The Dissertation Committee for Stephen Frederick Bourne Certifies that this is the approved version of the following dissertation:

High Density Thermal Energy Stores Utilizing Phase Change Materials for Shifting of Peak Cooling Loads

Committee:

Atila Novoselac, Supervisor

Richard Corsi

Michael Baldea

Ying Xu

Alexandre da Silva

High Density Thermal Energy Stores Utilizing Phase Change Materials for Shifting of Peak Cooling Loads

by

Stephen Frederick Bourne, B.S.; M.S. CIV & ENVIR ENG

Dissertation

Presented to the Faculty of the Graduate School of

The University of Texas at Austin

in Partial Fulfillment

of the Requirements

for the Degree of

Doctor of Philosophy

The University of Texas at Austin

May, 2016

Dedication

This work is dedicated to my parents, who have always strived to provide me with worthy role models; and to my wife Caryn, whose support and encouragement has made this work possible.

Acknowledgements

I would like to thank my advisor, Dr. Atila Novoselac, for his ongoing support of my studies at the University of Texas at Austin. I would also like to thank my PhD committee for their support and guidance during my research.

I would also like to acknowledge the ASHRAE Grant in Aid program, through which much of my experimental work was funded, and the Thrust Fellowship Program at the University of Texas. This work would not have been possible without the assistance provided by these organizations. Finally, I would like to thank Dr. Thomas Edgar and Risa Hartman for their support of my participation in the IGERT program at the University of Texas.

Most of all I wish to thank my wife, Caryn. I am grateful that she chose to accompany me on this journey, and I look forward to our next adventure together.

High Density Thermal Energy Stores Utilizing Phase Change Materials for Shifting of Peak Cooling Loads

Stephen Frederick Bourne, Ph.D.

The University of Texas at Austin, 2016

Supervisor: Atila Novoselac

Air conditioning cooling loads consume 11% of the electricity produced in the United States, and can be as high as 27% of total electric production in warm, humid climates. During the summer months these HVAC cooling loads can comprise more than 50% of peak electric load, with much of the demand coming from small commercial or residential electric customers.

Thermal storage systems offer the ability to shift these peak cooling loads to non-peak periods, which allows for a more efficient operation of baseload electric power plants by better utilizing capital equipment and available capacity. In addition, thermal storage systems allow for the more effective use of intermittent, renewable energy sources by shifting cooling loads to periods of renewable energy availability. Finally, thermal storage systems reduce the capital equipment cost for HVAC compressor systems by allowing the equipment to be sized for average, rather than peak, loads.

Given that residential and small commercial buildings generate the majority of peak cooling load in warm, humid climates, a thermal storage system compatible with these structures and sites is necessary. These sites may not have the space necessary for common chilled water thermal storage systems, which utilize the temperature change of a working fluid (frequently water) to store sensible energy in large storage tanks. For

residential and small commercial applications, a more compact, high-density thermal storage system will be required. Latent thermal storage, which utilizes the energy associated with a change in phase of a material to store thermal energy, shows promise for use in high-density thermal storage systems.

This research develops a latent thermal energy storage system based on phase change materials (PCM) suitable for use in applications where the size of the thermal store is critical, such as for existing residences and small commercial structures. Numerical, analytical, and experimental methods are used to design, test, and model a tube-encapsulated PCM-based thermal storage system with a capacity and performance suitable for HVAC applications. This research provides both general and specific design criteria sufficient to allow engineers to utilize this thermal store design for specific applications.

Table of Contents

List of Tables

List of Figures

Chapter 1: Introduction

1.1 Overview

Thermal energy stores, when used as part of a demand management system, can shift peak cooling load to off-peak hours or to periods when intermittent renewable energy sources are available. This enables more efficient use of baseline and renewable electric generation capacity and reduces dependence on less efficient and more costly peak energy power plants. High-density latent thermal energy stores can be an effective retrofit option for existing buildings and environmental control systems.

1.2 Electric energy generation and demand uncertainty

Sans any effective large-scale electric storage capability, electric power must be produced as it is used with generation precisely following demand. Uncertainty in both generation and demand require a means to regulate one or the other to maintain an ongoing balance. Current mechanisms focus mainly on the manipulation of generation using a mix of generation sources consisting of baseline, intermediate, and peak power plants.

Baseline power plants running continuously at constant output are used as a primary electricity supply. These baseline power plants are typically systems that require long startup periods and are slow to ramp up or down their output, but are generally less expensive to operate than other generation systems. Examples of these baseline systems include coal, nuclear, and combined cycle gas turbine power plants. Intermediate power plants, which can ramp up and down more quickly, are used to generate power needed to match predictable increasing demand throughout the course of a day. Peak demand power plants are fast-response generation systems, and are used to resolve issues associated with uncertainty in generation and demand. Peak demand power plants are less efficient and

more costly to operate, and are the last to be brought on-line to meet electric power demands [Masters, 2004].

The increased use of renewable but intermittent energy resources - such as wind and solar power - adds uncertainty to generation capacity. Figure 1 demonstrates the rapid growth in wind power for Texas, one of the largest wind producers in the U.S. Total U.S. solar and wind power generation is expected to grow by 46 and 42 gigawatts respectively by the year 2040 [US EIA, 2013]. Without mitigating action, the increased uncertainty in electric supply caused by the use of these intermittent renewable energy resources will require an increased capacity in less efficient peak demand power plants.

1.3 PEAK SHIFTING WITH DEMAND MANAGEMENT

Shifting peak load to non-peak periods can reduce the need for peak demand power plants. Shifting peak load to non-peak periods also allows for the more efficient operation of baseline power systems, making use of capacity and capital investment that might otherwise go idle during non-peak periods [Bentley and Evelyn, 1986].

To aid in the shift of peak power, electric generation and consumption systems can be moved from a model of on-demand generation to one that includes elements of as-available consumption [Hermanns and Weichmann, 2009]. In an as-available consumption model, demand management is used as part of a solution to match electric demand to available generation by shifting time-insensitive usage to periods when electric energy is available. In this manner peak electric loads can be reduced and electric energy can be produced at a lower cost and with higher efficiency. In addition, demand management systems allow for more efficient use of intermittent renewable sources - such as wind and solar - by driving energy use to periods when this type of power is available.

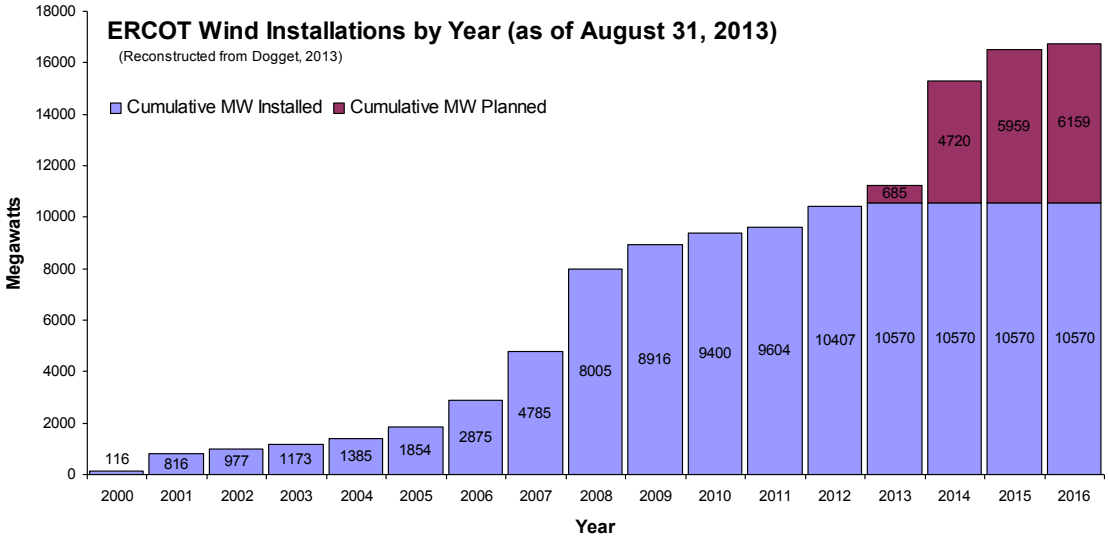

Figure 1: ERCOT projected wind capacity through 2016 [Doggett, 2013]. This demonstrates the rapid growth of wind generation capacity in Texas.

1.4 THERMAL ENERGY STORAGE AS A DEMAND MANAGEMENT TOOL

One tool for shifting peak electric load is the use of thermal storage systems. Overall, commercial and residential cooling loads account for 11% of all U.S. electric consumption [USEIA 2012], and can be a much larger share of peak electric demand in regions with warmer climates [Wattles 2011]. The Electric Reliability Council of Texas (ERCOT) reports that up to 54% of peak summer energy demand is due to weather-related loads, much of which is associated with environmental cooling [Doggett, 2013]. The demand for residential and commercial cooling will continue to increase, due to a projected growth rate in residential and commercial floor space and also to a shift in population towards states with warmer climates [US EIA 2013]. The use of active cold thermal storage systems offer the ability to shift building cooling loads to off-peak hours [Bentley and Evelyn, 1986]. Studies have shown that active thermal storage systems can be effective at both reducing peak energy demand and the overall cost of building energy

use by environmental systems when cost incentives – such as peak demand and time-of-day rates – are in use [Hajiah and Krarti, 2012a,b].

The use of thermal storage also eliminates the requirement that chiller equipment be capable of meeting peak cooling load demands, and thus reduces the peak demand seen by chiller equipment. The chiller equipment only needs to meet total load requirements (time-averaged load), rather than peak load requirements [He et al., 1999]. This reduces the capacity requirements and cost of chiller equipment and minimizes the refrigerant charge necessary for a given application. It also reduces the global warming impact of subsequent refrigerant leaks due to the smaller refrigerant charge required.

1.5 RETROFITTABLE THERMAL STORAGE

The ERCOT data shown in Figure 2 implies that fully 71% of weather sensitive peak load experienced in Texas is due to residential cooling loads. American Housing Survey data indicates that residential structures in 2011 had an average age of approximately 37 years [U.S. Census Bureau, 2013]. Similar data exists for commercial buildings, which account for 22% of Texas weather-sensitive load. According to the Commercial Buildings Energy Consumption Survey [U.S. Energy Information Administration, 2006], the median age of commercial properties in 2003 is approximately 28 years.

The long usable lifespan of residential and small commercial buildings, coupled with their weather sensitive load patterns, dictate that an effort be made to develop retrofittable thermal storage systems that can be deployed in existing structures that do not permit the addition of large sensible energy stores, such as chilled water tanks. High capacity, high-density thermal storage systems will be necessary for these retrofit applications.

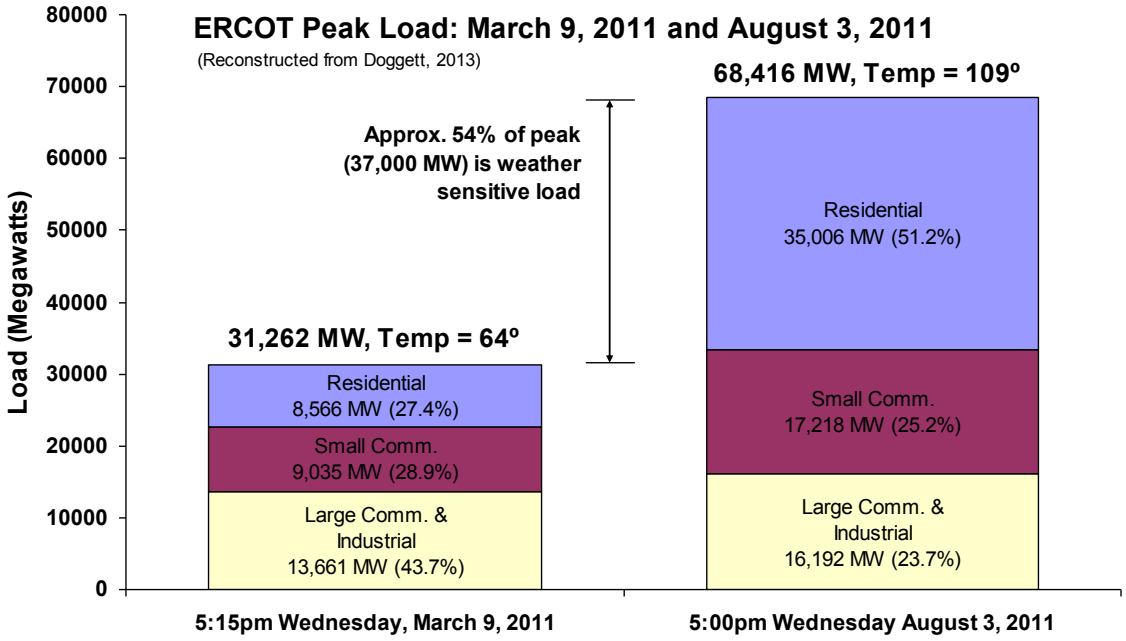

Figure 2: Extrapolated impact of weather on electric peak loads in Texas [Doggett, 2013]

1.6 LATENT THERMAL ENERGY STORES

Phase change materials (PCM) have been investigated for storing thermal energy in latent form [Hale et. al. 1971] [Humphries and Griggs 1977] [Abhat 1983] [He et. al. 1999]. Latent storage systems use the energy associated with phase change (solid-liquid, liquid-gas, or solid-gas) to store thermal energy [Baetens et. al. 2010]. Latent energy transformations are characterized by large changes in enthalpy at near isothermal temperatures, making them useful for compact, high-density thermal storage systems [Farid et. al. 2004]. Encapsulation systems to isolate the PCM from the heat transfer fluid (HTF) are required; rectangular [Shamsunder and Sparrow 1975], cylindrical [Bilir and Iilken 2005], and spherical containers [Assis et. al. 2007], have been modeled or experimentally investigated. However, many of these studies have concentrated on the phase change process rather than heat transfer with a working HTF (heat transfer fluid),

or assume a constant encapsulation surface or HTF temperature. This assumption is incompatible with a thermal store to be used in HAVC applications, where a change in temperature of the HTF is an express requirement. Simple tube-in-shell [Agyenim et. al. 2010] [Trp 2005] or spaced tubes of PCM [Kalaiselvam et. al. 2007] configurations have been investigated for use in thermal stores but these studies have aimed to maximize the performance (energy transfer rate) of the thermal store rather than the density of storage. A suitable thermal storage solution for retrofit applications would seek a balance between the highest possible thermal density while maintaining acceptable thermal performance for HVAC applications.

1.7 OBJECTIVES

There remains a need for research into a more efficient, high-capacity latent thermal store design specifically for HVAC applications - a design that maximizes storage capacity while offering acceptable heat transfer rate performance. In addition, there is a need for a model of this design that accurately represents important areas of interest, including the change in temperature of the HTF as it passes through the thermal store. Finally, experimental work is needed to validate both the design and the numerical model so that parametric studies can be performed to identify critical design criteria and so that engineering guidance can be developed. Therefore, the work in this dissertation is focused on fulfilling the following primary objectives related to these needs by developing and applying novel methods to:

1. Develop a design for and evaluate the feasibility of a high-density PCM-based latent thermal energy store, seeking a balance between performance and capacity suitable for HVAC applications;

2. Construct an experimental model of the proposed thermal store to determine critical design parameters, using this information for the development and validation of a numerical model that accurately represents the system; and
3. Use the validated numerical model for a parametric study to provide guidance for engineers seeking to implement this design.

These research objectives are fulfilled by three primary research investigations as described in this dissertation, which is divided into two distinct sections: 1) a research summary and 2) appendices. The research summary consists of an introduction, literature review, explicit research objectives, overview of methodologies used, and a summary of major findings from this research investigation. A more detailed description of specific phases undertook in the course of this dissertation are provided in the Appendices. There are 3 appendices (A – C), which include 3 full-length research papers, each containing the detailed methodologies, results and analyses summarized in section 1. Appendices A and B have been published in relevant journals, while Appendix C has been submitted and is currently under review.

Ultimately, this work provides new information on a high-density PCM-based thermal storage system that can be used in retrofit applications to reduce peak electric load.

1.8 SCOPE OF WORK

The scope of this work is limited to developing a thermal store design and providing design guidance for its use to engineers. The numeric model developed during this research produces graphs of performance data (energy recovery fraction) with respect

to encapsulation tube size for a set of flow rates (thermal demand) given specific materials (35% Propylene glycol HTF, aluminum encapsulation tubes, and tetradecane PCM). These are sufficient for an engineer to determine appropriate design parameters given thermal performance requirements.

The development from the data provided here of continuous equation forms that are suitable for control systems may be possible if the thermal store design is fully specified and the operating parameters sufficiently narrowed (input temperature and flow rate). These would take the form of empirical equations derived from the graphical data. This derivation, however, is not attempted here and is instead left for future work.

Chapter 2: Literature Review

2.1 Overview

The review of a number of topics is required to develop a thorough background in PCM-based thermal storage systems. These topics are covered in the following subsections.

2.2 Sensible v. Latent thermal storage

Thermal energy can be stored sensibly, through a change in temperature of a storage medium, or it can be stored latently as a change in phase of the medium. Phase change processes are characterized by large changes in energy at constant or near-constant temperatures. These characteristics of phase change/latent energy storage systems allow them to store energy at greater density and over a smaller temperature range than sensible energy storage systems, such as conventional chilled water tanks [Regin et al., 2008, Hasnain 1998]. As an example, note that the energy required to melt ice (0ºC ice changed to 0ºC water) is roughly equal to the energy required to heat the resulting water from 0ºC to almost 80ºC (334kJ/kg at a nearly constant 0ºC, vs. 4.2kJ(/kg·K) over 80ºC [Cengel et al., 2008]). Figure 3 depicts the relationship between enthalpy, temperature, and phase of a material as energy is supplied to drive the material from a fully frozen state to a fully vaporized state; note the constant temperature as thermal energy is added during the phase change process.

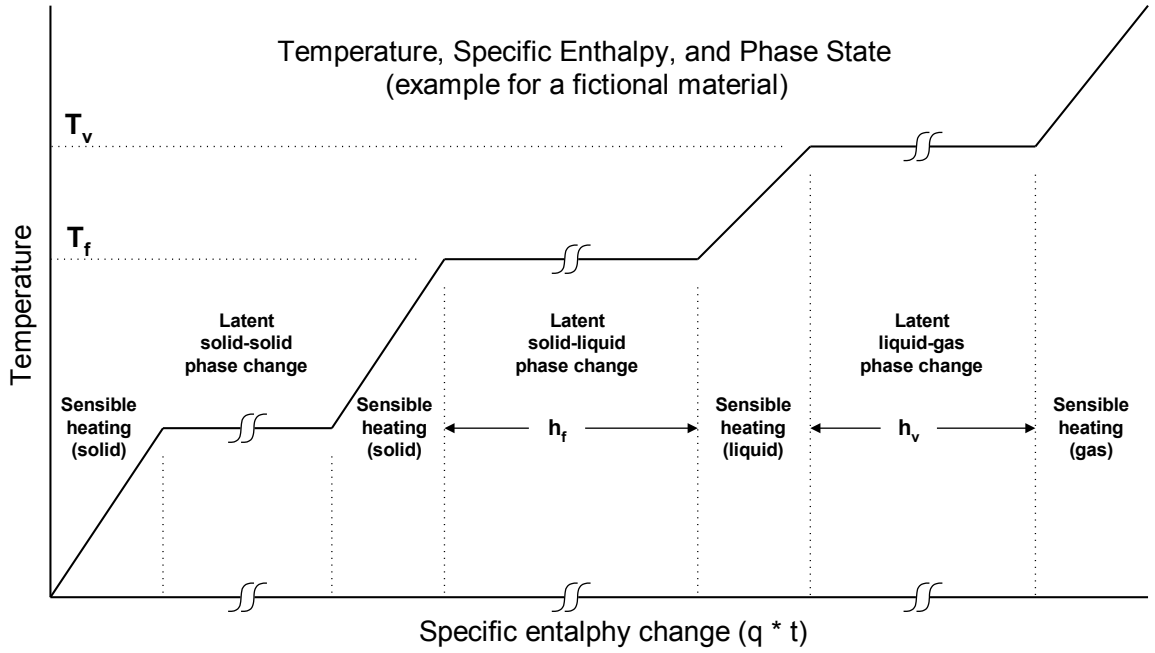

Figure 3: Temperature vs. enthalpy, phase state (not to scale) [derived from Regin et al., 2008].

2.3 PCM REQUIREMENTS FOR THERMAL STORES

Materials suitable for use in PCM-based thermal storage systems should exhibit several key properties: high volumetric and gravimetric heat of fusion, a narrow phase change temperature band in the desired range, reasonable thermal conductivity, chemical stability, and physical compatibility with common encapsulation materials [Abhat 1983][Baetens et al., 2010] [Humphries and Griggs 1977].

2.3.1 Heat of fusion and density

A large heat of fusion and high density are required to provide for a storage system that is size and capacity advantageous over a simple water-based sensible heat thermal storage system. Figure 4 shows the water volumes and temperature differentials

required to equal the energy storage a PCM with the heat of fusion densities listed (water properties taken at 0ºC). For a typical paraffin-based PCM (175 kJ/L heat of fusion), the comparable sensible water-based store using a temperature delta of between 5ºC and 6ºC would be approximate seven times larger in volume than a PCM-based store.

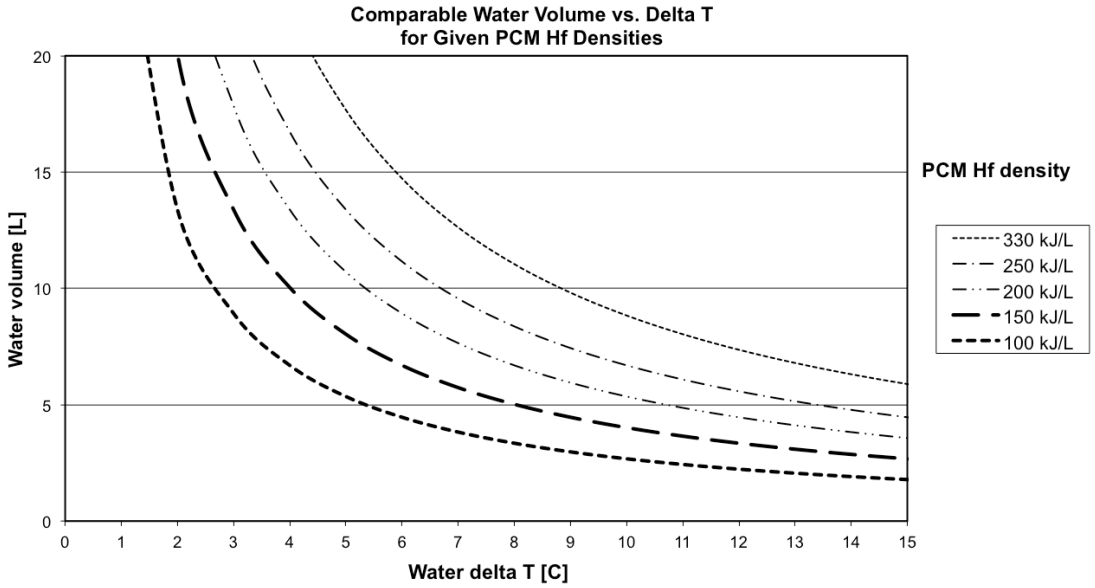

Figure 4: Water volume and temperature differential requirements for a sensible water store to equal the thermal storage capacity per liter of a PCM with the given thermal storage densities. Typical paraffin PCMs have a heat of fusion of about 175kJ/L; this would result in the PCM having a thermal density about 7 times that of a chilled water tank operating over 5 - 7°C.

2.3.2 Temperature range

The matching of phase change temperature range to the available equipment is important to insure that the storage system can cycle between its fully charged and discharged states while operating within the normal range of the chiller and fan coil systems [He et al., 2004]. Too wide a PCM temperature range might require a lower

temperature than possible from the chiller to become fully solidified - preventing a full charge of the store - or a higher temperature than usable by the cooling coil - preventing full discharge of the system. In any case, the temperature range of the PCM freeze-thaw cycle must be sufficiently narrow and be located between the maximum fan coil and minimum chiller operating temperatures. In addition, the gap between the PCM freeze-thaw temperature band and the extremes of the system must be sufficiently large to drive the thermal energy exchange at an acceptable rate. Figure 5 shows the limits to be considered.

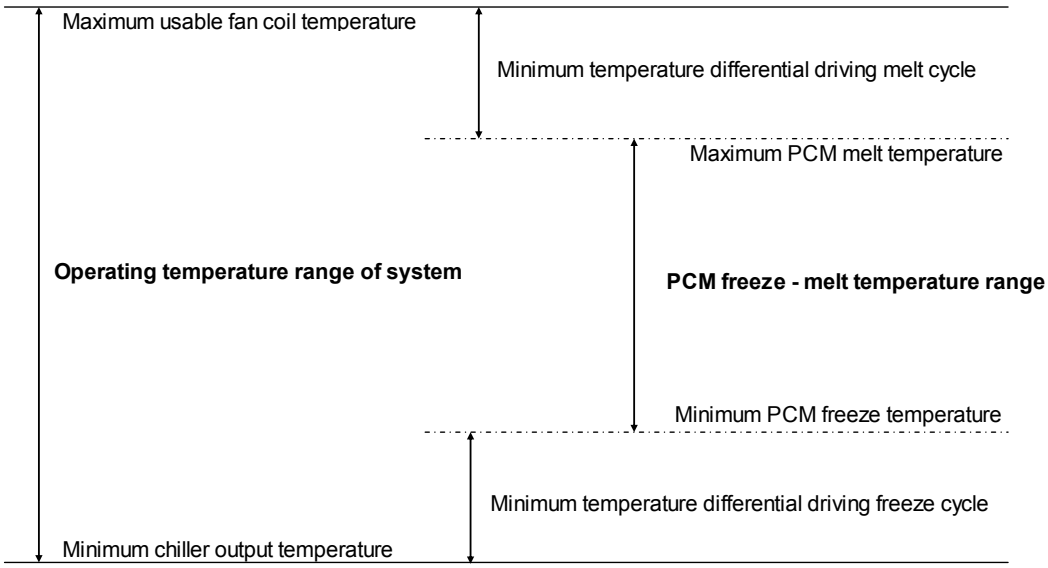

Figure 5: Relationship of system capability and PCM freeze-thaw temperature ranges for retrofit use. Note that the system must operate at a low enough temperature to fully freeze the PCM, and high enough to fully thaw it. Otherwise, capacity is lost.

2.3.3 Conductivity

Some common PCMs, such as paraffins and fatty acids, suffer from relatively low conductivity [Feldman et. a 1986], and this must be considered when designing a PCM-

based thermal storage unit. Good conduction through the PCM provides for acceptable charge and discharges rates with simple containment structures, although poor conduction rates can be overcome by PCM-embedded finned surfaces [Fan and Khodadadi 2011] or other conduction enhancements, such as lessing rings [Kenisarin and Mahkamov 2007] [Velraj et. al. 1999], metallic foams [Chen and Dukhan 2012], or by manipulating the encapsulation unit size/shape to improve the heat transfer area per unit volume [Feldman et al., 1986]. Alternatively, smaller encapsulation tubes or containers can be used to reduce the length of conduction paths.

2.3.4 Chemical stability/physical compatibility

Chemical stability is required to provide for both long service life and compatibility with encapsulation materials [Zalba et. al. 2003]. PCMs that chemically react with common and inexpensive materials will result in an unacceptable service life or additional costs. However, other physical matters must also be considered – such as storage density and volumetric/pressure changes that might occur during thermal cycling.

In thermal storage systems using phase change materials, phase changes occur in one or more of the following types of transitions: solid – solid (crystalline form change); solid – liquid (melting or freezing), solid – gas (sublimation), and liquid – gas (vaporization) [Regin et al., 2008] [Hale et. al. 1971]. Solid – solid phase changes are generally secondary, and in most cases store less energy than other phase changes. For instance, the paraffin n-Tridecane (C13H28) has a secondary solid-solid transition: a liquid-solid phase change at -5.4ºC with a heat of fusion of 155kJ/kg, and a subsequent solid-solid phase change at -41.6ºC for an additional 42kJ/kg. On the other hand, n-Tetradecane (C14H30) has a single liquid-solid phase change of ~230kJ/kg at 5.9ºC [Humphries and Griggs 1977]. Phase changes involving a gas phase introduce design

difficulties necessary to deal with the large volume or pressure changes encountered in such systems; these design issues can frequently make gas phase thermal systems impractical [Hasnain, 1998] [Humphries and Griggs, 1977]. Phase change materials that undergo a solid-liquid phase change are characterized by high density and high specific latent heat capacity (high thermal volumetric density) with low density changes (ease of encapsulation), making such materials useful for latent thermal storage systems.

Because of the advantages noted in this section, solid-liquid phase change systems are the focus of this research. Some of the solid-liquid phase change materials considered suitable for latent thermal storage systems include water, inorganic hydrates of salts, organic fatty acids and hydrocarbon paraffins, and eutectic compounds of each [Abhat, 1983] [Agyenim et al., 2010] [Farid et al., 2004].

2.4 COMMON SOLID-LIQUID PCMS

Water, salt hydrates, and organics such as fatty acids and paraffins are commonly used as PCMs. Each has distinct characteristics and properties that can affect its usability in specific PCM-based thermal store designs. These characteristics and properties are discussed in the following sections.

2.4.1 Water

Water, in the form of ice, is one of the first phase change thermal storage materials. Ice was delivered to homes in the United States as early as 1802 for food preservation using “ice box” systems [Stevenson, 1929]. Water has a high heat of fusion and high density (333kJ/kg and 1.043kg/liter [Cengel et. al. 2008]), making it volumetrically efficient at storing thermal energy. Water is also inexpensive and widely available.

However, freezing water for thermal storage requires temperatures lower than those for which typical HVAC chillers efficiently operate. Studies have shown that phase change temperatures should be in the range of 5 to 12ºC for space cooling applications [Li et al, 2012] [Dimaano and Watanabe, 2002], which is within the range of existing HVAC chiller systems but much higher than the freezing point of water. Also, the encapsulation of water for phase change applications is difficult because of the large decrease in density (expansion) of water when it freezes (999.8 vs. 916.7 kg/m3, or ~ 9.1% [Lide, 2001]). Since difficulties resulting from expansion arise when using encapsulated water for ice storage, phase change storage systems utilizing water use free ice instead. The free ice is stored in a tank through which HTF tubes pass, with the ice being regenerated during off-peak hours. Such ice-based systems require the use of specialized ice making equipment, in addition to existing HVAC equipment, making retrofit expensive.

2.4.2 Salt hydrates

Hydrates of salts and their eutectic compounds (mixtures of hydrated salts that produce the lowest freezing point) are highly reactive, have compatibility issues with many common encapsulation materials, and perform best when contained in hermetically sealed encapsulation vessels. In addition, only limited formulations of salt hydrates provide acceptable heat of fusion values (>200kJ/kg) while exhibiting congruent melt cycles (needed to prevent an irreversible separation of the material, which reduces the capacity of the system over time). Finally, salt hydrates typically exhibit a subcooling requirement that necessitates a lower initial temperature to induce phase change, which requires special efforts to improve initial nucleation [Kanwischer and Tamme 1985]. These issues make the use of hydrated salts in thermal stores more difficult than for other

materials, such as paraffins or fatty acids [Abhat 1983] [Farid et al., 2004]. Also, while material costs for hydrated salts are quite low, the encapsulation costs are much higher than for other PCMs [Feldman et al., 1986].

2.4.3 Fatty acids and paraffins

Straight-chain paraffins (n-alkanes) and saturated fatty acids are similar in constitution, each comprised substantially of hydrocarbon chains. However, while paraffins are typically of the form $CH^3(CH^2)_nCH^3$, fatty acids contain a carboxyl group and are typically of the form $CH^3(CH^2)_{2n}COOH$ [Li et al., 2012]. Both types of compounds exhibit the required properties for use as PCMs, with the exception of thermal conductivity [Feldman et al. 1986]. Their low thermal conductivity must be considered when designing thermal storage systems using these compounds [Velraj et al. 1999].

Both materials exhibit similar tendencies; for instance, longer hydrocarbon chains generally giving higher melting temperatures. This behavior in paraffins and fatty acids allows for the selection of a hydrocarbon chain length necessary to meet specific phase change temperature requirements.

Both paraffins and fatty acids are flammable, although paraffins suitable for cold thermal storage (tetradecane, hexadecane) have a high flash point (112ºC, 135ºC respectively) [Lide 2001]. They are also generally non-toxic, do not exhibit subcooling tendencies when freezing, and are unreactive with many materials suitable for encapsulation use [Hasan et al. 1994]. While the compatibility of paraffins and fatty acids with encapsulation materials is better than that for salt hydrates, fatty acids require special consideration due to their acidic nature.

2.4.4 Summary of PCMs

Thermal stores would differ only in their encapsulation materials/geometry and physical size when using different PCMs. This is due to the potential for reaction between a given PCM and its encapsulation material, and also to the different thermal capacities and conduction rates of the different PCMs. For the purpose of this research, any of the PCM materials described above is suitable. However, paraffins are well understood as PCMs, are readily available in a form possessing an appropriate freezing point temperature and temperature range, and are compatible with inexpensive and available encapsulation systems. For these reasons this research will utilize paraffin-based PCMs, with the understanding that the research is performed in a manner that allows application of its findings to other PCM materials as they become available or suitable for thermal store use. Paraffin PCMs will be reviewed further in the following section.

2.5 PARAFFIN PCMS

n-Paraffin (hereafter paraffin) waxes consisting of one or more compounds of the generic form CH3-(CH2)n-CH3 have been investigated for their use as PCMs (phase change materials) in thermal storage systems [Abhat 1983][Humphries and Griggs] [Hale et al, 1971]. As previously noted, phase change temperatures should operate in the range of 5 to 12ºC for space cooling applications [Li et al, 2012] [Dimaano and Watanabe 2002], and studies have shown that PCMs with the needed properties of specific melting point and heat of fusion can be crafted using paraffins with hydrocarbon chains of particular length or through the use of mixtures of such paraffins [He et al. 1999] [He et al. 2003] [He et al. 2004] [Choi et al. 1992]. These paraffin compounds are congruent through their melt-freeze cycles, chemically stable, non-toxic, possess high heats of fusion, and are available in a suitable temperature range for use in cold storage systems.

2.5.1 Research grade paraffins

Research grade paraffins (~99% or higher) with freezing temperatures (T_f) in the range of 0 to 40ºC (suitable for space conditioning) and an even number of carbon atoms do not undergo secondary solid-solid phase transitions near their normal freeze point [Humphries and Griggs 1977], giving them higher heats of fusion [Hale et. al. 1971]. These also have a narrower phase change temperature range, resulting in a more efficient thermal storage system because the equipment used to charge the thermal store does not have to work far from its normal operating range. Examples include n-Tetradecane (T_f = 5.6ºC) and n-Eicosane (T_f = 36.4ºC), which can be used for space cooling and heating, respectively. Table 1 gives relevant data on research grade paraffins with melting temperatures in a range useful for environmental control.

Name	Chemical Formula	Transition Temperature ºC (ºF)	Heat of Transition kJ/kg (Btu/lb)	Melting Temperature ºC (ºF)	Heat of Fusion kJ/kg (Btu/lb)
n-Dodecane	C12H26	N/A	N/A	-9.6 (14.7)	210.5 (90.6)
n-Tridecane	C13H28	-18.2 (-0.70)	41.6 (17.9)	-5.4 (22.3)	154.8 (66.6)
n-Tetradecane	C14H30	N/A	N/A	5.6 (42.1)	229.9 (98.9)
n-Pentadecane	C15H32	-2.30 (27.9)	43.2 (18.6)	10.0 (49.8)	163.7 (70.4)
n-Hexadecane	C16H34	N/A	N/A	18.2 (64.7)	228.9 (98.5)
n-Heptadecane	C17H36	11.1 (51.9)	45.5 (19.6)	22.0 (71.5)	168..3 (72.4)
n-Octadecane	C18H38	N/A	N/A	28.2 (82.7)	243.5 (104.7)
n-Nonadecane	C19H40	22.8 (72.9)	51.4 (22.1)	31.9 (89.4)	170.6 (73.4)
n-Eicosane	C20H42	36.2 (97.2)	0	36.4 (97.6)	247.3 (106.4)

Table 1: Properties of selected paraffins [excerpted from Humphries and Griggs, 1977]

Research grade n-Tetradecane (C14H30) has a narrow freeze/melt temperature range, an acceptable melting temperature (5.6ºC), a high heat of fusion (~225 kJ/kg) and no secondary solid-solid transition, which makes it well suited for cold thermal storage applications. However, pure paraffins are expensive and may not be cost effective in

thermal storage applications [Sharma, 2009]. A recent quote obtained for both laboratory (99%) and technical (95%) grades of Tetradecane confirms this claim, showing a cost factor of 2.7 for laboratory over technical grades of Tetradecane [Briggs, 2013].

2.5.2 Technical grade paraffins

Some paraffin products suitable in their pure form (99%) for cold thermal storage may not be suitable when found in technical grades (95%). This is because these products and their typical impurities (other n-alkanes) form mixtures that may have depressed freezing points, a lowered heat of fusion, and/or wider freeze-melt temperature ranges than their pure counterparts [He et al, 1999] [Trp, 2005]. For instance, a recent experiment using n-Tetradecane of the composition noted in Table 2 showed a freezing point depression from 5.9ºC to 4.1ºC. Such depressions may make the product unusable in a particular application, and care must be used when contemplating their use. Compositions and properties of these technical grade products should be confirmed before designing a thermal storage system based on these chemical grades.

Composition, n-Tetradecane, technical grade	
Tetradecane	95.14%
Branched Tetradecanes	2.80%
n-Paraffins < C14	0.73%
n-Paraffins > C14	1.33%

Table 2: Composition of a technical grade n-Tetradecane sample [Ruvalcaba, 2012]. This sample exhibited a freezing point temperature lower than that of pure n-Tetradecane (4.1ºC vs. 5.9ºC)

2.5.3 Binary mixtures of paraffins

Binary mixtures of tetradecane and hexadecane for cold thermal storage have been thoroughly investigated [He and Setterwall 2002] [He et al,2003] [He et al. 2004] [Choi et al. 1992] [Kousksou et al. 2010]. These results show that mixtures of these

products with needed thermal storage characteristics can be develop, but the mixtures result in a lowered heat of fusion, a wider freeze-melt temperature range, and sometimes include a solid-solid transition that may be outside of the temperature range of anticipated thermal store operation. These effects can reduce the capacity of the system in some applications, and may require changes in chiller or fan coil design to handle the wider thermal storage temperature range.

2.5.4 Thermal conductivity and enhancement of paraffin-based PCM thermal stores

Paraffin-based PCM materials that operate in a temperature range suitable for cold thermal storage generally exhibit poor thermal conductivity [Kenisarin and Mahkamov, 2007] [Velraj et al., 1999] [Feldman et al., 1986]. This poor thermal conductivity limits the rate at which energy from a PCM-based thermal store can be stored and recovered, and may require unique encapsulation methods or thermal enhancements to improve the effective conductivity of the PCM used [Agyenim et al., 2010].

However, it is not a matter of whether energy storage or recovery from a thermal store is fast, but rather is it "fast enough". The purpose of such a thermal store is to level or reduce peak period energy use, which – depending on the geographic location, time of year, mix of generation systems, and non-peak capacity – occurs over several hours each day. There is no requirement for the instantaneous recovery of all the thermal energy in a cold store, only that the needed portion of the stored thermal energy be recoverable within the peak energy period window at a temperature useful to typical environmental control systems. A successful thermal storage system based on macro-encapsulated paraffin PCM must balance the competing goals of performance (recovery rate and fraction), size, cost, and capacity.

Heat transfer performance in paraffin-based systems can be managed by using heat transfer enhancements internal to the encapsulation system, such as metallic foams or lessing rings [Chen and Dukhan, 2012] [Velraj et al., 1999], or by simply reducing the size of the encapsulation modules [Feldman et al., 1986]. Smaller encapsulation modules reduce the heat transfer path dimension and increase the surface area to volume ratio of the system at the expense of reduced overall capacity per volume of the thermal store due to a higher percentage of the total volume being used for the encapsulation material. Cylindrical and spherical encapsulation system sizes can be adjusted as needed to meet thermal recovery requirements. While surface area to volume ratios are higher with spherical encapsulation, cylinder encapsulation enables a higher theoretical packing density of 90.7% vs. 74.0% for spheres [Bezdek and Kuperberg 1990] [Hales 1998].

2.6 PCM-BASED THERMAL STORE EXPERIMENTATION AND MODELING

The number and type of physical thermal store designs and modeling methods found in the literature for PCM-based thermal stores are limited. As a result, other than a brief review of typical thermal store physical configurations and modeling methods, this review of previous research is grouped by author and ordered by date. This is because the uniqueness of a thermal store design or model is less in the configuration or technique used than in the assumptions made by specific authors.

2.6.1 Typical physical designs

A typical PCM-based thermal store physical design used in previous research is the shell and tube thermal storage system. This system utilizes a shell containing PCM with tubes for HTF flow passing through the shell [Agyenim, 2010] [Regin et al., 2008]. In some cases the system is reversed, and the PCM is contained in tubes while the HTF flows in the shell. This design lends itself to simple experimentation and modeling

because each tube is assumed to be surrounded by a similar shell of PCM or HTF, which is ostensibly a hexagonal area around the tube approximated using a cylindrical annulus. Since each tube and its associated annulus are identical, experiments and modeling need be performed only on a single set of tube and annulus elements. Other typical thermal store designs modeled or tested in the literature include slabs, tubes, or spheres of encapsulated PCM, either in a HTF bath or flow stream.

2.6.2 Typical modeling methods

Modeling of the phase change problem can be performed using a variety of methods. The most computationally complex entails solving the Navier-Stokes equations, for example as described by Versteeg and Malalasekera [1995]. However, this method is typically reserved for complex systems of fluid flow that require CFD (computational fluid dynamics) methods. In addition, it would require a means to alter the properties of the PCM during the phase change, producing a complex, non-linear problem. Ignoring natural, buoyancy-driven flows, as have most studies found on this subject, results in a system where the only fluid flow is related to external forced convection. This external forced convection can be modeled sufficiently using existing convection correlations, negating the need for such a computationally demanding solution.

Another method for solving phase change problems is by organizing them in the form of a Stefan, or moving boundary problem. This method is described in detail by Alexiades and Soloman [1993], and involves modeling the phase front as a moving interface whose velocity is related to the heat of fusion of the PCM and the net flux of energy across the moving phase interface. However, this method is complicated when the phase front moves in more than one dimension or direction, when both latent and sensible energy of the solid/liquid phases are significant, when multiple phase fronts are

encountered, or when the phase change temperature is not a single known value. While tractable, these complications diminish the benefits of utilizing such a method.

A more common approach is to use an enthalpy tracking model where the temperatures and enthalpies of nodes are solved using linear or linearized equations, or non-linear equations solved iteratively. This method is generally the least computationally intensive when a convection correlation exists for heat transfer between the HTF and the encapsulation surface, and linear/linearized equations are used. This method may require that the properties of the phase change material undergoing phase transition – which might be non-linear in nature – be linearized or otherwise handled in a manner that allows its effect to be reasonably represented in the model. This approach encompasses both finite volume and finite difference methods.

2.6.3 Previous research

Shamsunder and Sparrow [1975] comprehensively developed an implicit two-dimensional non-linear numerical solution for PCM solidification in a long rectangular container (square tubing), based on the enthalpy model and solved using iterative methods. Their non-dimensionalized solution utilizes the Ste (Stefan), Fo (Fourier) and Bi (Biot) numbers. This work, like some others in the realm of PCM solidification and melting, relies on a constant HTF (heat transfer fluid) temperature. This constant HTF temperature condition is unrealistic for the modeling of a thermal store, since the purpose of a thermal store is to transfer energy to/from a HTF that therefore must change temperature as it traverses the system. However, that model does give valuable insight into the development and solution of an enthalpy-based numerical model. The results show that a low Bi number is required for the store to produce a near-constant heat flux. This requirement is because for a low Bi number the resistance of convection dominates,

and in the modeled scheme the external resistant (1/[hA]) does not vary. Bi numbers larger than 1 produce significant drop-off in heat transfer with respect to time, and should be avoided unless mitigating action is taken. Ste numbers between 0.01 and 0.1 (within the realm of common PCMs) were modeled and shown to have little effect on solidification until near the end of the process.

Alexiades and Soloman [1993] have suggested these problems be solved as Stefan, or "moving boundary" problems. These problems can be solved using differential equations for the selected form of heat transfer on each side of the phase interface (in our case this is assumed to be conduction), but with a common condition at the moving interface (a fixed temperature). Energy conservation at the interface requires that the net difference in heat flux from each side of the boundary equals the rate of change of latent enthalpy, which can be related to the velocity of the phase front. This method allows for solving the time and position dependent values for temperature, latent enthalpy, and phase front position in a thermal store, and is similar to that used by Jiji and Gaye [2006]. However, modeling difficulties can arise when: the phase front moves in multiple dimensions, as found by Jesumathy et. al. [2012]; vertical advection and conduction must be considered; or multiple phase fronts result from partial discharge/charge cycles.

Ismail and Gonzalves [1999] numerically investigated the freezing of n-Eicosane (T_f = 36.4ºC) in a tube-in-shell system, where the shell contained the PCM and the tubes passing through the shell in a single-pass arrangement carried the HTF. Their enthalpy method model concentrates on a single similarity unit of HTF pipe and surrounding PCM annulus. Their numerical approximation is based on dimensionless parameters; the results are expressed in terms of a heat exchanger in the form of NTU, mass fractions of PCM solidified, effectiveness based on a dimensionless time, radii of the HTF tube, equivalent radius of the (effective) PCM annulus area (the "symmetry circle"), and formulation of a

Biot number involving the HTF pipe diameter. Their solution couples changes in the HTF with convection to the PCM. Their results show that increases in the R* ratio (the ratio of the outer PCM annulus diameter to the HTF tube diameter) reduces effectiveness and increases the time period for full solidification, much as would increasing the diameter of a shell encapsulating the PCM, or the thickness of a slab. In addition, they conclude that an R* value of 4 is optimal from the standpoint of both NTU and effectiveness.

Bilir and Ilken [2005] investigated the solidification time of PCM in both cylindrical and spherical containers using an enthalpy model and an explicit scheme. The model assumes a perfectly conducting shell (RT = 0), a constant HTF temperature and convection coefficient h, and radial conduction only (a reasonable assumption given solidification from the outside inward). Their model is similar to, and expands upon, that of Shamsunder and Sparrow [1975]. The results of an analysis of their model provides correlations for solidification times as a function of Stefan, Biot numbers and a superheat parameter for both cylinders and spheres.

Jiji and Gaye [2006] analytically investigated the theoretical solidification and melting of slab elements of PCM using a quasi-steady state model as an approximation. Their model also included internal energy generation. Their quasi-steady state method assumes that the system - from a sensible energy perspective - is always in equilibrium (sensible equilibrium is assumed to be reached immediately after the sensible/latent energy transformation has been completed). When the Stefan number is much less than one, this is a feasible assumption (sensible energy is a small part of the total energy exchange). The solution was found analytically, but required that the surface temperature of the encapsulation system be constant (the HTF temperature is also constant) resulting in a one-dimensional problem. The solution operates by assuming separate differential equations for conduction through the PCM – one for the solidified portion and one for the

liquefied portion of the PCM, each with its own boundary conditions – with a separate differential equation acting to connect the two at the moving interface boundary between the phases (using the quasi-steady state approximation referenced above). The rate of movement of the phase change interface is related to the difference between conduction from/to each of the phases and the heat of fusion of the PCM, coupled with the geometry of the system.

Ismail and Moraes [2009] investigated analytically and experimentally the use of spherically-encapsulated PCM. Their study assumed a constant HTF temperature outside of the spheres. Their study did not assume quasi-steady state, and instead used a finite-difference approximation to numerically model the freeze cycle, assuming only conduction inside of the spherical shell. Their numerical results correlated well with experimental results when diameters were small. They did not investigate melting cycles.

Jesumathy et al. [2012] investigated a single vertical annulus tube-in-shell design for a PCM-based thermal storage system. Their study showed that the PCM did not melt in a uniform manner; instead, the PCM melted from the top down in a manner similar to what we've observed in our own preliminary experiments, even though they had much higher relative flow rates that would tend to maintain a more constant and uniform thermal bath temperature. They also experimented by altering the Reynolds number of the flow around the encapsulation annulus, but limited the Re range to between 693 and 1175 (laminar flow). They surmising that this would alter the convection heat transfer coefficient, however, they noticed no significant change in the heat transfer coefficient. This may be because the Re numbers were in a range which is limited to laminar pipe flows, and in fully developed laminar flows the convection coefficient becomes a constant function of the Nusselt number, characteristic length and the thermal conductivity of the fluid. This study also notes that in certain cases internal

(encapsulation) convection results at the interface between the PCM and the encapsulation system, thus increasing heat flow internal to the encapsulation system, although this effect was not quantified.

Rathod and Banerjee [2014] experimented with a system similar to the tube and shell design investigated by Jesumathy et. al., except that the HTF flowed through a center tube rather than around the PCM annulus. Paraffin was used as a PCM. The HTF flow direction was set the same for melt or freeze cycles (bottom to top), which may have led to buoyancy-driven short circuit flows during melt cycle testing. Input HTF temperatures were recorded, but not output temperatures, so it is unclear if the input-output HTF temperature change was useful. The study concluded that internal convection (in the PCM) resulted in the observed melting pattern – from the top down, even though the HTF flow was from the bottom up – although buoyancy effects in the HTF may have contributed to this result. Natural convection in the PCM was considered insignificant during the freeze cycle. The study also found that pushing the HTF flow Reynolds number into the turbulent realm improved the melt cycle performance, as did increasing the temperature differential between the HTF and the PCM.

2.7 SUMMARY

The organic PCM compounds consisting of paraffins and fatty acids are the most promising due to their lack of subcooling, high heats of fusion, congruent melt cycles (no segregation), and compatibility with common encapsulation materials. Organic PCMs suffer from poor conductivity, but this can be overcome by internal conductivity enhancements – such as fins or metallic foams – or by manipulation of the encapsulation system dimensions or materials. The paraffin tetradecane has a suitable melting temperature range for use with HVAC systems and is readily available.

Most of the models found in the literature utilize some form of enthalpy tracking to monitor the phase state of the PCM elements. Few models considered vertical conduction in the system, however, any form of PCM conductivity enhancement - internally to the PCM or through manipulation of the encapsulation dimensions or material – could render vertical conduction important. Many models investigate the thermal performance of a single unit of a thermal store design using a constant external fluid or surface temperature, however, this is not useful for thermal store applications since our express interest is in changing the temperature of the HTF. Some studies did allow for a changing HTF temperature, but used high relative flow rates such that the change in temperature was too small to be useful. In addition, none of the studies or models specifically allowed for multiple simultaneous phase fronts, even though in the course of a partial discharge/recharge at least two-phase fronts are possible. Finally, no study made an attempt to model the thermal store in a stop-start mode, where intermittent demand would allow the store to thermally "reconfigure" itself between calls for cooling. Each of these are conditions that could be regularly encountered by a thermal store in operation with an HVAC system, and a flexible, robust model should attempt to represent as many of these potential conditions as possible.

A simple finite volume energy balance model can be used to track total enthalpy and phase states while solving for temperatures within the thermal store, and can incorporate the effects of advection (HTF), convection (HTF to encapsulation tube), and conduction (encapsulation and PCM) within a single model. Such a model enables operation with multiple phase fronts, supports a HTF that changes temperature as it passes through the store, incorporates vertical diffusion, and allows the store to thermally reconfigure during periods of zero HTF flow. The drawback to such a system is an

increase in computational requirements, but the scale of this project will not tax typical desktop computing power now commonly available.

Chapter 3: Specific Research Objectives

The literature review indicates that there are areas in need of further investigation with respect to latent heat thermal storage systems for HVAC applications. Specifically, a specialized high-density thermal store design for cooling load applications is needed. In addition, a numerical model that incorporates the parameters that are important to HVAC systems is needed for parametric analysis and to provide engineering guidance for application of the design. Therefore, as originally discussed in the Introduction section, the research focus of this dissertation addresses the following three objectives with the associated investigations in the form of journal publications as described below:

1. Apply novel methods to design and develop a high-density thermal storage system for HVAC applications and its associated numerical model based on a dense hexagonal packing of tube-encapsulated PCM. This objective is fulfilled by an investigation detailed in Appendix A, and summarized in this executive summary section.
2. Construct an experimental apparatus and apply analytical methods to identify critical thermal store parameters, using this information to refine the design and validate the model. This objective is fulfilled by investigations detailed in Appendix A, B, and C, and summarized in the executive summary.
3. Use the validated model to conduct a parametric analysis for the purposes of providing design guidelines to engineers seeking to implement this high-density thermal store design for specific applications. This objective

is fulfilled by the investigation detailed in Appendix C and summarized in this summary section.

These research objectives result in a new and novel thermal store design that can be used in retrofit applications to shift peak cooling loads, particularly where a high-density, low volume thermal store design is required. The parametric analysis is formulated so as to allow this thermal store design to be specified in a wide range of applications without additional modeling. The complete results of these research objectives and related investigations are presented in three journal articles compiled in the appendices.

Objective 1 is fulfilled by the journal article in Appendix A, " Compact PCM-based thermal stores for shifting peak cooling loads (published in Building Simulation, an International Journal). In this study the initial design, experimental apparatus, and model of the thermal store are developed.

Objective 2 is fulfilled in part by the journal article in Appendix A, " Compact PCM-based thermal stores for shifting peak cooling loads" (published in Building Simulation, an International Journal), and in part by the journal article in Appendix B, "Improved performance in tube-encapsulated phase change thermal energy stores for HVAC applications" (published in Building and Environment), and in part by the journal article in Appendix C, "Design guidelines for high-density thermal storage systems utilizing hexagonal packed tube encapsulated PCM" (submitted to Energy and Buildings). In these studies a critical dimensionless design parameter for the encapsulation system is identified, the numerical model updated, and then validated against experimental data.

Objective 3 is fulfilled by the journal article in Appendix C, "Design guidelines for high-density thermal storage systems utilizing hexagonal packed tube encapsulated PCM" (submitted to Energy and Buildings). In this study a parametric analysis of the thermal store design with respect to encapsulation tube size is performed, and the results used to provide guidance to engineers seeking to implement this design.

The methods used to fulfill the objectives described are found in Chapter 4, divided by group into analytical, numerical, and experimental methods. A summary of significant results is provided in Chapter 5, while an overall summary and suggestions for future investigations are provided in Chapter 6.

Chapter 4: Methods

4.1 Overview

This research is based on the hypothesis that a high-density thermal storage unit can be constructed using tube-encapsulated PCM tightly packed into a larger containment vessel or tank, with a heat transfer fluid flowing in the triangular-like spaces left at the interface between the tubes. Initial calculations indicate that a minimum four-fold thermal density improvement can be had over existing sensible thermal storage systems when using this method with standard CPVC encapsulation tubes, and even more when using thin-wall metallic tubes.

A finite volume numerical model is developed to confirm this hypothesis. The initial numerical model assumes that the tightly packed tubes can be modeled as tubes surrounded by an annular ring of HTF, where the area of the HTF flow is equal to the free area formed by the triangular flow paths between the tubes. As a result of this numerical model, a small-scale experimental thermal storage unit is constructed. The results of experiments using this test unit show that the numerical model accurately predicts thermal store performance when the tubes were slightly spaced (where an annular ring of fluid is actually present around the tubes), but breaks down at the desired high-density hexagonal packing of tubes.

A theory is developed that, while sufficient heat transfer occurs in the triangular-like flow paths formed with the hexagonal packed configuration, the heat transfer is not evenly distributed around the encapsulation tubes and thus forces the tube and PCM to internally redistribute the thermal energy. The CPVC tubing and PCM have poor conductivity, resulting in suboptimal performance and the discrepancy noted between predicted and actual performance of the thermal store. However, it is also theorized that if a sufficiently conductive material is used for the encapsulation tube that the tube itself

could be used to redistribute the thermal load around the PCM, improving the performance of this design. A dimensionless parameter – the resistance ratio – is developed to ensure that the conductivity around the encapsulation shell is at least an order of magnitude greater than the conductivity between the encapsulation shell and either the PCM or the HTF. A second configuration of encapsulation tubes using standard copper tubing that exceed the requirements of the resistance ratio parameter are constructed and installed in the experimental test thermal store. Testing confirms an improvement in thermal store performance sufficient for use in high-density thermal storage systems.

Using this information, the model is revised to treat the triangular-like flow paths formed by the tightly packed tubes as triangular pipes, with the assumption – made possible by the resistance ratio parameter – that the convected energy is well-distributed across the surface of these flow paths. The revised model is validated against the new experimental data, and the validated model is then used for a parametric analysis to provide design guidance for engineers seeking to implement this design. The parametric analysis shows that this design is well suited to retrofit applications for use in shifting peak cooling loads to off-peak periods.

The sections that follow summarize three specific methodologies used to achieve the stated objectives for this research, presented in the following order: analytical methods used to develop the resistance ratio parameter; numerical methods used to model this thermal store design for parametric analysis; and experimental methods used for design and numerical model validation. A summary of quality control measures is included at the end of this Methods section.

4.2 ANALYTICAL METHODS

An encapsulation tube design parameter, the tubing resistance ratio, is developed as a means to predict whether or not the physical properties and parameters of the encapsulation tube are capable of producing a well-distributed thermal condition around the PCM when a hexagonal packed configuration of encapsulation tubes is used. This condition allows for a simplified two-dimensional numerical model (the system is considered axisymmetric). This parameter is modeled after a Biot number, but differs in that it compares the resistance of the encapsulation tube to redistribute thermal energy around itself to that of the resistance of passing the thermal energy between either the HTF or the PCM.

The physical basis for the development of the resistance ratio is a numerical modeling element, which is comprised of a $\pi/3$ radian segment of an encapsulation tube of arbitrary step height L and its surrounding HTF, as shown in Figure 6. The segment is divided by a plane of symmetry as shown in Figure 7 (for clarity, Figure 7 does not show the HTF portion of the modeling element), which gives some of the critical dimensions used in calculating the resistance ratios.

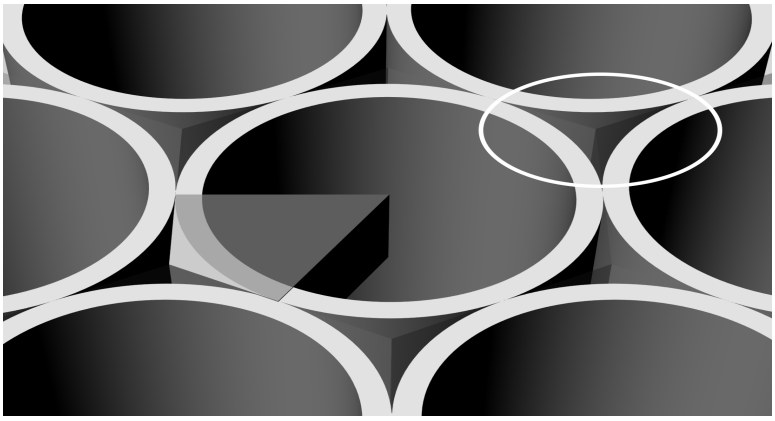

Figure 6: A modeling element (shown in the center tube), and the triangular-like flow paths for the HTF (example circled in white).

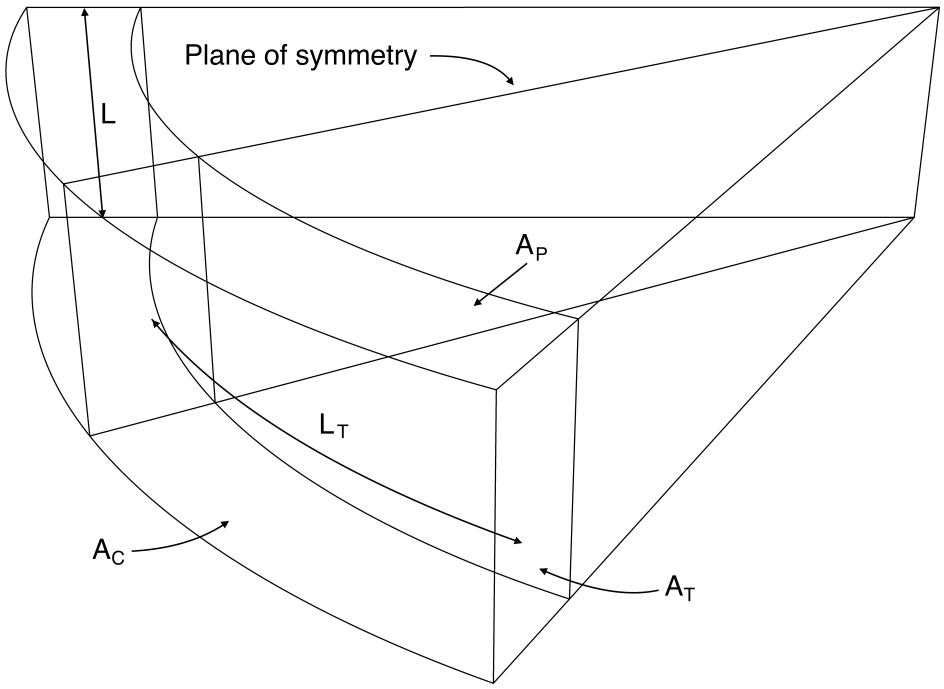

Figure 7: Dimensional parameters used for the calculation of the resistance ratio: L = arbitrary vertical step; Lt = characteristic length of conduction in the encapsulation material; Ac , At , Ap = areas associated with convection, conduction in the encapsulation tube, and conduction in the PCM respectively.

To develop the resistance ratio, the thermal resistances for heat transfer in each of the mediums are first calculated - convection from the HTF to the encapsulation tube, conduction from the encapsulation tube into the PCM, and conduction around the encapsulation tube. Equation 1 shows the calculation for the thermal resistance of convection to the encapsulation tube, R_c, for a symmetry section of the numerical model element shown in Figure 7. It is assumed that the thermal resistance for convection is based on the relevant surface area of the encapsulation shell and an average Nusselt number. The Nusselt number is estimated as 2.5, which corresponds to the Nusselt number for laminar flow in an equilateral triangular pipe [Cengel et. al.2008]. The

hydraulic diameter is calculated as four times the cross sectional area of the triangular-like HTF flow path divided by its wetted perimeter. Due to the relationship between hydraulic diameter and the convection surface area of the encapsulation tube in the hexagonal packed configuration, tube dimensional parameters cancel out and the resulting resistance is a constant function of the Nusselt number, HTF conductivity k_f, and an arbitrary length constant L corresponding to the height of the modeling element.

$$R_c = \frac{1}{hA_c} = \frac{D_h}{Nu\,k_f A_c} = \frac{4\left(\sqrt{3}-\frac{\pi}{2}\right)r_o^2}{\pi r_o} = \frac{12\left(2\sqrt{3}-\pi\right)}{\pi^2}\frac{1}{Nu\,k_f L} \tag{1}$$

The resistance of the PCM, R_p, is determined as it would normally be for a typical Biot number calculation involving a cylinder, with the characteristic length L_p set equal to $r_i/2$ (the volume of the an infinite cylinder divided by its surface area) [Incropera 2007]. Note that due to the relationship between the characteristic length L_p and the area of conduction A_p, the tube dimensional parameters cancel out and the resulting resistance is a constant function of the PCM conductivity k_p and the arbitrary length constant L. The resulting thermal resistance calculation is shown in Equation 2.

$$R_P = \frac{L_p}{k_p A_p} = \frac{\frac{r_i}{2}}{k_p \frac{\pi}{6} r_i L} = \frac{3}{\pi}\frac{1}{k_p L} \tag{2}$$

The area for heat conduction into the cylinder of PCM is taken as it is for a Biot number, upon which concept the resistance ratio parameter is based. For a Biot number,

the area for conduction into the body is set as equal to the surface area of convection; as a result the areas for convection and conduction are equal and thus cancel, producing a Biot number with no area components. In the case of the resistance ratio, convection to the cylinder is replaced by conduction from the encapsulation material, and thus the area used for conduction into the PCM is taken as A_p (the inside surface area of the encapsulation tube). However, a more accurate representation of conduction into the cylinder will use the log mean area for the areas at r_i and $r_i/2$, between which the heat transfer is assumed to occur. In this case the log mean area is calculated as 1/(2ln(2)) times the inside area of the encapsulation tube ($0.721*A_p$). When utilized in the calculation of the resistance ratio parameter, this results in a less conservative value than when using the inside area of the encapsulation tube. We will defer to the more conservative value of the resistance ratio and use the inside area of the encapsulation tube, following the example set in Biot number derivations.

It has been assumed that the thermal energy convected to the encapsulation tube surface is based on the surface area of the encapsulation shell and an average Nusselt number, but its distribution across the face of the encapsulation shell is unknown. Since our goal is to verify that the encapsulation shell can effectively redistribute the thermal energy around the PCM under the worst-case, most conservative conditions, it will further be assumed that the convected energy enters the encapsulation shell at the line of symmetry and is conducted around the encapsulation shell. The characteristic length for conduction within the encapsulation tube L_t is thus taken as the distance between the center of the encapsulation tube wall at the plane of symmetry and the center of the encapsulation tube wall at the edge of the modeling unit, where the apex of the triangular flow paths are formed by the intersection of the tubes. The cross-sectional area of the tube segment A_t is used for the area of conduction, since conduction is now assumed to

be along the cross-section of the tube, as shown in Equation 3. Note that this is the only resistance calculation that retains encapsulation tube dimensional parameters in its final form.

$$R_t = \frac{L_t}{k_t A_t} = \frac{\frac{\pi}{6}\left(\frac{r_o + r_i}{2}\right)}{k_t\left(r_o - r_i\right)L} = \frac{\pi}{6}\frac{\left(r_o + r_i\right)/2}{\left(r_o - r_i\right)}\frac{1}{k_t L} \tag{3}$$

The resulting resistance ratios R_t/R_c (between the encapsulation tube and the HTF) and R_t/R_p (between the encapsulation tube and the PCM) are shown in Equations 4 and 5. Note that both of these equations resolve to the product of a dimensionless constant multiplier C determined by the hexagonal packing geometry, a dimensionless geometry variable R_r describing the ratio of the average tube radius to its wall thickness, and a dimensionless conductivity variable K_r describing the conductivity ratio of the adjoining materials (including any Nusselt number modifier). These dimensionless quantities are summarized in Table 3.

$$\frac{R_t}{R_c} = \frac{\pi^3}{72\left(2\sqrt{3} - \pi\right)}\frac{\left(r_o + r_i\right)/2}{\left(r_o - r_i\right)}\frac{Nu\,k_f}{k_t} \tag{4}$$

$$\frac{R_t}{R_p} = \frac{\pi^2}{18}\frac{\left(r_o + r_i\right)/2}{\left(r_0 - r_i\right)}\frac{k_p}{k_t} \tag{5}$$

Resistance Ratio	C	Rr	Kr
R_t/R_c	$\frac{\pi^3}{72\left(2\sqrt{3}-\pi\right)}$	$\frac{\left(r_o+r_i\right)/2}{\left(r_o-r_i\right)}$	$\frac{Nu\,k_f}{k_t}$
R_t/R_p	$\frac{\pi^2}{18}$		$\frac{k_p}{k_t}$

Table 3: Dimensionless quantities C, Rr and Kr for Rt/Rc and Rt/Rp

Existing convention for Biot number calculations require a resistance ratio of less than 0.1, which is the criterion accepted here as well. When this condition is met it is assumed that the encapsulation shell is capable of redistributing thermal energy around the encapsulated PCM much more easily than to or from PCM or HTF, providing for even heat transfer into the PCM with respect to angular position. This creates an axisymmetric condition for heat transfer that simplifies modeling by permitting the system to be treated as two-dimensional (in r and z). The use of the resistance ratio parameter allows for the selection of encapsulation tube materials and thicknesses that can be accurately modeled using the two-dimensional model developed in this study, and provides for improved performance in thermal storage applications.

4.3 NUMERICAL METHODS

Numerical model development and validation are described in the following subsections.

4.3.1 Numerical model development

A linear numerical model, based on a finite volume method, is developed. The model considers advection of HTF flow, vertical diffusion in the HTF, convection from the HTF to the surface of the encapsulation surface, as well as vertical and radial

conduction within the encapsulation material and PCM. The model takes as input a set of matrices representing the previous time step temperature and latent energy values for each node (latent energy is set to 0 for surface and non-PCM nodes); values representing HTF input temperature and flow rate; and physical parameters and constants for the model. It returns a set of matrices representing the current time step temperature and latent energy values. Successive iterations can be used to model operation over any time interval. The default time step is one second.

Figure 8 shows an element that is the basis for the final numerical model. This element represents a 60° ($\pi/3$ radian) section of an encapsulation cylinder with arbitrary step height Δz, including its surrounding HTF and enclosed PCM, spanning between the contact points of the adjoining encapsulation cylinders. The vertical surfaces of the element are adiabatic, based on the assumptions that $dT/d\theta = 0$ in the PCM (axisymmetric, due to the incorporation of the resistance ratio condition discussed in the analytical methods section), and that HTF stratification in the tank results in a uniform temperature for all HTF cells at the same vertical location in the tank. This allows the thermal store to be modeled as a stack of these elements.

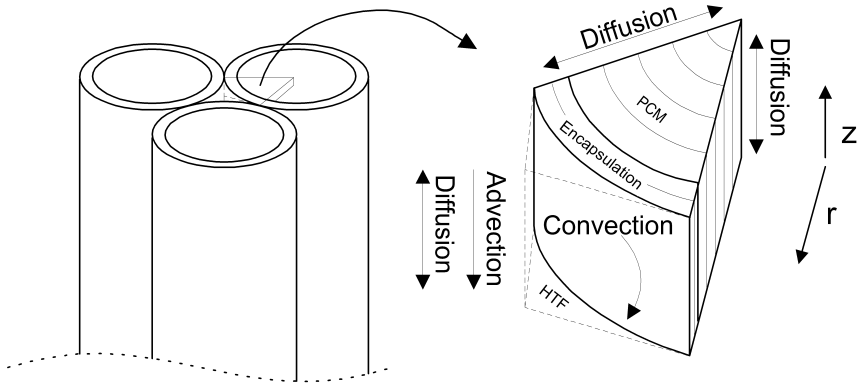

Figure 8: An element of the numerical model, which consists of components representing the HTF, encapsulation cylinder, and PCM. The model combines a vertical stack of these elements.

Each element consists of volumes representing the HTF, encapsulation material, and PCM, and each volume contains a node. In addition, some surface nodes are assigned where dissimilar materials or heat transfer mechanisms occur. Volume nodes are used to track temperature, and thus accumulate sensible energy. Volume nodes in the PCM are also used to track latent energy. Surface nodes track temperature, but do not accumulate thermal energy; they act only as transfer agents between volume nodes. An example representation of the nodes and volumes used in the model is shown in Figure 9.

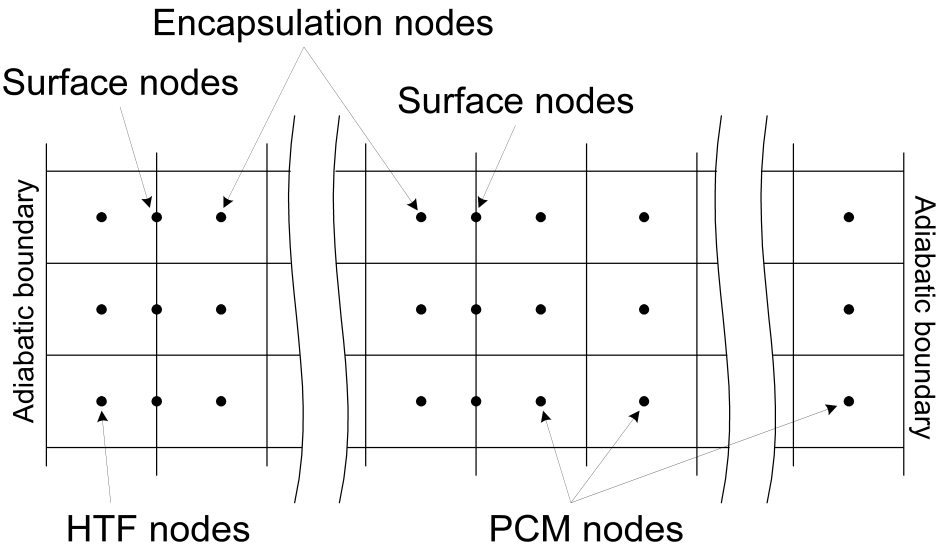

Figure 9: Example node breakdown for different elements of the model. HTF, encapsulation, PCM, and boundary surface nodes are depicted. The number of PCM and encapsulation nodes are configurable for each model run.

Tank stratification is maintained by using different flow directions for the charge and discharge cycles, which minimizes the potential for buoyancy-driven free convection in the HTF and so this potential is ignored. Only conductivity is considered in the PCM, regardless of phase; any buoyancy-driven convection effects in the PCM during phase

transition are assumed to be included in the effective conductivity of the PCM. Thermodynamic properties associated with the HTF and the encapsulation material are considered constant over the temperature range of the thermal store. These properties are evaluated at the mean operating temperature. Thermodynamic properties of the fully solid or fully liquid PCM are set dependent on phase state.

Heat transfer associated with the HTF is modeled using a single HTF node at each vertical step in the model. Advection and vertical diffusion is modeled between HTF nodes, and convection is modeled between the HTF nodes and the surface nodes of the encapsulation cylinder. In the initial numerical model, the free area in the tank available for HTF flow was evenly divided among the encapsulation tubes and modeled as an annular flow path around each tube; this method allows the same model to be used for spaced as well as packed encapsulation tubes. However, analysis of the initial experimental data and the need to maximize thermal density by using the hexagonal packed system of encapsulation tubes resulted in a revised model. This revised model treats the spaces formed by the confluence of the encapsulation cylinders as a set of triangular pipes. Reynolds numbers for the anticipated flow rates are on the order of 1, ensuring laminar flow. A Nusselt number for fully developed laminar flow in triangular pipes of 2.5 is used for convection purposes [Cengal et. al. 2008].

The hydrodynamic and thermodynamic entry lengths for laminar flow can be estimated as the products $0.05ReD_h$ and $0.05ReD_hPr$, respectively [Cengal et. al. 2008]. These values indicate that the typical hydrodynamic entry length is on the order of 1mm while the typical thermal entry length is on the order of 2cm, both of which are short compared to the active region of the experimental thermal store (0.908m). It should be noted that the thermal entry length calculation is predicated on a constant wall temperature, which is not present in this design. However, the rate of change of

encapsulation tube wall temperature in the tank during operation is small, so we will assume that the thermal entry acts as if the wall temperature is constant and that the flow is fully developed everywhere in the tank with respect to the model elements.

Each HTF node volume is assumed well mixed with a uniform temperature at each time step. The geometry and node configuration for a HTF node is shown in Figure 10, with the formula used to describe the energy balance and heat transfer with respect to the HTF given in Equation 6.

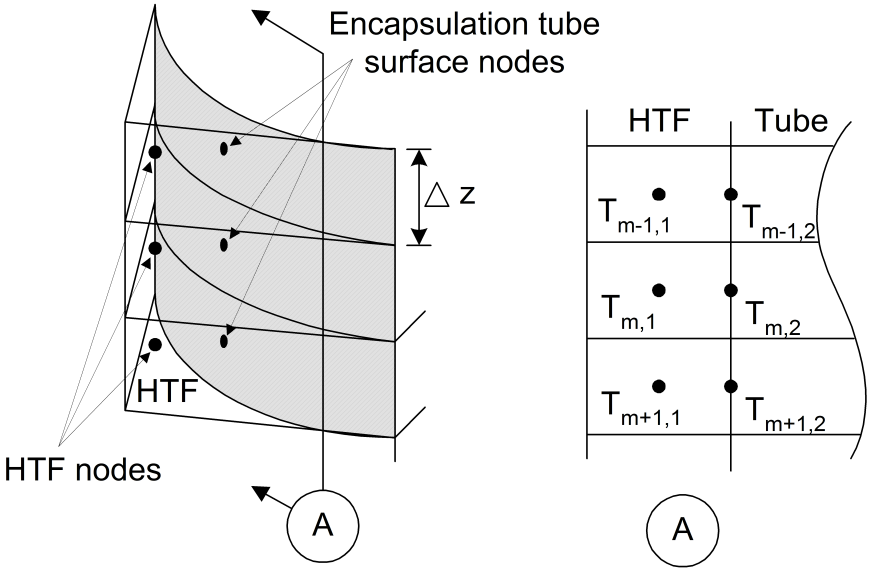

Figure 10: Geometry and node configuration for heat transfer in the HTF. This figure shows the HTF and convection surface nodes considered during the convection, advection, and diffusion modeling.

$$V_f \rho_f C_f \left(T_{m,1}^{t} - T_{m,1}^{t-\Delta}\right) = A_c h \left(T_{m,2} - T_{m,1}\right)\Delta t + A_a k_f \left(\frac{T_{m-1,1} - T_{m,1}}{\Delta z} - \frac{T_{m,1} - T_{m+1,1}}{\Delta z}\right)\Delta t + A_a w \rho_f C_f \left(T_{m-1,1} - T_{m,1}\right)\Delta t \quad (6)$$

This equation collapses to the differential form found in Equation 7.

$$\frac{\partial T}{\partial t} = \frac{A_c}{V_f}\frac{h}{\rho_f C_f}\left(T_s - T_f\right) + \alpha_f \frac{\partial^2 T}{\partial z^2} - w\frac{\partial T}{\partial z} \tag{7}$$

Heat transfer within the encapsulation cylinders and the PCM considers conduction only, in both the r and z directions, regardless of whether the PCM is solid, changing phase, or liquid. The geometry and node configuration is shown in Figure 11 (surface nodes are not shown). To improve the performance of the model, a log-mean value is used for conduction between radial nodes. This maintains model accuracy while allowing larger radial steps. Figure 11 is used to develop Equation 8, which is used to solve for unknown temperatures at each time step. This equation collapses to the heat equation (assuming k = constant) in cylindrical coordinates for the r and z dimensions as shown in Equation 9.

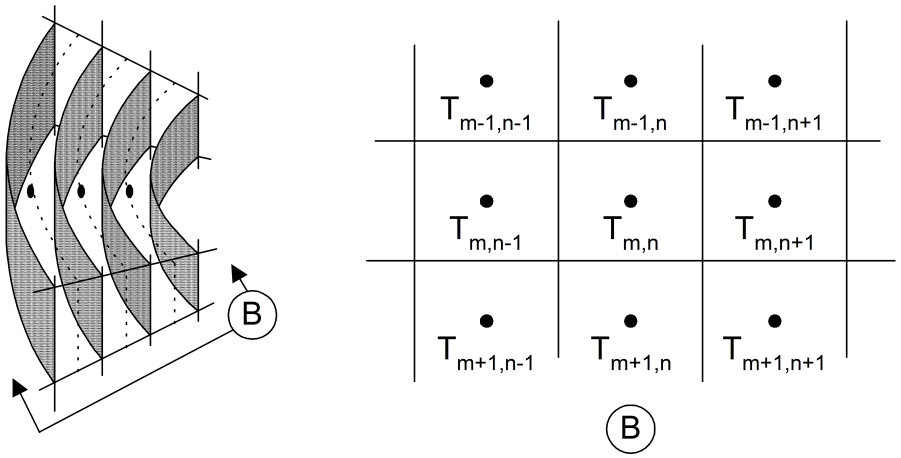

Figure 11: The node configuration for radial and vertical conduction in the encapsulation and PCM.

$$V_{(m,n)}\rho_{(m,n)}C_{(m,n)}\frac{T^{t}_{(m,n)}-T^{t-\Delta t}_{(m,n)}}{\Delta t}=$$
$$\left[k_{(m,n)}A_{o(m,n)}\frac{T_{(m,n-1)}-T_{(m,n)}}{\Delta r}-k_{(m,n)}A_{i(m,n)}\frac{T_{(m,n)}-T_{(m,n+1)}}{\Delta r}\right]+ \tag{8}$$
$$\left[k_{(m,n)}A_{h(m,n)}\frac{T_{(m-1,n)}-T_{(m,n)}}{\Delta z}-k_{(m,n)}A_{h(m,n)}\frac{T_{(m,n)}-T_{(m+1,n)}}{\Delta z}\right]$$

$$\frac{\partial T}{\partial t}=\frac{\alpha}{r}\frac{\partial}{\partial r}\left(r\frac{\partial T}{\partial r}\right)+\alpha\frac{\partial^2 T}{\partial z^2} \tag{9}$$

While the heat equation still applies to conduction during phase transition, a latent enthalpy tracking method must be used to determine the temperature of the phasing node at each time step based on its phase fraction. This is required because tests performed during this research have shown that the 99% tetradecane PCM utilized in the experiments melts over a temperature range estimated to be between 4.5°C and 6.5°C, rather than at a single temperature. A curve representing effective heat capacity with respect to temperature during phase change is estimated using a square function of temperature based on previous DSC (differential scanning calorimeter) studies of paraffin PCMs undergoing a slow rate of temperature change [He et. al 2004] and knowledge of DSC test output curves [O'Niell 1966], with the requirement that the integral of the curve equal the latent phase energy of the PCM element. This curve is used to estimate and set the temperature of a phasing PCM node to a new fixed value at each time step based on its phase fraction. The remaining unknown temperatures are then simultaneously resolved, and the resolved node temperatures used to calculate an update to the enthalpy of the phasing nodes. This process is repeated at each time step while the node is undergoing phase change.

In this manner the temperature of a phasing element can be treated as a constant value at each time interval – as it would be for an ideal phase transition of a pure substance – while still permitting the use of PCMs that change phase over a small but finite temperature range. Note that even though the temperature of a PCM node undergoing phase change is a non-linear function of its latent enthalpy, their temperature is fixed to a (new) constant value at each time step. It is only the remaining temperature node values that remain to be solved. Since the equations for the remaining nodes are linear in nature, typical linear programming methods are employed. In this case a sparse diagonal matrix of temperature variable coefficients and a corresponding answer vector are solved for the temperature matrix at each time step using widely available mathematics programming software (MatLab). The latent enthalpy energy matrix for PCM nodes undergoing phase transition is then updated using these temperatures and a variation of Equation 8. For additional information see section C2.1 in Appendix C.

4.3.2 Calibration/Validation of the numerical model

The model is calibrated/validated against the experimental data. Both sensible (at temperatures above and below the phase temperature range of the PCM) and latent experimental results are compared to model output. The calibration process is used for the tuning of only the PCM solid/liquid state thermal conductivities, and for verification of the PCM phase change specific heat vs. temperature curve (as described in section 4.3.1 and Appendix C section C2.1). All other properties of the materials used in the thermal store are set based on values found in the literature as described in Tables 6 through 8.

Adjustments are made to the base model for validation to account for real-world conditions not present in the base numerical mode, as noted in the following paragraphs

and described in Appendix A section A2.4 and Appendix C section C2.2. Note that all adjustments used for validation against existing experimental data are removed before use as a parametric analysis tool.

- The experimental apparatus has an additional volume of HTF at the top and bottom of the tank. A separate calculation is used to mimic the time shift and thermal diffusion effects that occur as a result of these pools.
- The numerical model assumes a perfect insulation system (no losses through the shell). The actual experiment has limited insulation resulting in some losses through the shell. To account for these losses, a separate loss calculation is added to the model based on a steady-state loss rate measured for each experimental run.
- The PVC shell of the experiment accounts for approximately 5% of the total thermal capacity of the thermal store, while the model assumes no mass in the shell. To compensate for this the sensible thermal capacity of the shell is proportionally added to the sensible capacity of the PCM.
- A finite amount of time is required set up the experimental apparatus for each run, resulting in a small thermal gain through the shell of the tank. This results in partial tank stratification, leading to a small temperature differential between the top and bottom of the tank. An adjustment is made in the initial temperatures of the model to duplicate the 0.2°C gradient in the tank that develops before each experimental run.

4.3.3 Design conditions

The conditions under which the model is evaluated (allowable output temperature range, acceptable energy recovery fraction, minimum encapsulation unit height, and

PCM product used) are based on typical parameters found in chilled water cooling systems, or conditions verified during experiments. This is done to ensure that this thermal store design can be integrated into existing chilled water systems or designs, and/or that the conditions are confirmed by experimental data. The basis for these design conditions is discussed in this subsection.

The chilled water supply temperature range is usually set between 4°C and 13°C [Croome-Gale and Roberts 1975], typically about 6.5 to 7°C. In addition, to maintain nominal indoor conditions (24°C, 50% RH) the return temperature is usually limited to approximately 13°C, resulting in a supply/return ΔT of 6°C [ASHRAE 2004].

Of the paraffins investigated, tetradecane exhibited freezing/melting temperatures most closely matching that of typical chilled water systems. Tetradecane has a freezing point of approximately 5.6°C [Humphries and Griggs 1977], but tests have shown that the 99% purity form used here melts over a range of between 4.5 and 6.5°C [Bourne and Novoselac 2015]. This falls within the acceptable range for use in chilled water systems as noted above, resulting in the selection of tetradecane for use in this thermal store system.

To optimize recovery of latent thermal energy in the store, the upper limit on output temperature must equal or exceed the melting temperature range of the PCM. For this reason the higher temperature value for acceptable HTF output is set to the upper melting temperature of the PCM, or 6.5°C. This results in a time-averaged output temperature value of between 5.0 and 5.5°C (due to the sensible energy discharged early in the cycle as the temperature of the thermal store is raised to the melting point of the PCM). Allowing for an expected ΔT of 6°C as noted above provides for a return temperature of between 11 and 11.5°C. A value of 11°C is selected for experimentation and modeling purposes.

A figure of merit (FOM) value is used to describe the available capacity (recoverable energy) of a chilled water thermal storage system. When operated within its design guidelines, a well-designed chilled water thermal storage system can have a FOM on the order of 90% [ASHRAE 2007], but it has been found that typical thermal storage systems operate at efficiencies of between 50 and 80% [Zhang et. al. 2011]. Since systems are not always operated within their design guidelines, and system operators should have knowledge of how the system will perform outside of the design parameters, the parametric analysis is performed over a range of thermal store recovery fractions from 70% to 100% of the total thermal store capacity.

The 1m minimum height of the thermal store modeled for the parametric analysis is based on the experimental apparatus, which utilizes encapsulation tubes filled with PCM to a level of just under 1 meter in height. While the maximum height is set at 3m for the parametric analysis, the performance of taller tubes (or any tube size greater than 1m) can be predicted using Equation 10 in section 5.3.3 [Analysis of general thermal store characteristics].

4.4 EXPERIMENTAL METHODS

The experimental apparatus and procedures are described in the following subsections.

4.4.1 Experimental apparatus

The tank is constructed of standard 4 inch (0.102m) schedule 40 PVC pipe. The top and bottom of the tank utilize a combination of PVC and brass fittings to allow for water flow and instrumentation. A PVC pipe flange is installed near the top of the tank to facilitate disassembly that allows for the installation and exchange of the PCM tubes. The tank is contained within a 12" (0.308m) cardboard tube and insulated using a

combination of polyurethane spray foam, foam insulation board, and polyurethane foam batting to a depth of approximately 4 inches (0.102m).

Two sets of PCM encapsulation tubes are utilized over the course of this study: one set of standard ½" CPVC tubes, and one set of standard ½" type M copper tubes. The CPVC tubes are used for the initial experiments during design and model development. All subsequent experiments utilized the copper tubes due to their compliance with resistance ratio requirements. The CPVC tubes are cut to a finished length of 1.14m and filled with 0.116 liter of tetradecane to a height of 0.973m. The copper encapsulation tubes are cut to a total finished length of 1.14m and filled with 0.150 liters of tetradecane PCM to a height of 0.908m. The remaining space in the tubes is to provide expansion room to minimize pressure changes during phase cycling. Experiments are conducted with a moderate-density (uniformly spaced tubes) configuration of 19 CPVC tubes, and high-density (hexagonal packed) configurations of 31 CPVC or 31 copper tubes. The CPVC and copper tubes have the same external dimensions.

Temperature measurements are made using Omega 44033 epoxy-encapsulated thermistors with an interchangeability of 0.1ºC. These thermistors are positioned at both the input and output of the thermal storage tank, and are placed directly in the restricted flow path of the entry/exit ports to minimize error and external influences. The thermistors are connected to GW Instruments iNet-100 A/D data acquisition hardware, which provides excitation current for each thermistor through a precision 4.7kohm resistor with an accuracy of +/- 0.025%-20ppm/ºC. The iNet-100 in this configuration has a temperature measurement accuracy of +/-0.1ºC. Temperature data is recorded at 10 second intervals during each test run. HTF flow rates are measured using Omega FLR1009 Pelton-type turbine wheel flow meters with a range of 50 to 500 ml/min and an

output of 0 to 5 volts. These devices have a repeatability of 0.2% of full scale. The flow meter in use for each experiment run is manually calibrated using direct measurement of the output flow from the tank at the beginning and end of each test run.

A portable chiller unit supplies chilled water to the thermal storage tank through a high-flow-rate supply loop adjacent to the thermal store to prevent changes in the temperature of the supply due to residence time in the loop. Short, small diameter polyethylene tubing connects the thermal store inputs/outputs to the supply loop. The output from the thermal store is switched between the top and bottom of the tank, depending on mode (charge or discharge), with the output going to an intermediate tank to permit flow rate verification before returning to the chiller. All tubes are insulated with foam rubber insulation to minimize losses. A schematic of the tank and its connections is shown in Figure 12.

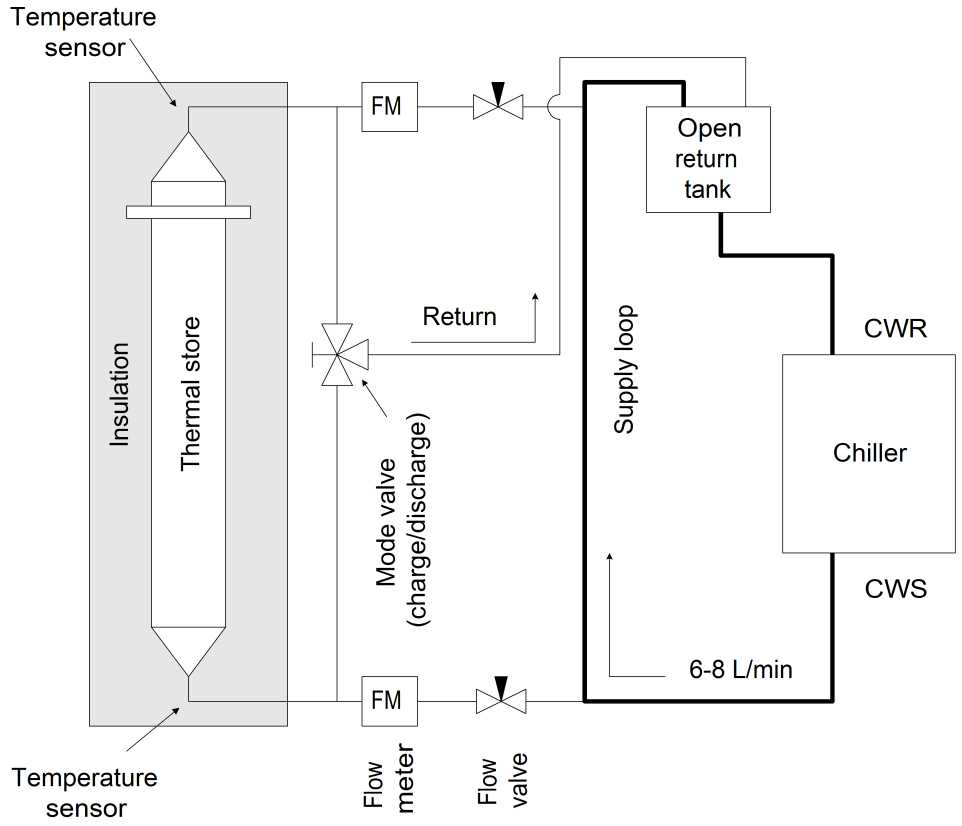

Figure 12: Experiment schematic. The high flow supply loop provides chilled water at a stable temperature to the tank inlets. The loop allows the low-flow inlet tubes to be as short as possible to limit heat gain from the environment. The open return tank allows for flow rate confirmation during each test.

4.4.2 Experimental procedure

During the charge cycle, HTF at approximately 2°C is pumped into the bottom of the tank to freeze the PCM and warms as it rises in the tank and solidifies the PCM. During the discharge cycle, HTF at approximately 11°C is pumped into the top of the tank and is cooled as it flows down the tank and melts the PCM. A 2°C charge temperature is selected as low enough to fully freeze the PCM while still being within the capability of typical chilled water systems. The 11°C temperature for the discharge cycle is selected as representative of a typical cooling coil chilled water return temperature.

By changing the direction of HTF flow depending on the cycle, a negative temperature gradient (measured from top to bottom) in the tank is preserved. This minimizes buoyancy-driven effects so as to prevent short-circuit flows through the tank. It also serves to encourage stratification within the tank.

4.5 QUALITY CONTROL

For experimental components, care is taken to minimize errors in the development of the apparatus and the acquisition of data. The uncertainty resulting from the test apparatus itself is heavily investigated during its design and development, as noted in this section. These efforts focused on ensuring the robustness of the system and the repeatability of experiments. Potential errors due to data acquisition and processing are also fully investigated, and a summary of the findings is presented here for review.

Errors in numerically modeled data are very difficult to quantify. In an effort to minimize errors associated with the numerical model, it is validated against existing data [see Methods: Numerical model validation]. Also, published values of high confidence found in the literature are used whenever possible for property values that can significantly affect errors. In addition, a grid sensitivity analysis (as described in this section) is performed to minimize errors while maximizing the computational performance of the model.

4.5.1 Experimental apparatus development and use

Several iterations of the experimental apparatus are constructed during this study in an effort to perfect the design and ensure accurate data collection. Over 200 separate experimental runs were made during the development, characterization, and use of the apparatus. Three separate tank systems, two different types of encapsulation tubes, three different PCMs, and three different tube packing configurations are investigated during

the development of this apparatus. The result of the development process was the final tank design and experimental procedure for testing the low-density (19-tube CPVC encapsulation) and high-density (31-tube using CPVC and copper encapsulation) tank configurations. Refinements to the apparatus and test procedure made in the course of development include:

- Re-configuration of the tank to minimize the water pools at the top and bottom of the tank. This modification serves to reduce the delay between HTF input flow and subsequent changes in the output flow temperature.
- The installation of a high-flow HTF delivery loop, with small-diameter tubes connecting the loop to the tank. This system reduces temperature changes in the HTF as a result of residence time in the delivery system. This is important due to the extremely low flow rates and a potentially long residence time in the supply loop.
- Incorporation of the HTF temperature sensors inside of the tank, placed directly in the restricted flow path at the point where the HTF actually enters or leaves the thermal storage tank. This system eliminates errors due to losses incurred between the point of measurement and the tank, and increases the accuracy of HTF temperature measurements.
- The use of polyurethane spray foam to fully insulate the tank surface, minimizing losses to the environment and sealing the system and tank from direct external convective heat flows. Remaining tank losses are estimated for each run based on a steady-state loss rate measurement made at the end of each test.
- A 99% tetradecane PCM was selected for use in the experiments; testing of a 95% technical grade showed that it did not exhibit the published

thermal properties of tetradecane. Most notably, the technical grade material had a lower freezing temperature (approximately 4°C vs. 5.6°C) that was unacceptable.

- Thermistors used to gather temperature data are calibrated simultaneously as a set prior to installation to minimize errors in calculations involving differences between their values.
- The installation of an open intermediate return tank in the flow loop for the thermal storage tank enables manual calibration of the flow meters before and after every test run. This allows for a very high degree of confidence in the flow rate measurements, which are critical in energy calculations.
- The energy removed by the HTF as a result of fully discharging the thermal store for each run is compared to the expected enthalpy change in the thermal store based the sensible/latent heat capacities of all its components, and are confirmed to be in good agreement for each test.

4.5.2 Experimental error analysis of measured values

The measured values used in the experimental calculations and their uncertainties are shown in Table 4, along with the net expected error of energy calculations. The relative uncertainty for values that operate over a range is determined using the median value of that range. Uncertainty parameters for measured data are taken from manufacturer specifications. Note that while the relative uncertainty of the loss rate is high (LR in Table 4), the loss rate portion of the total energy calculation is small and contributed very little to the uncertainty of the total energy calculations.

Description	Symbol	Value or range	Absolute error	Relative error*	Units	Source
Tin - Tout	ΔT	0 - 9 °C	0.14	3.1%	C	Calculated
Flow rate	F_{lpm}	0.100 - 0.300	0.003	1.5%	L/min	Measured
Density, HTF	ϱ_f	1036	3	0.3%	kg/m2	ASHRAE
C_p, HTF	C_f	3735	50	1.3%	J/(kg K)	
Tamb - Tavg	ΔT_{amb}	12 - 21°C	1	6.1%	C	Calculated
Loss rate	LR	0.2 - 0.3	0.05	20.0%	W/K	Measured
Overall (energy calculation)				3.7%		

* The relative error for parameter values given as a range is calculated at the median value.

Table 4: Experimental uncertainty values

4.5.3 Model grid sensitivity

A grid sensitivity analysis is performed during model validation to determine the necessary grid node density. The model is run for a typical configuration using different node grids, over a range of total nodes varying by more than an order of magnitude. The greatest variance between values of interest (time to T_{out} = > 6.5°C, percent of total energy recovered at T_{out} < 6.5°C, and kWh recovered at T_{out} < 6.5°C) was less than 4% over the range of node counts tested. The lowest grid node count that produced outputs differing by less than 2% from the highest node count is selected for the parametric analysis to optimize the accuracy of the results while minimizing computational resources and execution times.

Chapter 5: Results

5.1 RESULTS OF DESIGN ANALYSIS

An initial numerical model for the design is developed [see Methods: Numerical methods in section 4.3] and an experimental apparatus constructed [see Methods: Experimental methods in section 4.4] to validate the design and determine critical parameters. Tests are conducted using tetradecane encapsulated in both evenly spaced and hexagonal packed CPVC tubes, as well as hexagonal packed copper encapsulation tubes. This design analysis results in the development of the resistance ratio parameter, [see Methods: Analytical methods in section 4.2] which permits the use of hexagonal-packed tubes.

5.1.1 Low-density packing of CPVC tubes

The low density configuration consists of 19 tubes evenly spaced in the tank using tube-mounted spacer rings. This produces the pseudo annular ring packing as represented in Figure 13.

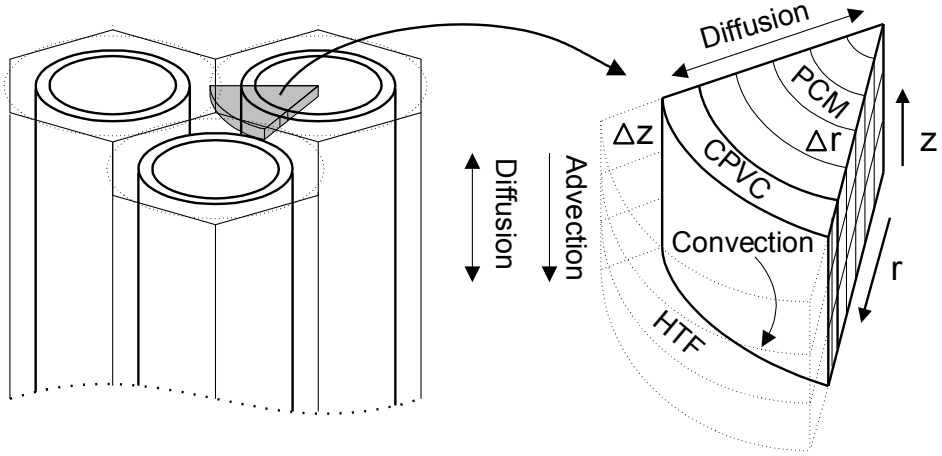

Figure 13: Elements, dimensions, and heat transfer considerations of the initial numerical model utilizing a loosely packed 19-tube configuration. Note that for the early numerical model of this design an equivalent circular cylindrical replaces the hexagonal annular cylinder.

Initial experiments found that the low density CPVC configuration, where the pseudo annular ring packing allows the HTF to flow evenly around the encapsulation tubes, has acceptable thermal performance but at a lower thermal density than the hexagonal packed configuration. This configuration results in a tube packing density of approximately 60% that of the high density configuration. Between 70% and 88% of the total thermal energy is recovered in the low density configuration, with typical results for the median flow rate tested given in Figure 14. In this example, 83% of the thermal energy was recovered at an output temperature of less than 6.5°C. Figure 14 shows both the actual experimental and predicted model output, which are in acceptable agreement for this configuration.

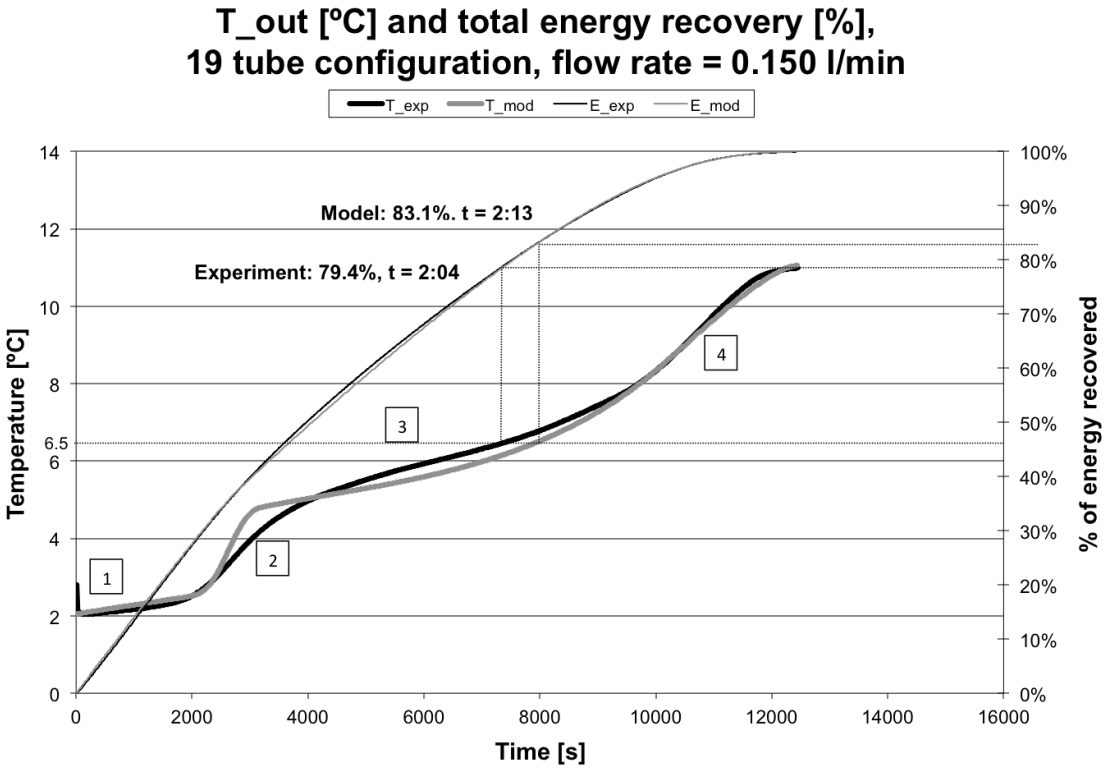

Figure 14: Output temperature and energy recovery with respect to time for both the experiment and numerical model at a flow rate of 150ml/min for the low density packing of 19 CPVC tubes. The numbered sections represent: 1) flushing of the HTF, and 2) sensible solid, 3) latent and 4) sensible liquid thermal changes.

The numbered markers in Figure 14 represent specific aspects of the thermal store discharge process, as listed below:

1. This initial output of the thermal store is a near-constant temperature, and represents the cold fluid that surrounds the encapsulation tubes as it is flushed out of the system by the incoming HTF.
2. The sharp rise in output temperature represents the sensible change in energy of the thermal store as it increases to the initial melting temperature of the PCM,

3. The lowered slope of the output temperature after the initial sensible warm-up period represents the phase change of the PCM as the tank discharges.
4. The rise in slope near the end of the discharge period represents the resumption of sensible temperature change as the PCM latent energy is exhausted.

5.1.2 High-density packing of CPVC tubes

Unlike the low-density packing configuration, the high density hexagonal packed system of CPVC tubes performs poorly. This configuration results in recovery of only 43% of total thermal energy in the tank at an output temperature of less than 6.5°C, even at the lowest tested flow rate and in spite of having a much higher PCM density over the 19-tube configuration. Example results of the CPVC 31-tube test configuration are shown in Figure 15. In this case the initial numerical model – which assumes that the thermal energy is well distributed around the encapsulation tube surface – does not accurately predict the performance of the thermal store, as it does for the 19-tube configuration.

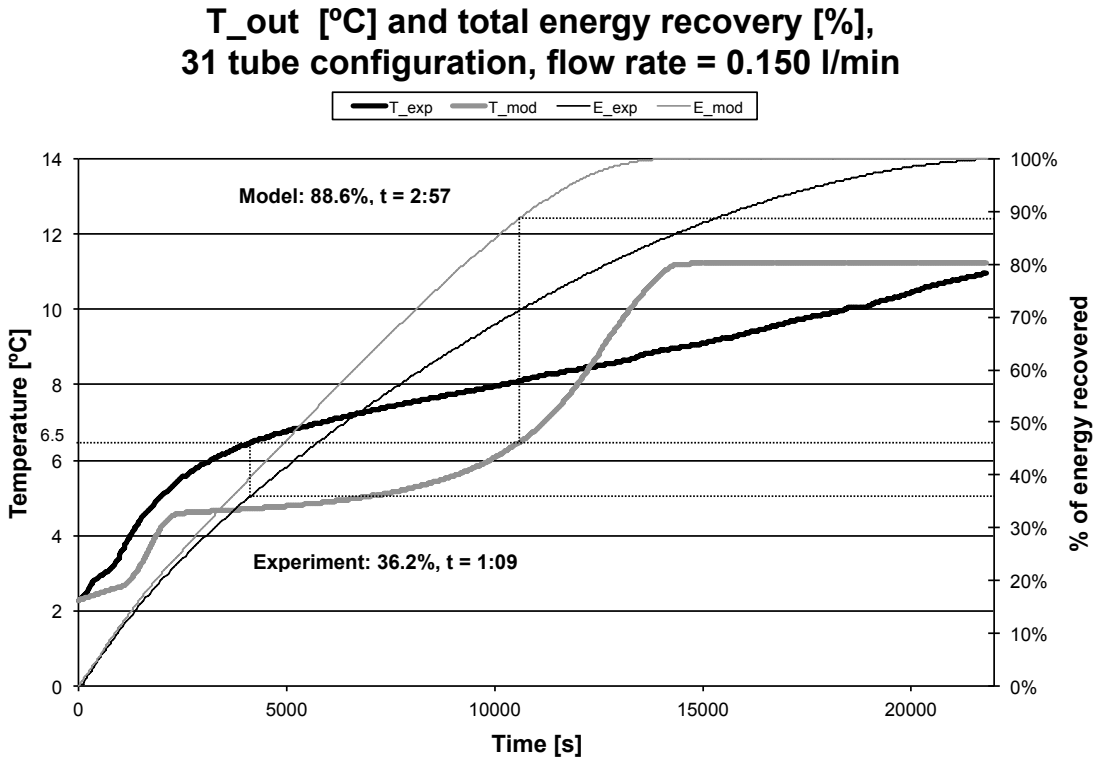

Figure 15: This plot shows the experiment and numerical model prediction for a hexagonal packed configuration of 31 CPVC encapsulation tubes. The model, which assumes well-distributed thermal conditions, predicts a much higher recovery rate than found in actual testing.

These results suggest that performance is dependent on the heat transfer being evenly distributed around the encapsulated PCM, leading to the development of the resistance ratio parameter [see Methods: Analytical methods]. This parameter is used to define the necessary thermal properties and dimensions of the encapsulation tubes such that the resistance to heat flow around the encapsulation tube is at least an order of magnitude less than the resistance to heat flow between the encapsulation tube and either the HTF or the PCM. In this way the tube can redistribute the thermal energy around the encapsulated PCM, restoring the well-distributed conditions of the low-density spaced CPVC tubes while maintaining the higher density of the hexagonal packed configuration.

Additional information on the resistance ratio parameter can be found in the Methods section of this document.

5.1.3 High-density packing of copper tubes

Tests are performed on the thermal store using hexagonal packed copper encapsulation tubes that exceed the requirement of the resistance ratio parameter developed in the Methods section. Multiple flow rates representative of expected loads on a per-unit basis are tested. Test results for this configuration are summarized in Figure 16, which gives the output temperature of the experimental thermal store and the net % of recovered energy with respect to time for flow rates between 100 and 300ml/min in 50ml/min increments. The results show that for a usable output temperature of equal to or less than 6.5°C (a minimum delta T of 4.5°C), approximately 73% to 93% of total recoverable thermal storage capacity (sensible and latent) can be recovered depending on flow rate.

These flow rates correspond to operating times of between 5.4 and 1.8 hours for 100ml/min and 300ml/min respectively, commensurate with a two to six hour peak power demand period. This works well in Austin, TX, where the local electric utility offers time of day pricing based on a 6-hour peak power demand period (3-hour if using thermal storage) [City of Austin 2016]. However, this thermal store design allows for varying the size and performance level of the thermal store to meet other regional market needs. The peak power demand period given here for the experimental apparatus is for reference use only.

Table 5 summarizes the flow rate, energy recovery, and run time results for copper and CPVC tube configurations. Figure 17 provides a graphic comparison of select output temperature results with respect to time.

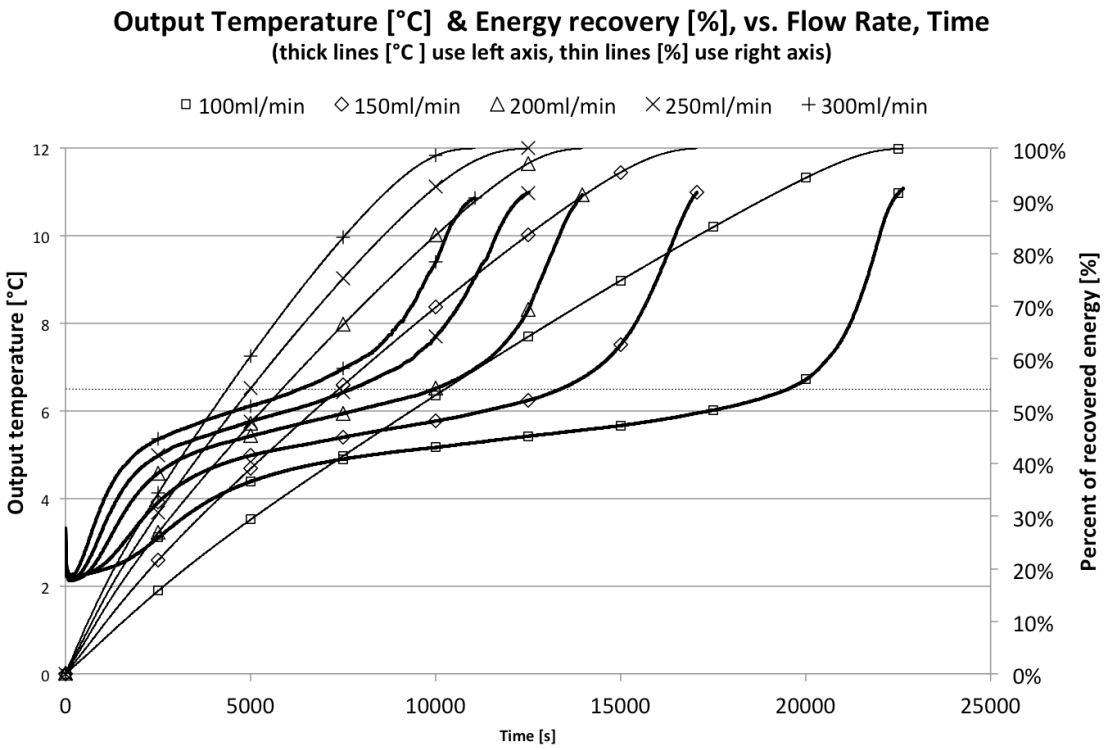

Figure 16: Energy recovery vs. output temperature. A reference output temperature of T <= 6.5C is provided by the dashed line, but the data can be used for any output temperature. To use this graph, find where a temperature plot for a specific flow rate crosses the reference temperature, them move up to the corresponding energy line and read the recovery percent on the right axis.

Encapsulation material	# of tubes	Flow rate [ml/min]	Net energy recovered (T<6.5°)	Run time [hours] (T<6.5°C)
Copper	31	100	93%	5.4
Copper	31	150	88%	3.7
Copper	31	200	83%	2.8
Copper	31	250	77%	2.1
Copper	31	300	73%	1.8
CPVC	31	100	43%	2.0
CPVC	19	100	88%	3.3

Table 5: Flow rate, energy recovery, and run time for copper and CPVC tubes

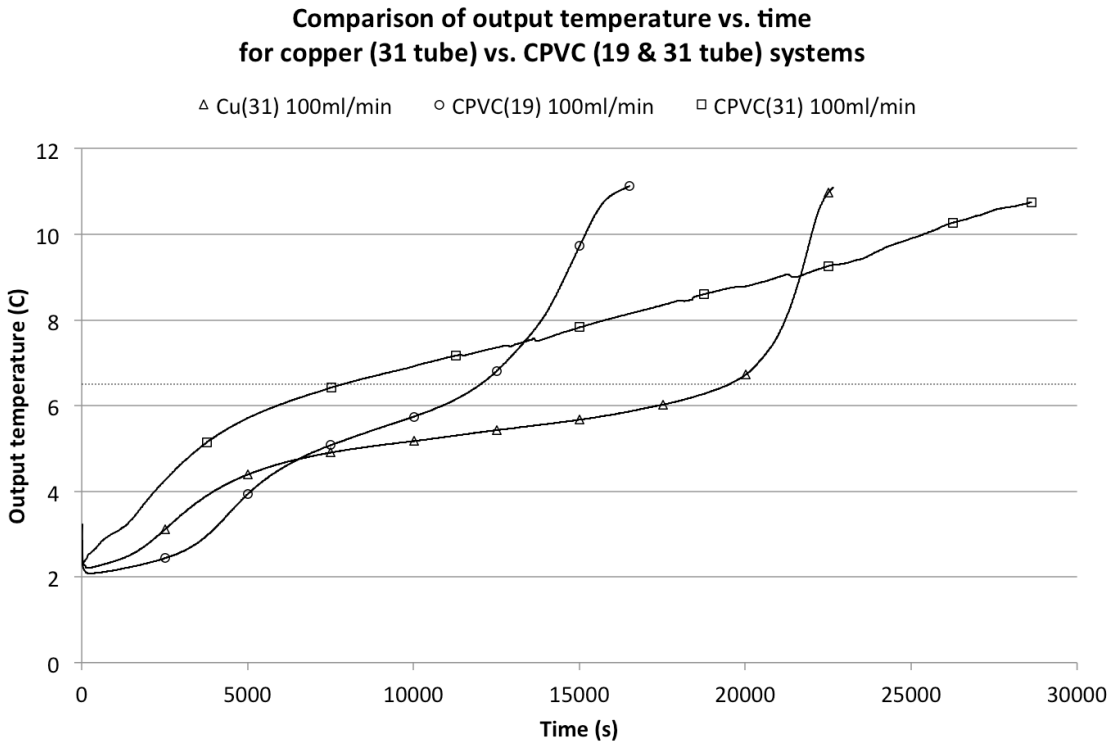

Figure 17: A comparison of performance between CPVC and copper encapsulation tubes. Note that both the 19 tube CPVC and 31 tube copper encapsulation tubes produced acceptable results with 88% and 93% of energy recovered, although the 31 tube copper system offered a much higher thermal capacity.

An analysis of all flow rates tested shows that energy recovery (as a percent of thermal store total capacity) and run times increase as flow rates decrease. These results are shown and characterized in Figures 18 and 19 for the flow rate and output temperature ranges given. A multivariable regression method [Stoeker 1989] is used to develop the empirical equations shown in Figures 18 and 19. These equations are functions of maximum output temperature (6.5°C ≤ T ≤ 7.5°C) and flow rate (0.1 L/min ≤ Q ≤ 0.3 L/min), and provide either the recovered energy percentage or run time as indicated.

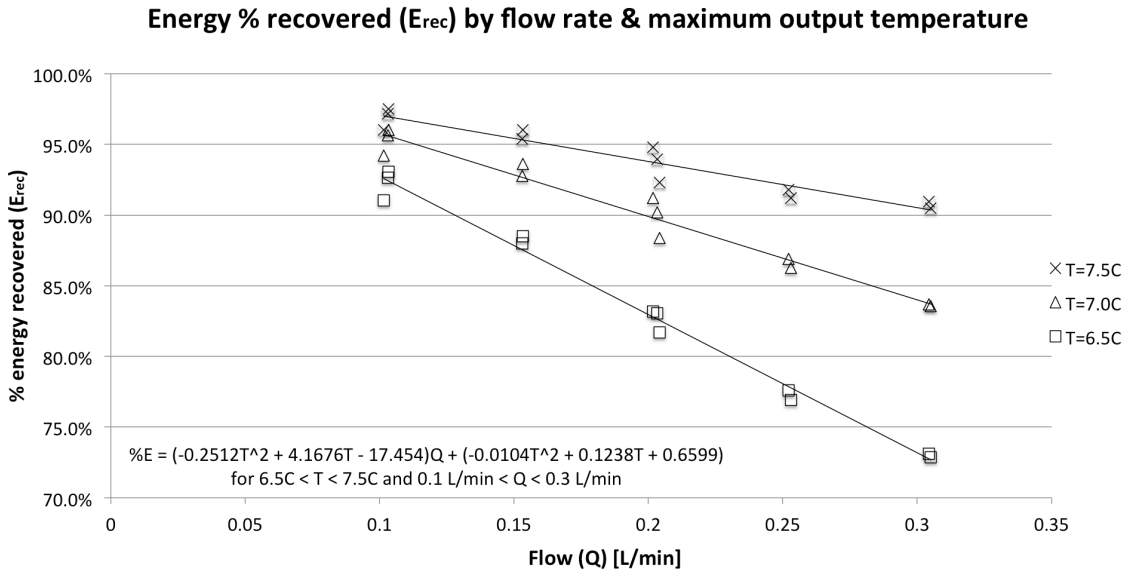

Figure 18: Energy recovery rate as a function of flow rate and maximum allowed output temperature. The equation shown is accurate to +/- 2% when compared to experimental results.

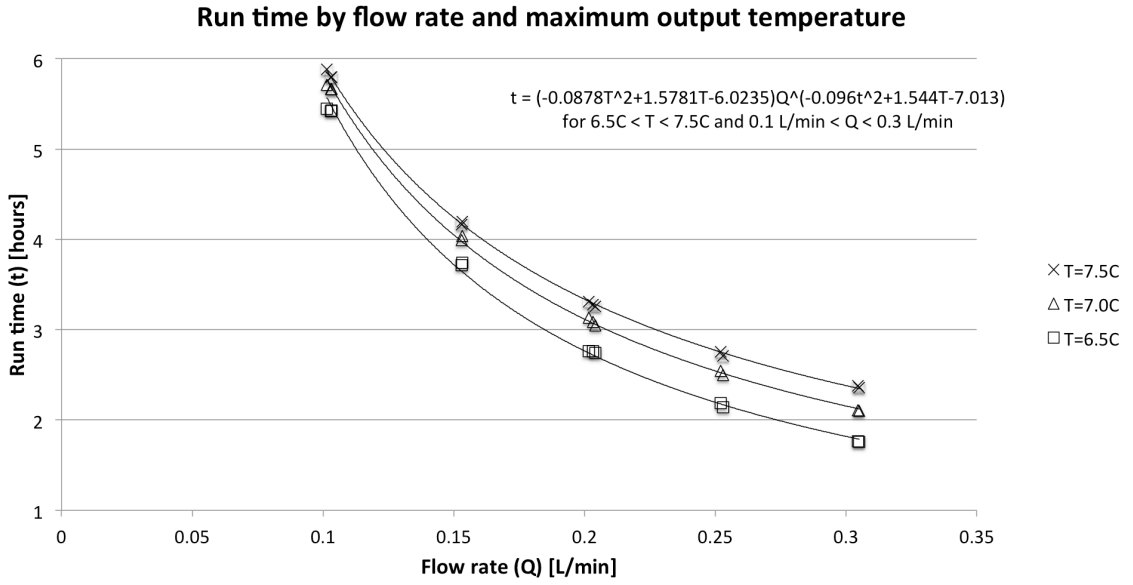

Figure 19: Run time as a function of flow rate and maximum allowed output temperature for the experimental thermal storage tank. The equation shown, based on a regression of the power equations, is accurate to +/- 3% when compared to experimental results.

5.1.4 Summary of design analysis results

The analysis results for hexagonal packed copper tubes confirm that this design is feasible for use in HVAC applications to time-shift peak cooling loads, given design compliance with the resistance ratio parameter. These results also give insight into how the HTF flow rate and acceptable output temperature range affect performance of this thermal store design.

5.2 RESULTS OF NUMERICAL MODEL CALIBRATION AND VALIDATION

The numerical model is updated to include the requirement for compliance with the resistance ratio parameter [see Methods: Analytical methods in section 4.2]. The numerical model is then calibrated/validated using experimental data for the high-density copper tube configuration of the thermal store from the initial design analysis [see Methods: Numerical Methods: Calibration/validation of numerical model in section 4.3.2]. For calibration/validation purposes, the model is modified to account for specific effects found only in the actual experiments and not in the base numerical model; these modifications are noted in sections 4.3.2 and Appendix C section C2.2. All modifications are removed for later parametric analysis studies. Validation allows for the use of the model as a parametric analysis tool.

5.2.1 High-temperature (liquid phase) calibration of model

A calibration/validation run is made at temperatures above the freezing point of the PCM. This allows calibration of the PCM liquid state conductivity, and validation of the model for sensible energy conditions. For this comparison, the thermal store is stabilized at a temperature slightly above 7°C (above the melting temperature of the PCM), and then 17°C HTF is input to the store at a normalized rate of approximately 30L/(min m^2 of PCM) until the temperature in the tank stabilizes. The model and

experimental data are then compared, as shown in Figure 20. The best fit resulted when using a conductivity value for the PCM in its liquid state of 0.15 W/(m °K), and results in the model data being almost indistinguishable from the experimental data. This value also agrees with published data [Shamsunder and Sparrow 1975].

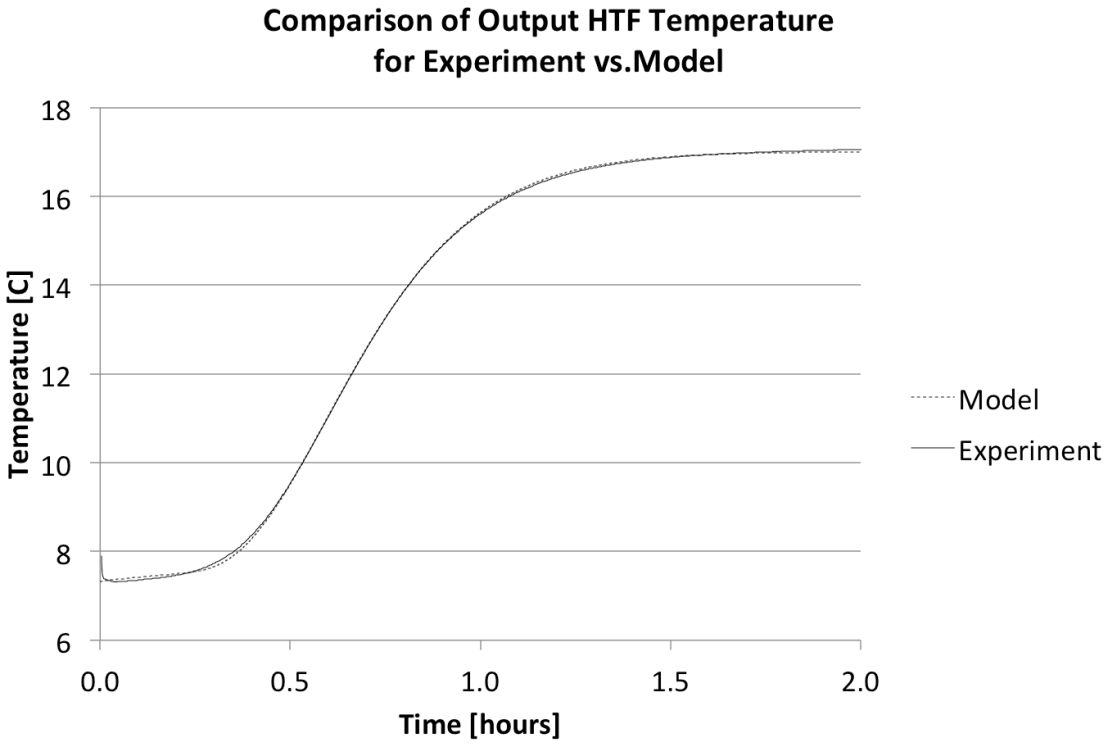

Figure 20: A comparison of the model to experimental data. The experimental thermal store is preconditioned to 7°C, then 17°C water is input until the thermal store stabilizes at the new temperature. This temperature range is chosen to ensure sensible thermal changes only are considered. The experiment and model show good agreement.

5.2.2 Low-temperature (liquid phase) calibration of model

A second calibration/validation run is made at temperatures below the minimum freezing point of the tetradecane PCM. This allows calibration of the solid state PCM conductivity, and validation of the model under a second sensible energy condition. In this case the thermal store is conditioned to a temperature of approximately -4°C, then HTF at a temperature of 3.5°C is input to the store while the output temperature is monitored. The model and experiment data are compared in Figure 21.

In this case, no single value of conductivity for the solid PCM allowed for a match over all of the data. However, visual inspection of a clear PVC tube containing frozen tetradecane noted a separation of the PCM from around the partial inside perimeter of the tube. The PCM has a higher density when solid, which indicates that the PCM shrinks when frozen. The observation and density data suggest that a high-resistance interface may be formed at the inside surface of the encapsulation tube due to the PCM shrinking and pulling away from the inside surface of the tube during the freeze cycle.

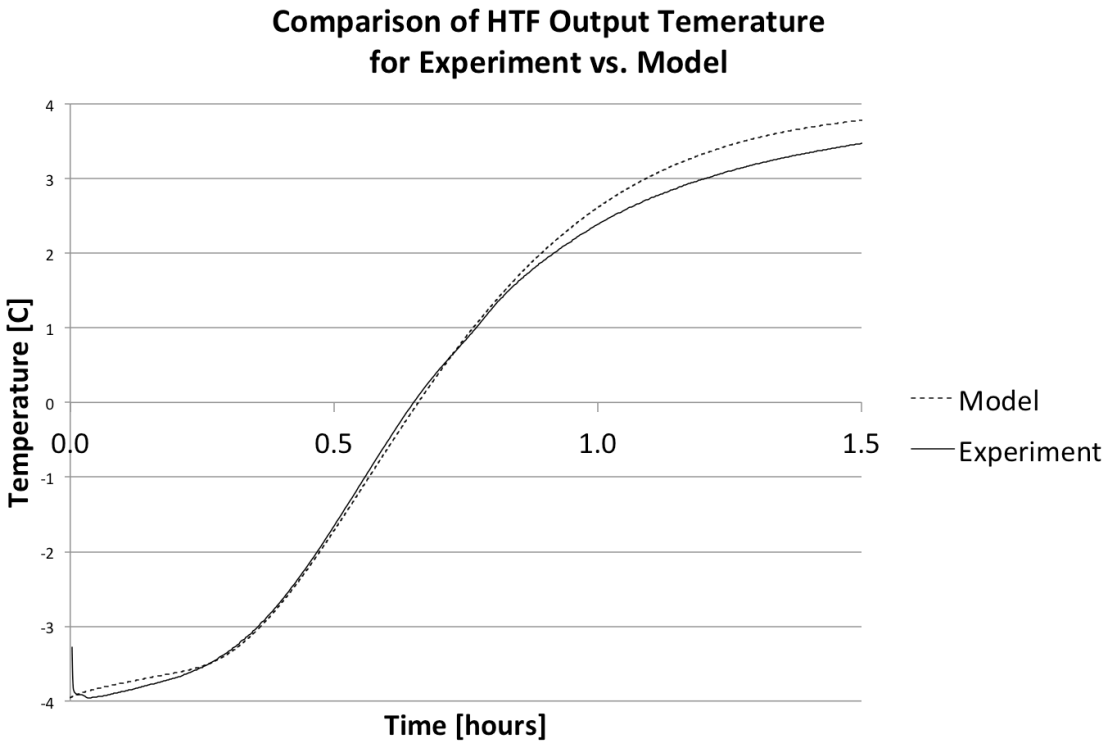

Figure 21: A comparison of the output HTF temperature between the model and the experiment. Using a two-stage conductivity value provides good agreement up to ~2°C. The remaining differences are attributed to early onset phase transition.

To compensate for this condition, the model utilizes a two-step conductivity value for the solid state PCM. The outermost PCM node only (adjacent to the tube surface) is given a conductivity value of 0.06 W/(m °K) to represent the increased resistance associated with the interface discontinuity formed by the gap between the PCM and tube. All other solid PCM nodes are assigned a conductivity value for the solid PCM phase equal to that of the liquid phase, or 0.15 W/(m °K). The interface discontinuity only exists while the node is fully solid. As soon as the melting process starts in a node that is adjacent to the tube surface, it is assumed that the melted PCM will fill in the discontinuity and at that point the PCM node is reassigned the standard solid phase

conductivity value of 0.15 W/(m °K). These values provide a reasonable match to the experimental data up to the point where the output temperature climbs above 1.5°C.

After 0.8 hours (output temperature above 1.5°C) the model and experimental data diverge significantly. However, a sensible energy analysis of the model and experiment do not account for the additional energy absorption of the experiment. A possible explanation for this discrepancy is that an early-onset of the phase transition is absorbing part of the energy using latent capacity. Since the additional energy cannot be accounted for in a sensible energy balance, it is assumed that an early phase transition is the cause of the divergence.

5.2.3 Latent (phase change) validation of model

A comparison between the model and the experiment over a complete cycle, including a phase transition, is also performed using the calibrated model. The comparison is made using the median experimental flow rate of 200ml/min (equivalent to 40L/(min m^2 of PCM)) and includes both output temperature as well as energy recovery as a percent of total energy in the thermal store. The thermal store is preconditioned to a temperature of 2°C, with the incoming HTF at a temperature of approximately 11°C. The results of the comparison are shown in Figure 22. These results shows some variance due to having estimated the thermal properties of the PCM during phase transition used by the model; however, the energy recovery as a percent of total thermal energy and the HTF output temperature with respect to time are in good agreement. When the particular value of interest for this study – the percent of total energy recovered at $T_{out} < 6.5$°C – is compared between the numerical model and the experimental data as provided in Figure 16, it shows an average error of approximately +/-4%. This value is similar to the

expected error of the experimental measurements, given as 3.7% [see Methods: Quality Control: Experimental error analysis in section 4.3.2].

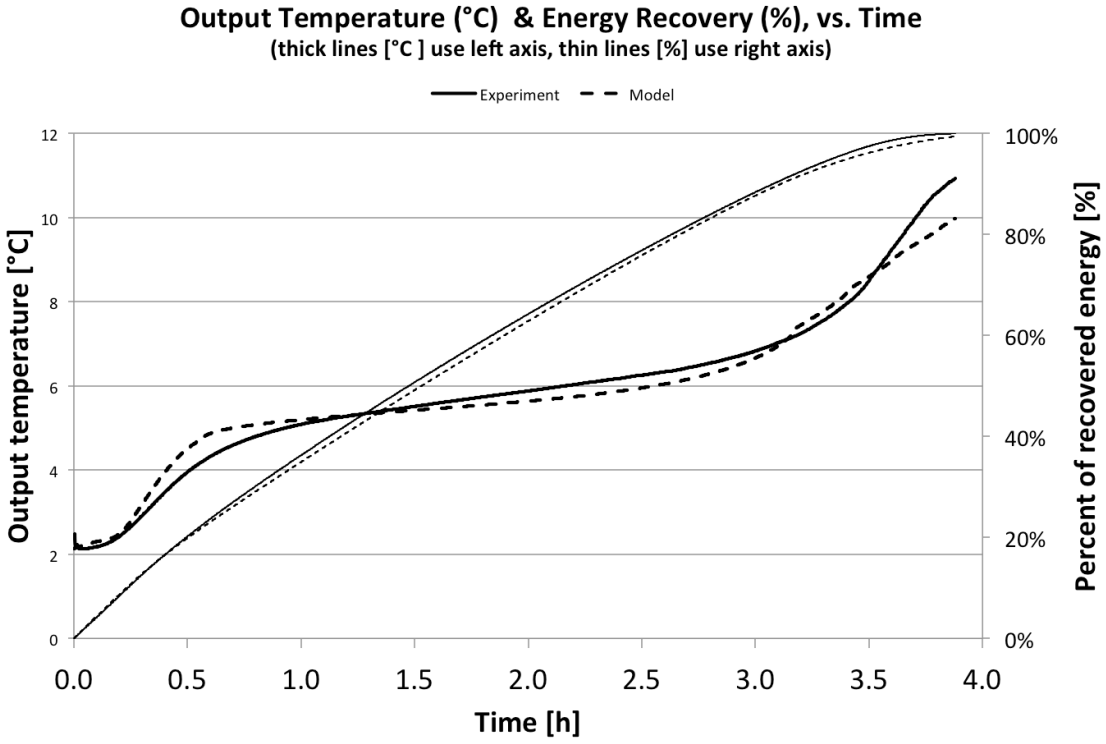

Figure 22: A comparison of experimental to model data shows good agreement. This plot shows both recovery rate as a percent of total thermal capacity and output temperature of the HTF. The discrepancies are likely due to the estimated thermal properties of the PCM as it undergoes a phase transition.

5.2.4 Summary of model calibration and validation results

The numerical model calibration and validation results show that the revised numerical model provides energy recovery values as a percent of total thermal store capacity that are very close to those calculated for the experimental data, with an error rate similar to that of the experimental measurements. This indicates that the model is

sufficiently accurate for the intended purpose as a parametric analysis tool for comparing these energy recovery values.

5.3 RESULTS OF PARAMETRIC ANALYSIS USING THE VALIDATED MODEL

A parametric analysis is run for a series of tube sizes and flow rates using the validated model to determine their affect on the percent of energy recovered at T_{out} < 6.5°C. The data from this analysis is provided in graphical form, and can be used to specify a thermal store of this type for particular load and capacity application An example is provided showing how to use the parametric data for this purpose. The results are also analyzed to provide additional details about thermal store characteristics that can assist in understanding thermal stores of this type and to extend the use of the parametric data

5.3.1 Parameters modeled for the analysis

The model is run for a series of encapsulation tube outside radius dimensions ranging from 0.007m to 0.016m [0.007, 0.010, 0.013, and 0.016m] and heights of 1 to 3 meters in 1 meter increments. Aluminum is modeled for the encapsulation tube material to minimize costs (for instance, by capitalizing on existing knowledge held by the soft drink and canning industry in the manufacture, filling, and protection of aluminum containers). The encapsulation tubes are configured to meet the requirements of the resistance ratio parameter previously defined. The selected PCM is tetradecane, $C_{14}H_{30}$, in a lab-grade (99%) configuration. The HTF is a 35% solution of propylene glycol in distilled water. The tank shell thermal mass is ignored, and the tank is also assumed to be perfectly insulated (no tank wall losses). The thermodynamic properties of the HTF, aluminum encapsulation material, and PCM are given in Tables 6 through 8.

Property	Value	Units	Source
Density	1038	kg/m^3	ASHRAE Fundamentals 2009
Kinematic viscosity	$6.73x10^{-6}$	m^2/s	
Conductivity	0.394	W/(m·°K)	
Specific heat	3735	J/(kg·°K)	

Table 6: Properties of 35% (by volume) propylene glycol in water at 6.5°C

Property	Value	Units	Source
Density	2700	kg/m^3	Lide,2001
Conductivity	236	W/(m·°K)	
Heat capacity	881	J/(kg·°K)	

Table 7: Properties of Aluminum at 6.5°C

Property	Value	Condition	Source
Freezing temperature	5.5ºC	N/A	Hale et al, 1971
Density (solid)	825 kg/m^3	4ºC	
Density (liquid)	771 kg/m^3	10ºC	
Latent heat	211 to 226 (kJ/kg)	(liquid)	
Conductivity	0.15 W/(m ºK)	20ºC	
Heat capacity (solid)	1.68 kJ/(kg ºK)	-20 to 0ºC	Kousksou et al. 2010
Heat capacity (liquid)	2.18 kJ/(kg ºK)	25ºC	

Table 8: Properties of Tetradecane

Flow rates are normalized per cross-sectional area [m^2] of PCM. The flow rates modeled, 20 to 60 liters/(min m^2 of PCM) in 10 liter/min increments, are proportional to those used in the experiments for development and validation of the numerical model. The initial state of the store is fully charged at 2°C, and the incoming HTF is set at a fixed 11°C. A temperature of 6.5°C is assumed to be the upper limit of usable output temperature, and is used for comparison purposes between different configurations and run parameters.

5.3.2 Analysis of tube size and flow rate on energy recovery

A separate numerical model run is performed for each possible configuration based on the range of values selected for tube radius, length, and flow rate. This amounts to a total of 60 unique model runs. Figure 23 shows an example of one of these runs, which includes both output temperature and cumulative energy recovery plots. Figure 24 summarizes the percent of total energy (sensible and latent) recovered at an output temperature of less than 6.5°C for aluminum encapsulation tubes by tube radius, length, and flow rate for all parametric model runs. These results show that smaller tube diameters allow for greater total energy recovery at any flow rate, but larger diameter tubes can be used where taller tanks, lower flow rates, or lower total energy recovery percentage values can be tolerated. Note that larger tubes can reduce costs associated with PCM encapsulation per unit of PCM volume.

The geometry associated with the use of the resistance ratio parameter (see section 4.2) results in a constant ratio of the encapsulation tube inside to outside radius for any particular HTF, PCM, and encapsulation tube material. This also fixes the ratio of HTF to PCM area in the tank, which allows the flow rates given in Figure 24 to be converted to velocities or residence times. For example, based on a HTF of 35% propylene glycol and water, a PCM of tetradecane, and an encapsulation tube material of aluminum, the ratio of HTF to PCM area is 0.1147 m^2/m^2. Dividing the flow rate (converted to $m^3/(sec\ m^2\ PCM)$) by the HTF to PCM area ratio gives the velocity of the HTF in the tank. For the example given, this results in velocities of 0.0029 to 0.0087 m/s for flow rates of 20 to 60 L/(min m^2 of PCM) respectively. Dividing the thermal store height by these velocities will also give residence times.

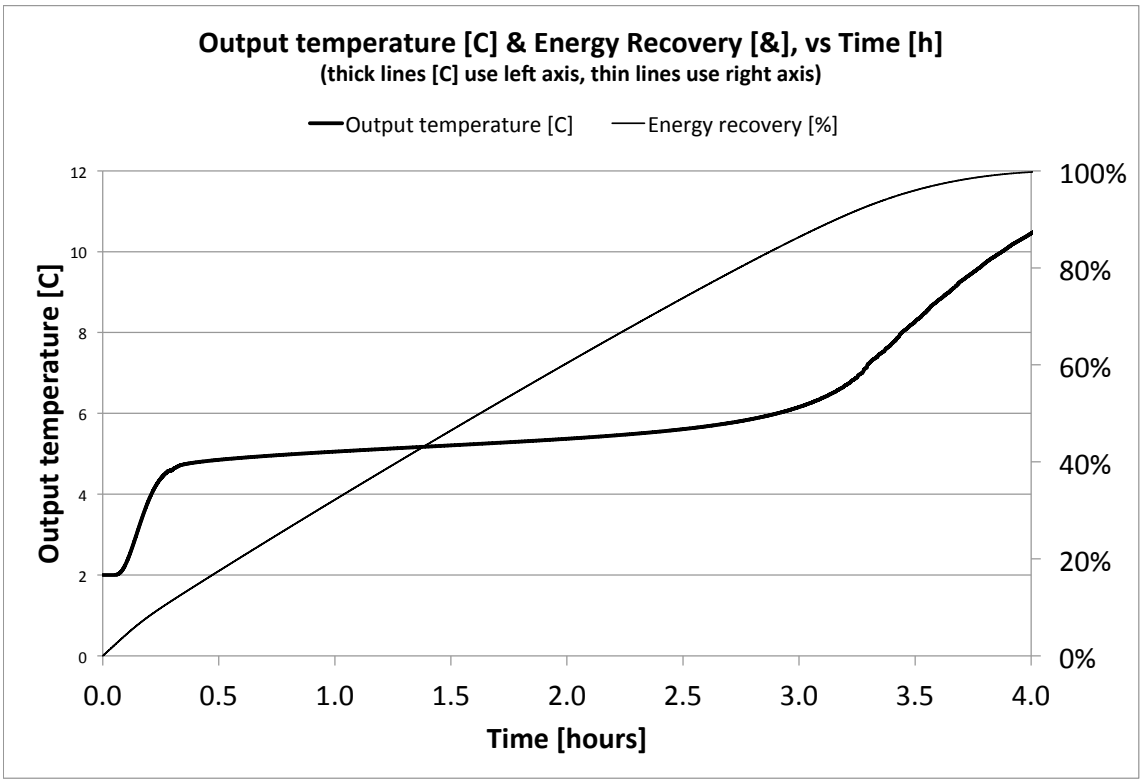

Figure 23: Example output from the model showing the HTF output temperature and energy recovery as a percentage of total capacity with respect to time for 0.007m radius encapsulation tubes and a 40L/(min*m^2 PCM) flow rate of incoming 11°C HTF. Find the time where the temperature reaches the maximum permissible output temperature and then move up to the energy recovery line to find the percent of energy recovered.

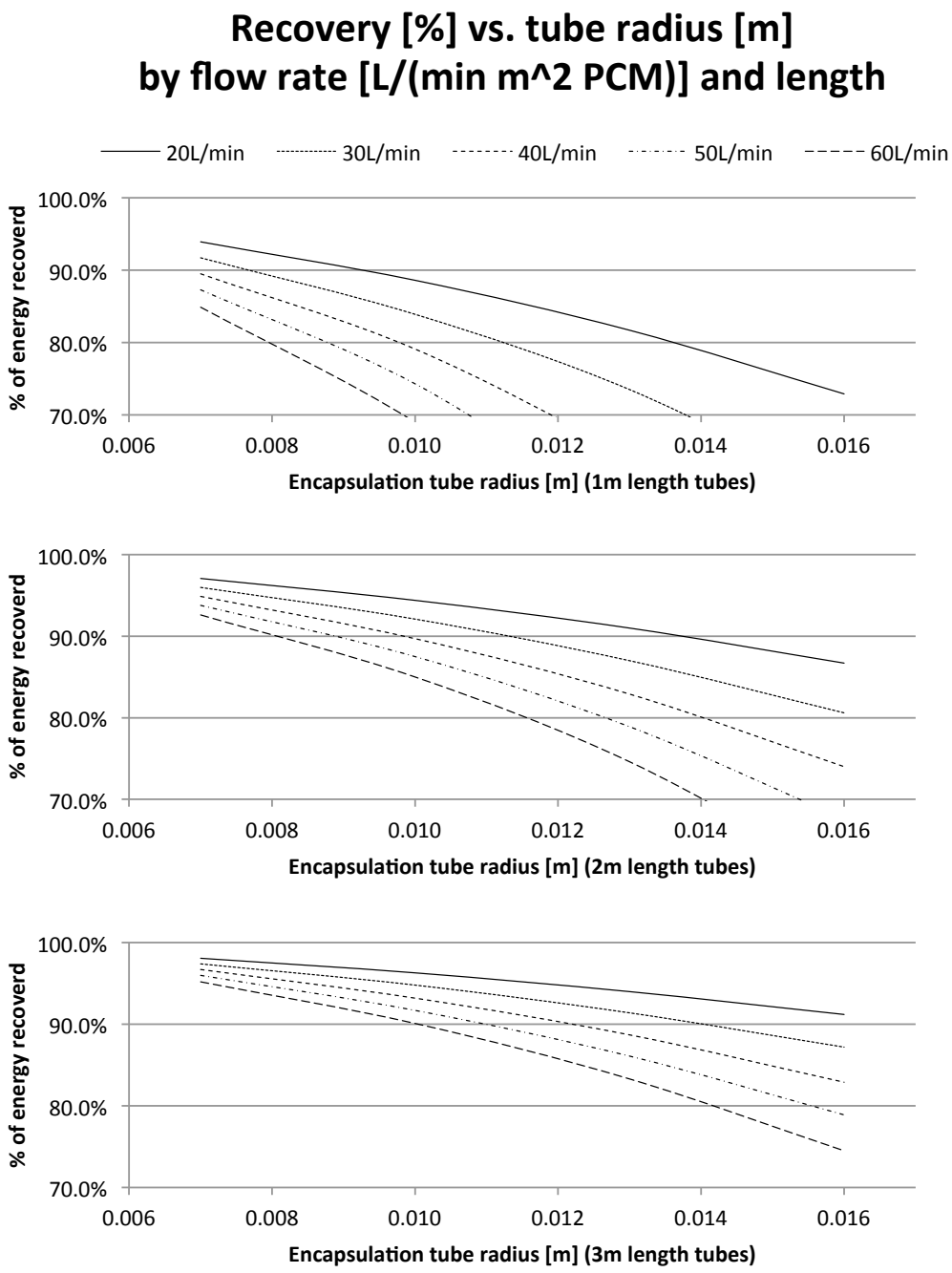

Figure 24: The recovery rate as a percentage of total thermal store capacity is plotted for various encapsulation tube radii by flow rate per m^2 of PCM cross-sectional area, for 1,2,and 3m long tubes, where the input temperature is 11°C and the output temperature is <6.5°C. The results show that as tube radius increases, flow rates must be slowed or the tubes lengthened to maintain a high recovery percentage.

5.3.3 Analysis of general thermal store characteristics

Additional information can be recovered from the data gathered during the parametric analysis. For instance, the impact of changes in tank size on system capacity and performance can be extrapolated from the raw performance data gathered during the model runs. A general review of the thermal store design can also provide additional details useful for engineers. This additional information extends the usability of the parametric analysis data, making it more useful for design purposes. This subsection summarizes this additional information.

Since the flow rate of the parametric model data is normalized to a $1m^2$ cross sectional area of PCM, adding diameter to the tank provides an increase in flow rate and capacity proportional to the increased cross-sectional area of the thermal store while maintaining the recovery rate and run times predicted for the smaller unit. For example, a thermal store with a PCM cross-sectional area of $2m^2$ and a height of 1m would allow for a flow rate of 40L/min while following the energy recovery projection for a 20L/(min m^2 of PCM) flow rate with a thermal store 1m in height from Figure 24. It would also effectively double the capacity of the thermal store. This same concept can also be used to define thermal stores with lower flow rates or smaller diameters.

The effect of taller encapsulation tubes can also be estimated based on information taken from the parametric analysis. Increasing the height of the thermal store will - like adding diameter to the tank - add capacity to the thermal store, but it has a different impact on recovery/flow rate performance. A further analysis of the model data shows that as the system is operated a temperature gradient is formed in the thermal storage tank. Once established, the temperature gradient maintains a relatively stable slope and shape as it moves down the tank during the discharge cycle until it meets the tank output, after which the output temperature rises quickly. This is demonstrated in

Figure 25, which is model data showing snapshots of the tank HTF temperature with respect to vertical position within the tank at ½ hour time intervals. This suggests, so long as the length of the thermal store is longer than the final temperature gradient formed in the tank at the point the maximum acceptable output temperature is reached, that any length added to the thermal store encapsulation tubes will add capacity that is completely recoverable. Thus, adding height while maintaining flow rate improves the overall recovery rate as a percent of total energy recovered, as well as adding equivalent capacity.

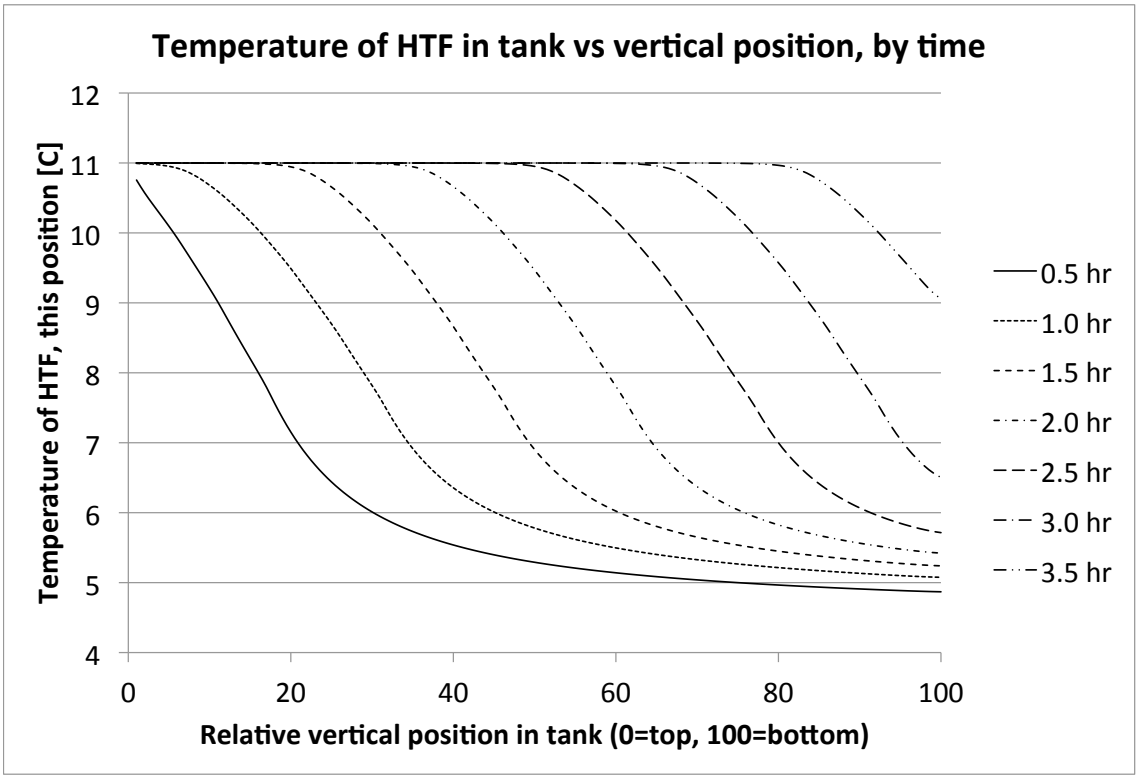

Figure 25: The temperature gradient initially formed in the tank is pushed down the tank as it discharges. In this case (0.007m radius encapsulation tubes, 40L/(min*m^2 of PCM flow rate) the gradient profile is fully developed by the one-hour mark. Once established the gradient travels down the tank until it reaches the tank exit, after which the output temperature begins to rise quickly.

The change in energy recovery resulting from a height increase over any of the reference heights given on Figure 24 (1, 2, or 3m) can be estimated using Equation 10. In this equation, $\varepsilon_{r'}$ is the adjusted energy recovery percent, ε_r is the recovery percent taken from the appropriate graph in Figure 24, z_R is the reference PCM tube height for the graph used in Figure 24, and Δz is the height added above the reference height. All of the tested configurations, when recovery is above 70%, met the requirement that the thermal store length be greater than the temperature gradient. This allows the use of Equation 10 to estimate the effects of adding height to a thermal store for any of the configurations shown in Figure 24.

$$\varepsilon_{r'} = \frac{\varepsilon_r z_R + \Delta z}{z_R + \Delta z} \tag{10}$$

The numerical model uses only the outside radius as a specification for the encapsulation tubes; it uses the resistance ratio parameter requirement to set the inside radius of the encapsulation tubes based on thermal properties of the tube material, PCM, and HTF. Because of the nature of the hexagonal packed tube configuration, this results in a constant ratio of PCM packing ε_p (the ratio of PCM cross-sectional area to tank cross-sectional area, or PCM volume to tank volume) for any given encapsulation material, HTF, and PCM configuration. For 35% propylene glycol HTF and tetradecane PCM encapsulated in copper tubes this ratio is 0.849, while it is 0.811 for aluminum tubes. These ε_p values can be used to determine the overall uninsulated size of a given storage capacity, or the potential storage capacity from the required maximum uninsulated size of the tank.

While copper tubes have a higher thermal conductivity and a higher PCM storage density than aluminum tubes, thermal stores consisting of equal amounts of PCM (and

thus equal latent storage capacity) will require more aluminum tubes than copper tubes. This is a result of the resistance ratio parameter guidelines, which require a thicker wall for an aluminum tube due to its lower thermal conductivity. This results in a larger overall thermal store size but also greater surface area and thus heat transfer rate and energy recovery when using aluminum tubes.

For the PCM, HTF, and range of aluminum tube sizes and heights modeled, the latent energy capacity is approximately equal to 90% of the total thermal energy capacity (including sensible energy). This permits the estimation of total thermal store capacity by dividing the latent capacity by 0.90 (based on the mass of PCM in the tank).

Chilled water thermal storage systems have thermal storage densities typically on the order of 5.8 to 8.1 kWh (thermal)/m^3 of HTF, based on a 5 to 7 °C change in temperature of the HTF as it passes through an HVAC system. Newer systems are capable of operating over a larger temperature change of up to 13°C, thus increasing their thermal storage density to 15.3kWh/m^3; however, these systems require specialized chiller equipment [Andrepont 2012]. The proposed latent thermal storage system has an estimated storage density when using aluminum encapsulation tubes of 41.5kWh./m^2, which equates to a storage density 2.7 to 7.2 times that of a chilled water system. In addition, this system can work with standard HVAC chiller equipment.

An analysis of internal temperatures of the thermal store produced by the model shows that the typical peak rate of change of temperature of PCM nodes during phase transition is at most 1°C per minute, and typically much lower. This is important because the rate of change of temperature used during DSC testing for PCM properties can affect the measured properties of the PCM [He et. al. 2004].

5.3.4 Application of the parametric analysis results

The necessary engineering parameters for a thermal store to meet specific load and capacity requirements can be determined using the data provided in this parametric analysis. An example of using this data to specify a thermal store is given below.

Let's assume that a residential-scale thermal store is required. The operating parameters are a capacity of 60kWh(thermal) with cooling demand rate of 9kW(thermal), and a desired recovery rate as a percent of total capacity of 80%. Lets also assume that space is limited for this residential unit, and that the uninsulated diameter of the base can be no more than 1m (radius = 0.5m). The steps to design this thermal store are as follows:

1. Divide the thermal store desired capacity by the desired recovery percent; this gives the actual needed capacity of the thermal store at 75kWh.
2. Find the cross-sectional area of the PCM in the thermal store, based on the allowed size (radius = 0.5m, area = 0.79m^2) multiplied by the packing ratio parameter for aluminum tubes of 0.811; this gives a PCM cross-sectional area of 0.64m^2.
3. Calculate the necessary HTF flow rate to meet the demand rate using an average temperature change between HTF supply and return of 5.5°C, and the specific heat property for the HTF as given in Table 6. This calculation shows that the application will require a flow rate of 26 L/min.
4. Divide the required flow rate by the PCM cross sectional area to obtain the flow rate normalized to a 1m^2 cross sectional area of PCM, as is used in the graphs of Figure 24. This gives a normalized flow rate of 40L/(min m^2 of PCM).
5. Multiply the required thermal capacity by the typical ratio of latent to total thermal energy (90%), and then divide this value by the latent capacity of

the PCM and PCM density to estimate the total PCM volume needed. For this application the total PCM volume required is 1.5m^3 of PCM.

6. Divide the total PCM required by the PCM cross sectional area to obtain the minimum height of the thermal store, in this case 2.4 meters.
7. Using Equation 10, calculate the actual recovery percentage ε_r from the desired recovery percentage $\varepsilon_{r'}$ using a reference height of 2m (because we will use the 2m chart in Figure 24) and an actual height of 2.4m; for this application the value comes to 75%.
8. Using the chart for a 2m tall thermal store in Figure 24, locate the tube size where the 40 L/min flow rate crosses a horizontal line drawn corresponding to a 75% recovery rate; any tube radius equal to or smaller than the identified radius will function in this application. In this case the 40 L/min flow rate line does not go below 75% at the largest tube radius listed, (0.016m radius) so any tube radius this size or smaller is acceptable..

For this application, a thermal store with uninsulated dimensions of a 1m diameter base and 2.4m height using 0.016m radius aluminum encapsulation tubes will provide for the desired 9kW demand rate and 60kWh total usable thermal storage. The storage system will contain 1.5m^3 of tetradecane PCM. Other thermal stores of this design can be specified in the same manner, however, in some cases there will be multiple degrees of freedom that may result in multiple possible solutions. This was avoided in the example by specifying a particular base diameter for the store.

5.3.5 Summary of parametric analysis results

The parametric analysis provides insight into the internal workings of a thermal stores utilizing hexagonal packed aluminum encapsulation tubes with tetradecane as a PCM. The analysis provides design guidance for engineers seeking to specify a thermal store of this type. An example for use of the graphical parametric data is provided. The parametric data can be used to specify thermal storage systems of size limited only by the physical constraints of the tanks and encapsulation tubes.

Chapter 6: Summary

The work presented in this dissertation investigates the development of a high-density latent energy thermal storage system suitable for use in HVAC cooling applications. Such a high-density thermal storage system can be used in applications where traditional chilled water tanks, due to their size, are impractical – for instance, the retrofit of thermal storage into existing residential or small commercial buildings. These buildings contribute greatly to the total peak load in hot and humid climates, underscoring the importance of this research.

Specifically, this research first evaluates the feasibility of a novel thermal store design based on hexagonal-packed tubes of encapsulated PCM, with a focus on maximizing storage density while maintaining sufficient thermal performance for HVAC applications (Objective 1). This is accomplished using a mix of experimental and numerical methods. Secondly, this research investigates the design by applying analytical methods, using this information to define critical parameters and to refine and validate a numerical model of this thermal store design. (Objective 2). Finally, the validated numerical model is used to perform a parametric analysis of the design so as to provide engineering guidance to those wishing to apply this thermal store design to specific HVAC applications (Objective 3). The model also allows additional analysis of this design to gain further insight into its operation.

A total of 3 different research studies are conducted to meet the three specific research objectives identified in this dissertation. Each research study resulted in a full-length journal article, and these three articles are included as Appendix A, B, and C. These research studies are summarized in the Introduction, Methods, and Results sections

of this dissertation. The major findings and results of these research studies are summarized below.

- A thermal storage system utilizing tube-encapsulated phase change material (PCM) is proven feasible by both experimentation and modeling. This thermal store design is shown to provide suitable performance for HVAC applications while providing a storage density 2.7 to 7.2 times that of a chilled water system.
- To meet the desired performance characteristics and to simplify numerical modeling, the encapsulation shell must have specific thermal properties relative to the HTF and PCM used. Analysis of this thermal store design has produced the resistance ratio parameter that - if applied to the specification of encapsulation tubes - ensures that the conductivity requirements are met for any particular HTF, PCM, and encapsulation material selection.
- A finite-volume numerical model of the thermal store is developed for parametric analysis of the design, validated against experimental data. The parametric analysis provides engineering guidelines for determining design parameters for thermal stores of this type for a wide variety of capacities and performance levels. Instructions for utilizing the parametric data and an example are provided.
- Further analysis of the design using the numerical model gives additional insight, including:
    - Due to the nature of hexagonal-packed encapsulation tubes, thermal store PCM volume fraction is fixed for any specific HTF, PCM, and encapsulation material when the resistance ratio is

applied; encapsulation tube radius will not affect PCM density in such cases. For the PCM and HTF used in this study with aluminum tubes, the PCM fraction is 0.811; for copper tubes it is 0.849

- Increases in tank diameter proportionally increases capacity at any given flow rate while maintaining the fraction of recoverable energy. An increase in height increases the capacity as well as the fraction of recoverable energy (subject to limitations involving the temperature gradient – see section 5.3.3). An equation is provided to estimate this effect. This extends the usefulness of the parametric modeling data.

These findings contribute to the body of knowledge available for the design of high-density tube encapsulated PCM based thermal storage systems. The new and novel thermal store design proposed here allows for the application of thermal storage systems where - due to space requirements - they might not otherwise be possible. This work addresses a segment of energy use that can account for more than 50% of the peak energy load in hot and humid climates during summer months [Doggett 2013] , and is growing [US EIA, 2013]. The application of this design to existing residential and small commercial buildings has the potential to significantly reduce peak energy demand related to HVAC cooling loads, while shifting these loads to periods when baseload capacity or intermittent renewable resources are available. This will reduce energy costs, allow for the expanded use of intermittent renewable energy resources, and reduce the pollution and environmental impact associated with the use of fast-response peak power plants.

6.1 FUTURE WORK

This study provides many answers associated with the design and use of high-density PCM-based thermal stores; however, new questions have surfaced during this work. These questions become topics for future investigations and are summarized here along with suggested research.

6.1.1 Variable HTF return temperatures

The numerical model presented in this study assumes a constant return HTF temperature; a variable flow rate rather than temperature is used to simulate variations in demand. However, there may be times where the demand is variable in both flow rate and HTF return temperature.

One assumption in the model is that the system avoids buoyancy-driven flows by maintaining tank stratification. The introduction of variable-temperature return HTF would violate that assumption. It is likely that this would be resolved in the thermal store by buoyancy driven flows allowing the incoming HTF to seek a level in the tank appropriate for its temperature. Some mixing would occur in the tank as a result of these flows; however, the impact on overall performance, if any, is not yet known.

Additional experiments can be conducted using the experimental apparatus developed in this study, or by constructing a full-scale model for testing. The tests should introduce variations in return HTF temperatures to determine their impact on thermal store performance.

6.1.2 Internal convection

In the present model, the potential for natural convection internal to the encapsulation tubes, between tube surface and the frozen surface of the PCM, are either ignored or assumed included in the calibrated value for conductivity of the solid and

liquid forms of the PCM. During testing, and confirmed by the model, it is found that the PCM in the tube melts in such a way so as to form cone-shaped surface in the tube of height approximately equal to the length of the temperature gradient formed in the tank and demonstrated in Figure 25.

If the potential for internal convection is found, it may be possible to use this phenomenon to further improve the performance of this thermal store design. The angle of the tubes with respect to vertical has been shown to impact internal convection heat transfer in thermo syphon systems [Larsen and Hartnett 1961, Budihardjo et.al. 2007], and tilting the tank or encapsulating tubes may increase internal heat transfer rates.

A purpose-specific test apparatus will need to be constructed to perform tests to investigate internal convection. One possible test configuration would be a conical insert for a test pipe, the shape of that taken by the PCM inside an encapsulation tube during the discharge cycle, that can be maintained at a specific surface temperature, either by circulating a HTF behind its surface or through other means, which would mimic the near-isothermal conditions found at the surface of the melting PCM. The upper portion of this tube could be filled with a fluid, and the outside of the tube then subjected to a temperature exceeding that of the internal conical surface. The steady-state temperatures of the internal/external tube surfaces, internal conical surface, and/or internal fluid (average) could be used to back-calculate the effective heat flux for comparison between different tube radii and conical insert heights.

6.1.3 PCM properties during phase transition

The model estimates the properties of the PCM during phase change; specifically, the effective specific heat capacity with respect to temperature during phase transition. A better understanding of this phenomenon can allow for a more accurate modeling of this

design. DSC testing of paraffin PCMs has been researched; however, DSC temperature scan rates can have an impact on measurements. Slower scan rates produce more accurate results and, - given the slow rate of temperature change that occurs in this thermal store design - additional tests at the slowest possible scan rates would be useful in properly characterizing the PCM. This would improve model accuracy and allow for more detailed analysis of the design. Existing standard DSC equipment can be used for this analysis, so long as it has the capability to test at below ambient temperatures using scan rates on the order of 0.1°C/min or lower.

6.1.4 Cost analysis

A cost-benefit analysis of this thermal store design would enable proper sizing for specific applications and economic conditions (electric rates, rebates, tax incentives). Such a study would need to investigate electric utility as well as customer motivations, and also examine the possibility of utility versus customer-controlled operation. This is an important consideration since each of these stakeholders is driven by different concerns. For instance, a customer would seek maximum economic return; this would encourage the customer to turn on their thermal store as soon as daily peak electric rates applied to ensure the maximum discharge, and hence economic recovery, from the thermal store. However, if all customers were to act accordingly, the thermal stores might all be depleted prior to the end of the peak period, resulting another peak later in the day. If utility controlled, the utility could phase the thermal stores into operation such that an overall reduction in energy use is achieved without producing a secondary peak in energy use. A cost analysis study could provide guidance to engineers on how to consider these issues when sizing thermal storage systems.

Appendix A

PAPER 1: COMPACT PCM-BASED THERMAL STORES FOR SHIFTING PEAK COOLING LOADS

Stephen Bourne, Atila Novoselac (graduate advisor)

(Published in Building Simulation, 2014: DOI 10.1007/s12273-015-0243-6)

ABSTRACT

Thermal energy stores, when used as part of a demand management system, can shift peak cooling loads to off-peak hours or to periods when intermittent renewable energy sources are available. This enables more efficient use of baseline and renewable electric capacity, and reduces dependence on less efficient and more costly peak energy power plants. High density thermal stores can be an effective retrofit option for existing buildings and environmental control systems. This paper investigates the development of a simple, compact, high density thermal storage unit suitable for use in small to medium residential or commercial applications that utilize, or can be retrofitted to use, chilled water cooling coils. This thermal store design is based on the use of a widely available phase change material (PCM), macro-encapsulated into cylindrical tubes that are packed into a containment tank. An experimental scale model of this thermal store is constructed for test purposes, and tests are conducted to determine the feasibility of this design and to characterize its operation. A numeric model is developed to demonstrate the feasibility of modeling such a store using simplified assumptions, both for design purposes and real-time predictive control strategies. The results show that such a design increases thermal capacity over that of a simple chilled water tank, and that a simplified numeric model for use by control systems can predict the short-term performance of the store in near real-time.

Keywords: PCM, thermal store, tetradecane, renewable energy, cooling load

LIST OF SYMBOLS

Symbols

A_a	*Cross-sectional area associated with advection [m²]*
A_c	*Surface area associated with convection [m²]*
A_i	*Area of the inside face (relative to the radius) of a modeled element [m²]*
A_o	*Area of the outside face (relative to the radius) of a modeled element [m²]*
A_h	*Area of the horizontal face of a modeled element [m²]*
$A_{lm,i}$	*Log-mean area of the inside face of the modeled element [m²]*
$A_{lm,o}$	*Log-mean area of the outside face of the modeled element [m²]*
C	*heat capacity [J/(kg · ºK]*
F	*Flow rate [m³/s]*
F_{lpm}	*Flow rate [L/min]*
h	*Thermal convection coefficient [W/(m² · ºK]*
HF	*Heat of fusion for PCM (Tetradecane) [J/kg]*
HF_p	*Heat of fusion remaining as of the previous time step for a specific PCM element undergoing phase change [J]*
HF_m	*The maximum heat of fusion calculated for a specific element [J]*
k	*Thermal conductivity [W/(m · ºK]*
r	*Radial dimension [m]*
t	*time [s]*
T	*Temperature*
T_{amb}	*Ambient temperature [ºC or ºK]*
T_s	*Surface temperature for convection heat transfer [ºC or ºK]*
T_S	*Highest temperature at which the PCM begins to solidify [ºC]*
T_M	*Lowest temperature at which the PCM begins to melt [ºC]*
U_z	*Velocity of the heat transfer fluid flow*
V	*Volume [m³]*
w	*Velocity in the z direction of the HTF (heat transfer fluid) [m/s]*
z	*vertical dimension [m]*
Δt	*Time step [s]*
Δr	*length dimension of the current radial step [m]*
α	*Thermal diffusivity [m²/s]*
ρ	*Density [kg/m³]*

Subscripts

c	*PCM parameter*
f	Heat transfer fluid (HTF) parameter
m	Vertical integer coordinate of the referenced node (vertical node number)
n	Radial integer coordinate of the referenced node (radial node number)
v	*CPVC parameter*

Superscripts

t	Current time step
$t-\Delta t$	Previous time step

Chapter A1: Introduction and background

A1.1 Overview

Without any effective large-scale electric energy storage capability, electric power must be produced as it is used and precisely follow demand. Uncertainty in both generation and demand requires a means to regulate one or the other to maintain an ongoing balance. Typical regulation mechanisms focus on the manipulation of generation by using a mix of generation sources consisting of baseline, intermediate, and peak power plants. [Masters, 2004].

The increased use of renewable but intermittent energy resources - such as wind and solar power - adds uncertainty to generation capacity. Total U.S. solar and wind power generation is expected to grow by 46 and 42 gigawatts respectively by the year 2040, with total renewables producing almost 20% of all electric power [US EIA, 2013]. Without mitigating action, offsetting the increased uncertainty in electric supply caused by the use of these intermittent renewable energy resources will require an increased capacity in fast-response but less efficient and more costly peak demand power plants. The need for more peak demand power plants can be mitigated by shifting peak electric load to non-peak periods [Bently and Evelyn, 1986], or to times when intermittent renewable energy is on-line.

Commercial and residential environmental cooling loads account for 11% of all U.S. electric consumption [USEIA, 2012], and can be a much larger share of seasonal peak electric demand - particularly in regions with warmer climates [Wattles, 2011]. The Electric Reliability Council of Texas (ERCOT) reports that up to 54% of peak summer energy demand in Texas is due to weather-related loads, much of which is associated with environmental cooling [Doggett, 2013]. The demand for residential and commercial cooling is expected to increase due to a projected growth in residential and commercial

floor space, and to a shift in population towards states with warmer climates [US EIA, 2013].

Active thermal energy stores, when used as part of a demand management strategy, can time-shift these cooling loads. Studies have shown that active thermal storage systems can be effective at both reducing peak energy demand and the overall cost of building energy use by environmental systems, particularly when cost incentives – such as peak demand and time-of-day rates – are in use [Hajiah and Krarti, 2012a,b]. The use of thermal storage systems can also reduce the peak demand seen by environmental chiller equipment, eliminating the requirement that chiller equipment be capable of meeting peak cooling load demands. Instead, chiller equipment only needs to meet total load requirements (time-averaged load) [He *et al*., 1999]. This reduces the capacity requirements and cost of chiller equipment, and minimizes the refrigerant charge necessary for a given application.

The data in Figure A1 shows that up to 71% of weather sensitive load experienced in Texas is due to residential demand associated with environmental cooling load. The American Housing Survey data indicates that residential structures in 2011 had an average age of approximately 37 years [U.S. Census Bureau, 2013]. Similar data exists for commercial buildings, which account for 22% of Texas weather-sensitive load and have a typical 28 year lifespan [USEIA, 2006]. The long usable lifespan of residential and commercial buildings dictates that an effort be made to develop retrofittable thermal storage systems that can be deployed in existing structures, structures that may not permit the addition of large conventional sensible thermal energy stores such as chilled water tanks. High capacity, high density thermal storage systems will be necessary for these retrofit applications.

Thermal energy can be stored sensibly through a change in temperature of a

storage medium, or it can be stored latently as a change in phase of a material – for instance, from a solid phase to a liquid phase or vice versa. Phase change processes are characterized by large changes in enthalpy at constant or near-constant temperatures. These characteristics of phase change/latent energy storage systems allow them to store energy at greater density and over a smaller temperature range than sensible energy storage systems, such as conventional chilled water tanks [Regin *et al*., 2008]. For example, the energy required to melt ice (0ºC ice changed to 0ºC water) is roughly equal to the energy required to heat the resulting water from 0ºC to almost 80ºC (334kJ/kg at a nearly constant 0ºC, vs. 4.2kJ(/kg·K) over 80ºC [Cengel *et al*., 2008]).

PCMs (phase change materials) suitable for use in an environmental cooling latent energy thermal storage system should exhibit several key properties, including: high volumetric and gravimetric heat of fusion; a narrow phase change temperature band in a range compatible with existing chiller equipment; acceptable thermal conductivity; chemical stability; and physical compatibility with common encapsulation materials [Abhat 1983][Baetens *et al*.,2010] [Humphries and Griggs 1977]. For environmental space cooling applications, phase change temperatures should operate in the range of 5 to 12ºC [Li *et al*, 2012] [Dimaano *et al*, 2002]. Potential cooling-mode PCMs include water, salt hydrates, fatty acids, and paraffin hydrocarbons.

n-Paraffin (hereafter paraffin) waxes consisting of one or more compounds of the generic form CH_3-$(CH_2)_n$-CH_3 have been heavily investigated for their use as PCMs (phase change materials) in thermal storage systems [Abhat 1983][Humphries and Griggs 1977] [Hale *et* al, 1971]. Studies have shown that paraffin-based PCMs with the needed properties of melting temperature and heat of fusion can be crafted using paraffin with hydrocarbon chains of particular length, or through the use of mixtures of such paraffin [He *et al*., 1999] [He *et al*., 2004] [Choi *et al*., 1992]. These paraffin compounds

are congruent through their melt-freeze cycles, chemically stable, compatible with available low-cost encapsulation materials, non-toxic, possess high heats of fusion, and are available in suitable temperature ranges for use in cold storage systems. Paraffins do suffer from poor thermal conductivity (approximately 0.2 W/(m□K), however, encapsulation dimensions can be adjusted or internal thermal conduction enhancements used when necessary to improve thermal performance. Such paraffins can be used to construct high-density thermal storage system for environmental cooling applications.

This paper investigates the development of a simple, compact, high-density paraffin-based PCM thermal storage unit suitable for residential or small commercial retrofit applications. A simplified numeric model for this store is developed for design and real-time control applications. The model utilizes a finite volume approach so as to preserve both the change in temperature of the HTF as it passes through the store as well as the capability for multiple phase fronts that may develop during partial charge/discharge cycles. Experiments are conducted to determine the feasibility of this design and to characterize its operation, and numeric modeling is performed to predict the performance of the thermal store under varying loads.

A1.2 PREVIOUS PHASE CHANGE MODELS AND EXPERIMENTS

Shamsunder and Sparrow [1975] comprehensively developed an implicit two-dimensional non-linear numeric solution for PCM solidification in a long rectangular container (square tubing), based on the enthalpy model and solved using iterative methods. Their non-dimensionalized solution utilizes the Ste (Stefan), Fo (Fourier) and Bi (Biot) numbers. This work, like some others in the realm of PCM solidification and melting, relies on a constant HTF (heat transfer fluid) temperature. This constant HTF temperature condition is inconsistent with the operation of an actual thermal store, since

the express purpose of a thermal store is to transfer energy to/from a HTF that must change temperature as it traverses the system. However, their model does give valuable insight into the development and solution of an enthalpy-based numeric model. Their results show that a low Bi number is required for the store to produce a near-constant heat flux; this is because for a low Bi number the resistance of convection dominates, and in the modeled scheme the external resistant (1/[hA]) does not vary. Bi numbers larger than 1 produce significant drop-off in heat transfer with respect to time. Ste numbers between 0.01 and 0.1 (within the realm of common PCMs) were modeled and shown to have little effect on solidification until near the end of the process.

Jesumathy et al. [2012] investigated a single vertical annulus tube-in-shell design for a PCM-based thermal storage system. Their study showed that the PCM did not melt in a uniform manner; instead, the PCM melted from the top down, even though they had attempted to maintain a constant and uniform thermal bath temperature. They also experimented by altering the Reynolds number of the flow around the encapsulation annulus, but limited the Re range to between 693 and 1175 (laminar flow). This study also notes that in certain cases internal (encapsulation) convection may result at the interface between the PCM and the encapsulation system, increasing heat flow internal to the encapsulation system

Jiji and Gaye [2006] analytically investigated the theoretical solidification and melting of slab elements of PCM using a quasi-steady state model as an approximation. This method assumes that the system - from a sensible energy perspective - is always in equilibrium (sensible equilibrium is assumed to be reached immediately after the sensible/latent energy transformation has been completed). When the Stefan number is much less than one, this is a feasible assumption (sensible energy is only a small part of the total energy exchange). The solution was found analytically, but required that the

surface temperature of the encapsulation system be constant. The solution operates by assuming separate differential equations for conduction through the PCM – one for the solidified portion and one for the liquefied portion of the PCM, each with its own boundary conditions – with a separate differential equation acting to connect the two at the moving interface boundary between the phases (using a quasi-steady state approximation). The rate of movement of the phase change interface is related to the difference between conduction from/to each of the phases and the heat of fusion of the PCM, coupled with the geometry of the system.

Ismail and Moraes [2009] investigated analytically and experimentally the use of spherically-encapsulated PCM. Their study assumed a constant HTF temperature outside of the spheres, and used a finite-difference approximation to numerically model the freeze cycle while assuming only conduction inside of the spherical shell. Their numeric results correlated well with experimental results when diameters were small. They did not investigate melting cycles.

Ismail and Gonzalves [1999] numerically investigated the freezing of n-Eicosane (T_f = 36.4ºC) in a tube-in-shell system, where the shell contained the PCM and the tubes passing through the shell in a single-pass arrangement carried the HTF. Their enthalpy method model concentrates on a single similarity unit of HTF pipe and surrounding PCM annulus. Their numerical approximation is based on dimensionless parameters, and the results are expressed in terms of a heat exchanger in the form of NTU, mass fractions of PCM solidified, and effectiveness based on a dimensionless time, radii of the HTF tube, equivalent radius of the (effective) PCM annulus area (the "symmetry circle"), and the formulation of a Biot number involving the HTF pipe diameter. Their solution couples changes in the HTF with convection to the PCM. Their results show that increases in the R^* ratio (the ratio of the outer PCM annulus diameter to the HTF tube diameter) reduces

effectiveness and increases the time period for full solidification. In addition, they conclude that an R^* value of 4 is optimal from the standpoint of both NTU and effectiveness for this particular design.

Bilir and Ilken [2005] investigated the solidification time of PCM in both cylindrical and spherical containers using an enthalpy model and an explicit scheme. The model assumes a perfectly conducting shell ($R_T = 0$), a constant HTF temperature and convection coefficient h, and radial conduction only (a reasonable assumption given solidification from the outside inward). Their model is similar to, and expands upon, that of Shamsunder and Sparrow [1975]. The result of an analysis of their model provides correlations for solidification times as a function of Stefan, Biot numbers and a superheat parameter for both cylinders and spheres.

These efforts have focused on the speed and manner in which an encapsulated PCM can store or recover energy. Most utilize some form of enthalpy tracking, and model the thermal performance of a single unit of a thermal store design. However, in many cases the idealized model or experiment is inconsistent with application as a thermal storage system. For instance, the assumption of a constant temperature HTF is inconsistent with use as a thermal store, as the express purpose of the store requires that HTF temperature change as it passes through the system. In other cases a model may allow only a single phase front, however, in a partial discharge/recharge operation multiple phase fronts are possible. Finally, these models have concentrated on optimizing freeze/melt rates; however, energy storage and recovery in a thermal store does not necessarily have to be fast, but only fast enough for a particular application. Peak energy demand during cooling season typically occurs over a two to six hour period, and if a large portion (75%+) of a thermal store's capacity can be recovered in this time frame then performance will be acceptable for such an application. Thermal storage systems for

retrofit applications thus need to be optimized for storage density, with a goal of making them “fast enough” for the intended purpose of shifting cooling loads away from peak energy periods. A balance between speed and storage density should be sought.

Chapter A2: Methods

An experimental thermal store design is constructed utilizing PCM encapsulated in CPVC tubes arranged in a pseudo annular-ring configuration inside of an insulated PCV tank. Cylindrical encapsulation is used due to its higher potential density of encapsulated volume over spherical encapsulation (theoretical maximums of approaching 90.7% vs. 74.0% respectively), and also to minimize manufacturing costs. The thermal performance of this design can be manipulated by altering the diameter, length, spacing, and number of the PCM encapsulation tubes.

A finite-volume numeric model, suitable for use in thermal storage applications, is also developed to demonstrate that simplified models for design and real-time operation/control are feasible for this thermal store design.

A2.1 Experimental apparatus

The PCM encapsulation system for the thermal store consists of CPVC tubes. CPVC is chosen due to its chemical resistance to n-alkane paraffins and its availability in an appropriate size. Standard ½ inch (12.7mm) CPVC tubing is used. Tubes are cut to a finished length of 1.14m with the end caps installed. This length is chosen to maintain a manageable size for the test apparatus. Each tube is filled with 0.116 L of PCM, then fitted with end caps. The completed tubes contain approximately 0.167m of clear space above the liquid PCM to allow for expansion/contraction of the PCM without large changes in internal pressure.

The tank is constructed of standard 4 inch (0.102m) schedule 40 PVC pipe. The top and bottom of the tank utilize PVC fittings to allow for water flow and instrumentation. A PVC pipe flange is installed at a level coincident with the top of the PCM encapsulation tubes to facilitate installation of the PCM tubes and instrumentation.

The main body of the tank, which contains the full height of the encapsulated PCM tubes, is placed into a 0.305m diameter cardboard form tube and supported by 0.102m of Styrofoam insulation board at its base. The remaining space around the tube is filled with polyurethane spray foam insulation. The upper flange and top portion of the tank is manually insulated with polyurethane foam batting and covered by a 0.305m diameter cardboard cylinder.

The temperature measurement system utilizes Omega 44033 epoxy-encapsulated thermistors with an interchangeability of 0.1ºC. These thermistors are positioned at both the input and output of the thermal storage tank, and are placed directly in the restricted flow path of the entry/exit ports to minimize error and external influences. Return tank, loop, and ambient temperatures are also measured using these thermistors, as is the water bath and PCM temperatures during PCM water bath melt/freeze testing. The thermistors are connected to GW Instruments iNet-100 A/D data acquisition hardware, which provides excitation current for each thermistor through a precision 4.7kohm resistor with an accuracy of +/- 0.025%-20ppm/ºC. The iNet-100 in this configuration has a temperature measurement accuracy of +/-0.1ºC. Temperature data is recorded at 10 second intervals during each test run.

HTF flow rates are measured using Omega FLR1009 Pelton-type turbine wheel flow meters with a range of 50 to 500 ml/min and an output of 0 to 5 volts. These devices have a repeatability of 0.2% of full scale. One flow meter is used per tank port (at the top and bottom of the PCM tank), however, since the flow meters are not bi-directional only the device acting as the input is utilized for each test run; the unused device is bypassed. These devices are dependent on fluid viscosity, and so require calibration to the fluid in use. The flow meter in use for each run is manually calibrated using direct measurement of the output flow from the tank at the beginning and end of each test run.

Testing is performed by pumping chilled water through the storage tank. A Polyscience 5706T portable chiller unit supplies chilled water. To minimize temperature changes in the HTF during delivery to the tank, the tank is supplied from a high-volume-flow loop that delivers the HTF at constant temperature to points very near the tank inputs. Small diameter polyethylene tubing connects the supply loop with the input/output terminals of the tank to minimize residence time in the tubing. All tubes are insulated by wrapping the tubes in foam rubber pipe insulation having a minimum R-value of 0.5 (SI). A schematic of the tank and its connections is shown in Figure A2, and a picture of the complete apparatus is shown in Figure A3.

The direction of HTF flow in the tank is devised to preserve any temperature gradient developed in the tank, and is dependent on the cycle (charge or discharge). During the charge (freeze) cycle, chilled water at approximately 2ºC is pumped into the bottom of the tank. During the discharge (melt) cycle, chilled water at approximately 11ºC is pumped into the top of the tank. The 2ºC charge temperature is selected as low enough to fully freeze the PCM while also being within the capability of typical chilled water systems. The 11ºC temperature for the discharge cycle is selected as representative of a typical cooling coil chilled water return temperature. HTF flow rates for the recharge (freeze) cycle are fixed at 300ml/min. Flow rates for discharge are constant during each run, but vary between runs at rates from 100ml/min to 200ml/min.

Two PCM/tank configurations are investigated: a high density configuration utilizing 31 tightly-packed encapsulated PCM tubes, and a moderate-density configuration utilizing 19 evenly-spaced encapsulated PCM tubes. When the thermal store is configured for high density mode, the close-packing arrangement fails at the inside surface of the tank, resulting in additional flow paths around the inside edge of the tank. The total area of these flow paths are large with respect to the total flow path

between the tubes. To minimize the impact of these flow paths they are blocked with 5/8" closed-cell foam backer rod; this provides for more uniform and consistent heat transfer between the PCM tubes and the HTF. When in the moderate-density 19 tube configuration, this perimeter area is small relative to the total free cross section area of the tank and so is ignored. A picture of the 19-tube packing configuration is shown as an inset in Figure A3.

A2.2 PCM TESTING

Tetradecane is used for the phase change material. A lab grade product of approximately 99% purity is selected over a technical grade product (95%) grade due to early experiments conducted with a technical grade formulation. In those experiments it was found that the freezing point of the tetradecane was depressed by the impurities found in the technical grade product, making it unsuitable for this application. The essential properties of pure tetradecane are taken from the literature, as indicated in Table A1.

The melting of paraffins occurs over a range of temperature. Thermal testing is performed on the PCM using a water bath protocol to determine the freeze and melt temperature range of the tetradecane PCM. A 20ml sample of PCM is placed in a section of clear ½" schedule 40 PVC pipe, and a thermistor installed in the approximate center of the sample. The temperature reading of the thermistor is monitored as the PCM sample freezes and melts while in a temperature-controlled water bath. The freezing temperature range is found using a water bath temperature of 2ºC, and the melting temperature range using a water bath temperature of 9ºC. A picture of the water bath apparatus is shown as an inset in Figure A3.

A2.3 NUMERIC MODEL

The numeric model of this experiment is developed based on a finite volume energy balance of an annular ring configuration of cylinder(tube)-encapsulated PCM, as shown in Figure A4. The finite volume energy balance method was chosen for the initial model to allow maximum flexibility, including the ability to later model a partial freeze-melt-freeze cycle where multiple phase fronts might exist.

The model is a two-dimensional (in r and z) finite volume representation of the unit shown in Figure A4, which comprises a 60º segment of an individual PCM encapsulation tube and its share of the associated HTF flow path. The example segment shown in Figure A2 is assumed to have adiabatic boundaries along its exposed vertical surfaces, based on the assumptions that $dT/d\theta$ is equal to zero (the model is axisymmetric) and that a uniform temperature exists within HTF cells at the same vertical location. Temperature nodes are located at the center of each volume element, with surface temperature nodes used at surfaces separating dissimilar materials. Volume element nodes can accumulate latent and/or sensible energy, while surface nodes are used only to transfer energy between adjacent dissimilar materials.

The model accepts as input two matrices that represent the last state (temperature and available latent energy) for each temperature node and volume element, as well as model physical properties (dimensions, material properties), some pre-calculated constant dimensions and parameters to speed processing, and the current incoming HTF temperature. It outputs the new node state for the current time step, including the current output temperature, as well as the latent enthalpy for each PCM node. Successive iterations of the model allow for run times of any length.

The actual annular area associated with each encapsulation tube is a hexagonal cylinder, but for modeling purposes the hexagonal cylinder is replaced by a circular

cylinder of equivalent cross-sectional area equal to an appropriate share of the free cross-sectional area of the tank; this is done to preserve the relationship between HTF (heat transfer fluid, i.e.: propylene glycol and distilled water solution) volumetric flow rate and velocity within the tank. Advection due to HTF flow, vertical diffusion in the HTF, convection between the HTF and the surface of the encapsulation tubes, and conduction through the encapsulation material and PCM are all considered in the model. Diffusion is considered only in the z direction for the HTF, but for both the r and z directions in the encapsulation material and PCM. For this iteration of the numeric model the heat capacity (C) and conduction (k) of the components are assumed constant, regardless of phase or temperature. Due to the change in phase and resulting change in heat capacity, the heat capacity value used for the PCM is a temperature/phase averaged value, as shown in Table A1. To maintain model simplicity and speed of operation, the potential for buoyancy-driven free convection within the encapsulated PCM or within the thermal storage tank itself is ignored. Only conduction is considered internal to the PCM encapsulation tubes, regardless of phase state, while conduction, advection, and forced convection are considered in the HTF. The model is calibrated so that any free convection effects are included in the effective heat transfer coefficient, h, or the material thermal conductivity, k.

The energy balance between the HTF and the surface of the encapsulation is described by an equation based on the geometry and nodes as shown in Figure A5. The energy balance for the HTF element is such that:

net enthalpy change = net convection + net diffusion + net advection

Performing an energy balance on the elements shown in Figure A5 gives the equation:

$$V_f \rho_f C_f \left(T_{f,n}^{t} - T_{f,n}^{t-\Delta t}\right) = A_c h \left(T_{c,n} - T_{f,n}\right)\Delta t + A_a k_f \left(\frac{T_{f,n-1} - T_{f,n}}{\Delta z} - \frac{T_{f,n} - T_{f,n+1}}{\Delta z}\right)\Delta t + A_a w \rho_f C_f \left(T_{f,n-1} - T_{f,n}\right)\Delta t \quad \text{(A1)}$$

This equation collapses to the more recognizable differential form:

$$\frac{\partial T}{\partial t} = \frac{A_c}{V_f}\frac{h}{\rho_f C_f}\left(T_s - T_f\right) + \alpha_f \frac{\partial^2 T}{\partial z^2} - w\frac{\partial T}{\partial z} \quad \text{(A2)}$$

Boundary surface nodes are used between dissimilar interfaces. These nodes are used solely to transfer energy, and do not have any sensible or latent energy storage capabilities. In addition, these operate in the r dimension only, unlike normal element nodes, which operate in both the r and z dimensions. In these boundary surface nodes, net energy in = net energy out.

Two modes of energy transfer are defined for internal (encapsulation and PCM) nodes: Sensible energy mode and latent energy mode. Sensible energy mode applies to the internal element nodes of the encapsulation material, or to the PCM nodes when they are either fully frozen or fully melted. In this mode, an energy balance for the internal, conduction-only nodes follows a similar process (net in = net stored). However, this mode is complicated by the changing area over which heat transfer occurs in the radial direction, as shown in Figure A6. Formulating a finite volume energy balance based on the geometry shown in Figure A6 gives the equation:

$$V_{(m,n)}\rho_{(m,n)}C_{(m,n)}\frac{T^{t}_{(m,n)}-T^{t-\Delta t}_{(m,n)}}{\Delta t}=$$
$$\left[k_{(m,n)}A_{o(m,n)}\frac{T_{(m,n-1)}-T_{(m,n)}}{\Delta r}-k_{(m,n)}A_{i(m,n)}\frac{T_{(m,n)}-T_{(m,n+1)}}{\Delta r}\right]+ \quad \text{(A3)}$$
$$\left[k_{(m,n)}A_{h(m,n)}\frac{T_{(m-1,n)}-T_{(m,n)}}{\Delta z}-k_{(m,n)}A_{h(m,n)}\frac{T_{(m,n)}-T_{(m+1,n)}}{\Delta z}\right]$$

This equation collapses to the more recognizable form of the heat equation (for k = constant) in cylindrical coordinates for the r and z dimensions:

$$\frac{\partial T}{\partial t}=\frac{\alpha}{r}\frac{\partial}{\partial r}\left(r\frac{\partial T}{\partial r}\right)+\alpha\frac{\partial^2 T}{\partial z^2} \quad \text{(A4)}$$

Latent energy mode applies to the internal PCM elements only, and only when they are undergoing phase-change. Thermal energy transfer is by conduction/diffusion between the PCM elements and other PCM elements and/or the encapsulation material elements, regardless of phase, and so normal conduction/diffusion calculations apply. However, in this mode the available latent enthalpy of a PCM element is tracked and updated at each time step. In addition, the temperature of a PCM element undergoing phase change is set to a new fixed value for each time step; this temperature is a linear value between its melting temperature T_M (the lowest temperature at which it begins to melt) and its solidification temperature T_S (the highest temperature at which it begins to solidify) based on the percentage of latent capacity remaining in that element. This calculation is shown in Equation A5. The model then simultaneously solves for the remaining unknown temperatures in the thermal store for the current time step. The final temperature field is used to calculate the net energy in to or out of each phasing PCM

element, and these values are used to update their available latent energy. New fixed temperatures for the next time step are calculated from the updated latent energy values for the phasing PCM elements. The net affect of this mode is similar to allowing the PCM to have a higher heat capacity during its latent heat phase change than during its sensible temperature change.

$$T_{(m,n)} = T_M + \left(1 - \frac{HF_p}{HF_m}\right)\left(T_S - T_M\right) \tag{A5}$$

If we consider heat transfer in the radial direction as occurring between temperature nodes, then the radial heat transfer can also be thought of as occurring across a cylinder of material with a temperature node on each surface. Integration of Fourier's law in cylindrical coordinates applied over the r dimension for this case yields Equation A6, where the effective thermal area over which the heat transfer occurs is the logarithmic mean of the surface areas associated with each temperature node [McAdams, 1942). For this reason the log mean area of each associated set of nodes is used as the effective area of thermal transfer between them for the radial direction in the discretized equations.

$$Q = kA\frac{dT}{dr} \quad \rightarrow \quad \frac{k}{\left(r_{n+1} - r_n\right)}\left(\frac{A_{n+1} - A_n}{\ln\left(A_{n+1} \big/ A_n\right)}\right)\left(T_{n+1} - T_n\right) = \frac{k}{\Delta r} A_{lm} \Delta T \tag{A6}$$

A2.4 DIFFERENCES BETWEEN THE NUMERIC MODEL AND EXPERIMENTAL APPARATUS

There are fundamental differences between the numeric model and the experimental model, with the numeric model being an idealized subset of the experiment. A schematic comparing the experimental and numeric models is found in Figure A7. To

make the two comparable - necessary for validation of the numeric model - adjustments are made to the model as described in the following paragraphs.

The experimental apparatus has a small pool of HTF at the top and bottom of the tank, as well as some water surrounding the non-active (air containing) portion of the encapsulation tubes (a total volume of approximately 1.46 liters for the 19-tube configuration), as shown in Figure A7. These water pools both delay and skew the output temperature of the tank relative to the numeric model. To compensate for these water pools, the incoming water temperature for the numeric model is pre-conditioned through the use of a separate numeric model that accounts for advection, diffusion and delay due to the HTF pools. These preconditioned temperatures are used as the input to the numeric model. To accurately account for the total energy change in the thermal store, including the energy changes associated with these water pools, the input temperatures to the preconditioning model are used for the overall energy calculations.

The numeric model is developed to simulate an idealized thermal store of any size based on a representative unit of the store. Since knowledge of the tank shell construction and size are not known, it is not considered by the base numeric model. For the case of our experimental apparatus, the construction of the shell and its impact are known with the result being a specific overall increase in the sensible heat capacity of the system. This is compensated for in the numeric model by proportionally increasing the heat capacity of the CPVC used in the encapsulation tubes, such that the net sensible energy storage in the PVC tank shell is incorporated into the total sensible energy storage of the CPVC tubes. The thermal effects of the non-PCM-containing portion of the CPVC tubes that are excluded from the numeric model are handled in the same manner.

The numeric model assumes perfect insulation, with no shell losses. However, the experimental system has limited insulation and non-negligible losses through the shell.

To compensate for this, the numeric model incorporates a loss function that is integrated with the HTF energy/temperature calculations (since the shell losses would be transferred to the HTF first). The loss rates for the experimental apparatus are determined by observing the energy loss of the experimental apparatus during steady-state operation. Losses are determined for each flow rate and test mode so that all losses – including those due to the input/output plumbing – are properly determined for each experimental run configuration. Typical loss rates noted are between 0.2 and 0.3 W/ºK.

A finite amount of time is required to shift the experiment from charge mode to discharge mode. During this time, the experimental apparatus experiences heat gain from the environment, warming the tank contents, as well as causing some thermal stratification. To compensate in the numeric model for this heat gain and stratification the model applies an initial linear gradient to the tank where the top of the tank is 0.2ºC higher than the charge temperature, while the bottom of the tank remains at the charge temperature. This approximates the average net energy gain due to losses to the environment during the time it takes to shift from charge to discharge mode, and is commensurate with the gain observed in the experimental apparatus during the mode reconfiguration process.

For validation with the experimental apparatus, each of the above adjustments are made to the numeric model and used for all simulations presented here. However, for general parametric study purposes the bare model can be used without these adjustments. The bare model is meant to be generic and not require a specific containment vessel material or insulation level.

Chapter A3: Results/Discussion

PCM testing is performed to characterize the PCM. Test runs are then performed to characterize the Nusselt number associated with convection between the HTF and the encapsulation tube surface, and to characterize the latent heat capacity of the PCM. Tests are then performed on the thermal store using multiple flow rates representative of expected loads on a per-unit basis and compared to the corresponding results of the numeric model.

A3.1 PHASE CHANGE MATERIAL TESTS

The temperature range of melting for paraffins is dependent on the method used for testing and the temperature differential or rate of change of temperature between the sample and its surroundings. The thermal storage unit described in this paper is essentially a water bath with a water temperature that varies depending on the cycle type (freeze or melt). To estimate the effective temperature ranges of freezing and melting, a sample of encapsulated PCM is placed in alternating water baths of 2 degrees Celsius (freeze cycle) and 9 degrees Celsius (melt cycle) while the temperature of the PCM sample is monitored. This temperature range was selected so as to center the thermal response near the reported melting temperature of pure tetradecane. The water bath test results for the 98.8% tetradecane used in these experiments are provided in Figure A8. These results show that the PCM freezes at between 5.6 and 5.4ºC, with a sub cooling requirement of 5.2ºC before freezing begins. The results also show that the PCM melts over a wider range of between 4.5 to 6.5ºC. The numeric model is designed to model cooling system support (and therefore the PCM melt cycle), so the melt cycle temperatures are used in the model (T_{melt} = 4.5ºC, $T_{solidify}$ = 6.5ºC) for this investigation. These temperatures are also used in the model to set the temperature of the melting PCM

as a linear function of the phase state for each PCM element.

A3.2 THERMAL STORE CALIBRATION

Calibration for the effective Nusselt number for heat transfer between the HTF and the PCM encapsulation tube is required because, while modeled as an annular-ring configuration, it is different from such in several respects. For instance, the outer ring surface is virtual, adiabatic, and is not constrained by dz/dt=0 (dz/dt equals the free stream velocity U_z at the virtual outer annular surface). In addition, the flow velocities are very low and exhibit Reynolds numbers on the order of 1, which is lower than typical correlations for annular flow.

The tank is calibrated for effective Nusselt number using a loose-packed configuration of 19 CPVC tubes, each filled with 120 ml of distilled water. The parameters used for the distilled water in its liquid state are shown in Table A2. The tank is pre-chilled to 6ºC, and then supplied HTF through the upper input at 17ºC while the output temperature is recorded. The results are used in conjunction with the numeric model to determine the effective Nusselt number for external heat convection to the PCM-containing tubes. A comparison of the experiment to the calibrated numeric model (using the adjustments to the numeric model as defined in the methods section) is shown in Figure A8. The Nusselt number is found to be approximately between 2 to 3, with 2.5 being selected for use in the numeric model.

The tank is also calibrated using 19 CPVC tubes filled with tetradecane as per the methods section. The parameters used for the tetradecane calibration are those in Table A1 for the liquid form of tetradecane. To avoid the possibility of phase change in the tetradecane, the temperature range for this test is limited to 7ºC and 17ºC. This calibration cycle also determined the appropriate Nusselt number to be approximately 2 to 3. These

results are shown in Figure A9.

In addition, the tank is calibrated for the effective value of the PCM latent heat. The tetradecane used in this experiment is 98.8% tetradecane, 0.8% tridecane, and 0.4% other impurities. However, studies have shown that small amounts of some impurities in tetradecane can reduce the latent heat of fusion (He *et al*., 1999). The PCM latent heat of fusion value is adjusted to provide the best match of the expected total energy recovery from the thermal store to the total energy actually recovered (including projected losses). Based on the recovered energy from three experimental runs (at flow rates of 100ml/min, 150ml/min, and 200 ml/min), the value of the latent heat for the PCM is estimated to be 215kJ/kg. This is only slightly lower (5%) than the 226kJ/kg expected for pure tetradecane.

A3.3 THERMAL STORE TEST RESULTS

Thermal store test results for HTF flow rates of 100ml/min, 150ml/min and 200ml/min using the 19 tube moderate density configuration are shown in Figures A10, A11 and A12. These plots include the output temperature and net % of recovered energy with respect to time (note that recovered energy includes losses through the tank wall, since it is possible to recover these losses with better insulation). The results show that for usable output temperatures of up to 6.5ºC (a minimum delta T of 4.5ºC), between 70% to 88% of total recoverable thermal storage capacity (sensible and latent) can be utilized, depending on flow rate through the tank.

The error between experimental and modeled data for the 19 tube configuration are calculated relative to the range of operation for temperature, total energy recovered, and percent of total energy recovered. Three runs at each of the experimental flow rates of 100ml/min, 150ml/min, and 200ml/min were compared to the predicted output.

Temperature measured with respect to time and compared to predicted values had differences of no more than 10.0% for all runs. The total energy recovered, calculated from HTF temperature changes, flow rates, and estimate losses, differed by no more than 2.4% between runs. When recovered energy is compared as a percentage of total recovered for the model vs. the experiment, this figure drops to 1.5%.

A3.4 DISCUSSION ON HIGH-DENSITY CONFIGURATION

Experimental runs using the 31-tube high-density configuration were inconclusive. This is because the annular ring assumption of the numeric model breaks down as the spacing between the encapsulation tubes approaches zero. The model uses the HTF trapped between the encapsulation tubes (as shown in Figure A13) to form a virtual volume for the annular ring configuration. However - unlike a true annular ring configuration - the convective heat transfer is not distributed evenly around the circumference of the encapsulation tube. Instead, the energy is concentrated near the center of the triangular-shaped HTF flow areas formed by the confluence of the encapsulation tubes, forcing the energy to be redistributed by and through the low-conductivity PCM and impeding performance of the store. Future experiments will investigate the minimum tube spacing required to support the annular ring assumption of the model, and if the difficulties encountered with the high-density configuration can be overcome by a more conductive encapsulation material or by thermal conductivity enhancements to the PCM itself.

Plots comparing the results of a high-density experimental run and the corresponding numeric model are shown in Figure A14. Previous experiments using densely packed tubes produced similar experimental results (Bourne 2014), however, there is a large discrepancy between the output temperatures of the experiment and those

predicted by the numeric model. The higher than expected output temperatures of the experiment indicate a much lower heat transfer rate than that anticipated by the numeric model, for the reasons discussed above.

A3.5 DISCUSSION ON FREE CONVECTION

The numeric model ignores the potential for internal or external free convection related to the PCM encapsulation tubes and their contents. Instead, the model uses Nusselt number and conductivity values that represent average effective heat transfer rates. The experimental and numeric results, however, indicate that free convection may play a role in overall heat transfer. This is evidenced by higher heat transfer rates early in the discharge cycle, when temperature differences between the HTF and PCM are highest, and lower heat transfer rates later in the cycle. The effective Nusselt number associated with free convection is a function of the Grashof number, which is dependent on the temperature difference between the fluid and the surface involved in convective heat transport; this could explain the discrepancies between the experiment and the numeric model results. Further experiments are required to determine when and if free convection plays a role, and whether or not it needs to be accounted for separately in the numeric model.

A3.6 EXAMPLE OF MODEL APPLICATION

The calibrated numeric model can be used to predict the performance of this thermal store. For instance, the performance of a fully charged store relative to run time, flow rate, or desired energy recovery rate can be examined. Figure A15 demonstrates this capability by plotting the predicted performance of this thermal store for these variables using typical loss rates. The model predicts that the percentage of energy recovered at output temperatures of < 6.5ºC varies nearly linearly within our expected range of

operation (0.1 L/min to 0.2 L/min).

A3.7 EXPERIMENTAL ERROR ANALYSIS

The values used in the experimental calculations and their uncertainties are shown in Table A3. The relative uncertainty for values in Table A3 that operate over a range is determined using the median value of that range. Temperature uncertainty is taken directly from thermistor manufacturer data (based on NIST certification), while energy flow uncertainty is calculated from the relevant parameters. While the relative uncertainty of the loss rate is highest (LR in Table A3), the loss rate portion of the total energy calculation is small and contributed very little to the uncertainty of the tank total energy calculations. The major contributor to uncertainty in the energy calculations is found to be the temperature differential value ΔT. The overall typical relative uncertainty of the experimental energy flow calculations is found to be approximately 4.0%.

Uncertainty in the model is driven by the calibration of the model through the manipulation of the Nusselt number (for convective heat transfer) and the conductivity of the PCM. These uncertainties exceed all other uncertainties associated with the modeling methods utilized. For example, computation grid and time step were refined to get grid and time step independent solutions, and geometry parameters were taken from ASTM standards for PVC/CPVC pipe dimensions (ASTM, 2014). The process of model calibration through the manipulation of the Nusselt number is described in the Results/Discussion, Thermal store calibration section of this paper.

A3.8 LIMITS ON MODEL APPLICATION

The model in its current form is limited to applications where it can be calibrated to a physical apparatus. This is because the model assumes that any free convection effects, either in the HTF or in the encapsulated PCM, can be adequately represented by

adjusting the constant Nusselt number and PCM conductivity values. Future research will need to expand the model by identifying when such natural convection effects become significant, and integrate their effect into Nusselt and conductivity values that vary as appropriate during runtime.

Chapter A4: Summary

This study shows that PCM-based thermal stores of this design can be used to store and recover thermal energy with a timescale and recovery rate sufficient for their use in the intended application. In addition, the investigation shows that simple, near real-time finite-volume numeric models can predict the performance of this type of thermal store with sufficient accuracy so as to allow their use in an appropriate control system. The approach of calibrating the annular ring model so that average effective convection and thermal conductivity coefficients are determined allows for simplifications that eliminate the need to account for the possibility of internal and external free convection flows. Further research is required to validate the use of the annular ring finite volume model to general thermal stores of this design, eliminating the need for calibration with a specific thermal store configuration.

It is also noted that the simplified annular ring model breaks down as the actual spacing between the encapsulation tubes approaches zero, and that a high-density hexagonal packing of the CPVC encapsulation tubes performs poorly. This is possibly the result of the lower effective convective heat transfer rate offered in this configuration, and/or the poor thermal performance of the either the PCM or the CPVC encapsulation material. Future research to improve the modeling and performance of the hexagonal-packed configuration of this thermal store will investigate how a highly conductive encapsulation material, or conductivity enhancements to the PCM itself, might improve the performance, energy storage density, and modeling capabilities of the high density hexagonal-packed configuration of this thermal store design.

A4.1 Acknowledgements

This work was funded by Pecan Street Inc. (a 501(c)3 non- profit public-private

partnership in Austin, Texas) and the University of Texas at Austin.

References

Abhat, A. 1983. “Low Temperature Latent Heat Thermal Storage: Heat Storage Materials.” Solar Energy Vol 30 (4): 313–332.

2009 ASHRAE Handbook - Fundamentals. 2009. Atlanta GA: American Society of Heating, Refrigeration and Air-Conditioning Engineers, Inc.

ASTM International. (2014). *D2846-14: Standard Specification for Chlorinated Poly(Vinyl Chloride) (CPVC) Plastic Hot-and-Cold-Water Distribution Systems*. West Conshohocken, PA.

Baetens, Ruben, Bjørn Petter Jelle, and Arild Gustavsen. 2010. “Phase Change Materials for Building Applications: A State-of-the-art Review.” Energy and Buildings 42 (9) (September): 1361–1368. doi:10.1016/j.enbuild.2010.03.026.

Bentley WG, Evelyn JC (1986). Customer thermal energy storage a marketing opportunity for cooling off electric peak demand. *IEEE Transactions on Power Systems*, 1: 57–61.

Bilir, Levent, and Zafer lken. 2005. “Total Solidification Time of a Liquid Phase Change Material Enclosed in Cylindrical/spherical Containers.” Applied Thermal Engineering 25 (10) (July): 1488–1502. doi:10.1016/j.applthermaleng.2004.10.005.

Bourne, S., Novoselac, A. Compact Phase Change Based Thermal Stores: Experimental Apparatus, Methodology, and Results. ASHRAE Winter Conference New York, ASHRAE Papers CD: 2014 ASHRAE Winter Conference, New York, NY

Cengel, Yunus A., Robert H. Turner, and John M. Cimbala. 2008. Fundamentals of Thermal-Fluid Sciences. 3rd ed. New York, NY: McGraw Hill.

Choi, Eunsoo, Young I. Cho, and Harold G. Lorsch. 1992. “Thermal Analysis of the Mixture of Laboratory and Commercial Grades Hexadecane and Tetradecane.” International Communications in Heat and Mass Transfer 19 (1): 1–15.

Dimaano, Maria Natalia R., and Takayuki Watanabe. 2002. “The Capric–lauric Acid and Pentadecane Combination as Phase Change Material for Cooling Applications.” Applied Thermal Engineering 22 (4): 365–377.

Hajiah A, Krarti M (2012a). “Optimal Control of Building Storage Systems Using Both Ice Storage and Thermal Mass – Part I: Simulation Environment.” Energy Conversion and Management (April). doi:10.1016/j.enconman.2012.02.016. http://linkinghub.elsevier.com/retrieve/pii/S0196890412000799.

Hajiah A, Krarti M (2012b). optimal controls of building storage systems using both ice storage and thermal mass—Part II: parametric analysis. *Energy Conversion and Management*, 64: 509–515. doi:10.1016/j.enconman.2012.02.020.

Hale, D, M Hoover, and M O'Neill. 1971. "Phase Change Materials Handbook". United States. http://hdl.handle.net/2060/19720012306.

He, Bo, E. Mari Gustafsson, and Fredrik Setterwall. 1999. "Tetradecane and Hexadecane Binary Mixtures as Phase Change Materials (PCMs) for Cool Storage in District Cooling Systems." Energy 24 (12): 1015–1028.

He, B, V Martin, and F Setterwall. 2004. "Phase Transition Temperature Ranges and Storage Density of Paraffin Wax Phase Change Materials." Energy 29 (11) (September): 1785–1804. doi:10.1016/j.energy.2004.03.002.

Humphries, William, and Edwin Griggs. 1977. "A Design Handbook for Phase Change Thermal Storage Control and Energy Storage Devices". National Aeronautics and Space Administration Scientific and Technical Information Office. http://hdl.handle.net/2060/19780007491.

Ismail, K.A.R., and M.M. Goncalves. 1999. "Thermal Performance of a PCM Storage Unit." Energy Conversion and Management 40: 115–138.

Ismail, K.A.R., and R.I.R. Moraes. 2009. "A Numerical and Experimental Investigation of Different Containers and PCM Options for Cold Storage Modular Units for Domestic Applications." International Journal of Heat and Mass Transfer 52 (19-20) (September): 4195–4202. doi:10.1016/j.ijheatmasstransfer.2009.04.031.

Jesumathy, Stella P., M. Udayakumar, and S. Suresh. 2012. "Heat Transfer Characteristics in Latent Heat Storage System Using Paraffin Wax." Journal of Mechanical Science and Technology 26 (3): 959–965.

Jiji, Latif M., and Salif Gaye. 2006. "Analysis of Solidification and Melting of PCM with Energy Generation." Applied Thermal Engineering 26 (5): 568–575.

Kousksou, T., A. Jamil, T. El Rhafiki, and Y. Zeraouli. 2010. "Paraffin Wax Mixtures as Phase Change Materials." *Solar Energy Materials and Solar Cells* 94 (12): 2158–65.

Li, Gang, Yunho Hwang, and Reinhard Radermacher. 2012. "Review of Cold Storage Materials for Air Conditioning Application." International Journal of Refrigeration 35 (8): 2053–2077.

Masters, Gilbert M. 2004. Renewable and Efficient Electric Power Systems. Hobnoken, NJ: John Wiley & Sons, Inc.

McAdams WH (1942). Heat Transmission, 2nd edn. New York: McGraw-Hill.

Regin, A. Felix, S.C. Solanki, and J.S. Saini. 2008. "Heat Transfer Characteristics of Thermal Energy Storage System Using PCM Capsules: A Review." Renewable and Sustainable Energy Reviews 12 (9) (December): 2438–2458. doi:10.1016/j.rser.2007.06.009.

Shamsundar, N, and Sparrow, E.M. 1975. “Analysis of Multidimensional Conduction Phase Change Via the Enthalopy Method”. ASME. http://heattransfer.asmedigitalcollection.asme.org.ezproxy.lib.utexas.edu/article.aspx?articleid=1436183.

Trip Doggett. 2013. “ERCOT - A Strategic View of the Future” presented at the Gulf Coast Power Association Fall Annual Conference, October 2. http://www.ercot.com/content/news/presentations/2013/GCPA - 02 Oct 2013 FINAL.pdf.

U.S. Census Bureau. 2013. American Housing Survey for the United States: 2011. U.S. Government Printing Office. https://www.census.gov/content/dam/Census/programs-surveys/ahs/data/2011/h150-11.pdf

U.S. Energy Information Administration. 2006. “Commercial Building Energy Consumption Survey”. U.S. Energy Information Administration. http://www.eia.gov/consumption/commercial/about.cfm.

U.S. EIA Energy Information Administration. "Frequently asked Questions: How much electricity is used for cooling in the United States?”. 21 Jan 2012. [Accessed 10 Mar 2013]. http://www.eia.gov/tools/faqs/faq.cfm?id=98&t=3

U.S. Energy Information Administration. 2013. Annual Energy Outlook 2013. Washington D.C.: U.S. Energy Information Administration. http://www.eia.gov/forecasts/aeo/pdf/0383(2013).pdf.

Wattles P (2011). ERCOT Demand Response—Overview and Status Report. Available at http://www.ercot.com/content/meetings/dswg/keydocs/2011/0830/3_ERCOT_presentation_workshop_083011. pdf.

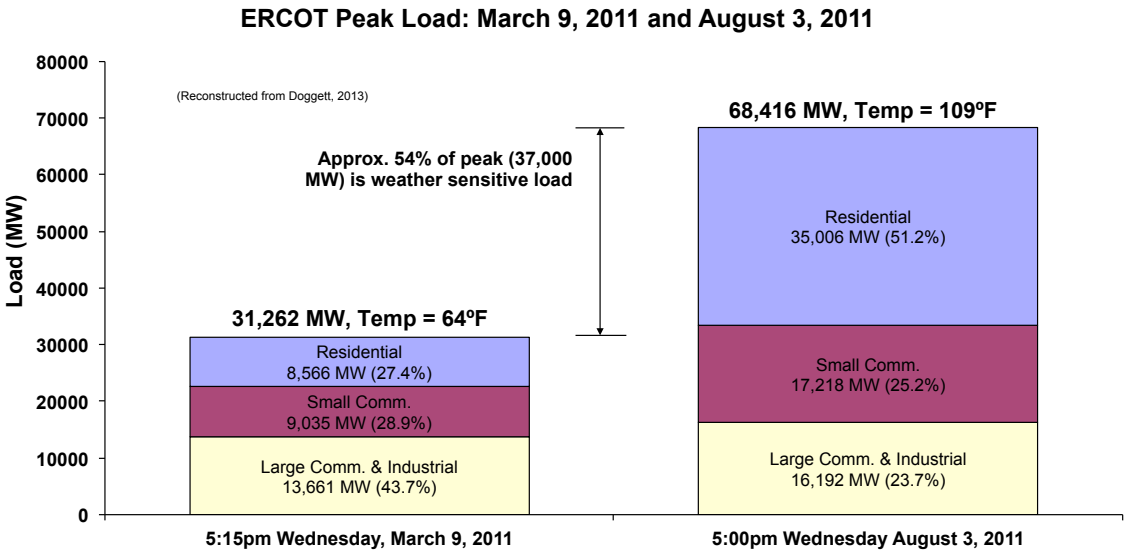

Figure A1: Extrapolated impact of weather on electric peak loads in Texas [Doggett, 2013]. Note that the increase in peak power use due to weather-sensitive load is primarily due to an increase in energy use by residential customers.

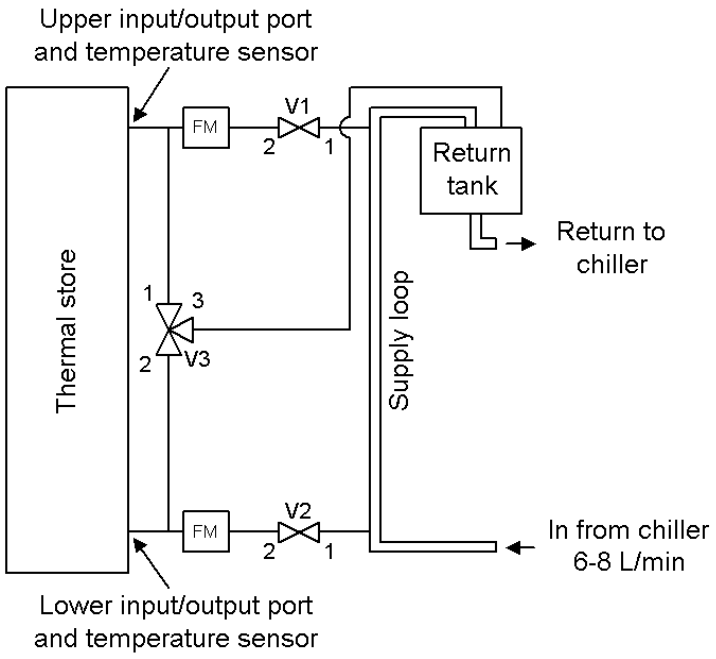

Figure A2: Schematic of the test tank and its connections. Note that two modes of operation are possible: Charge mode with V1 closed, V2 open, and V3=1-3; or discharge mode with V1 open, V3 closed, and V3=2-3. The supply loop delivers a constant flow rate of 6 to 8 liters/minute so that the temperature in the loop is constant, and so that the supply links to the tank are as short as possible. The return tank is open to allow for flow rate confirmation by direct measurement.

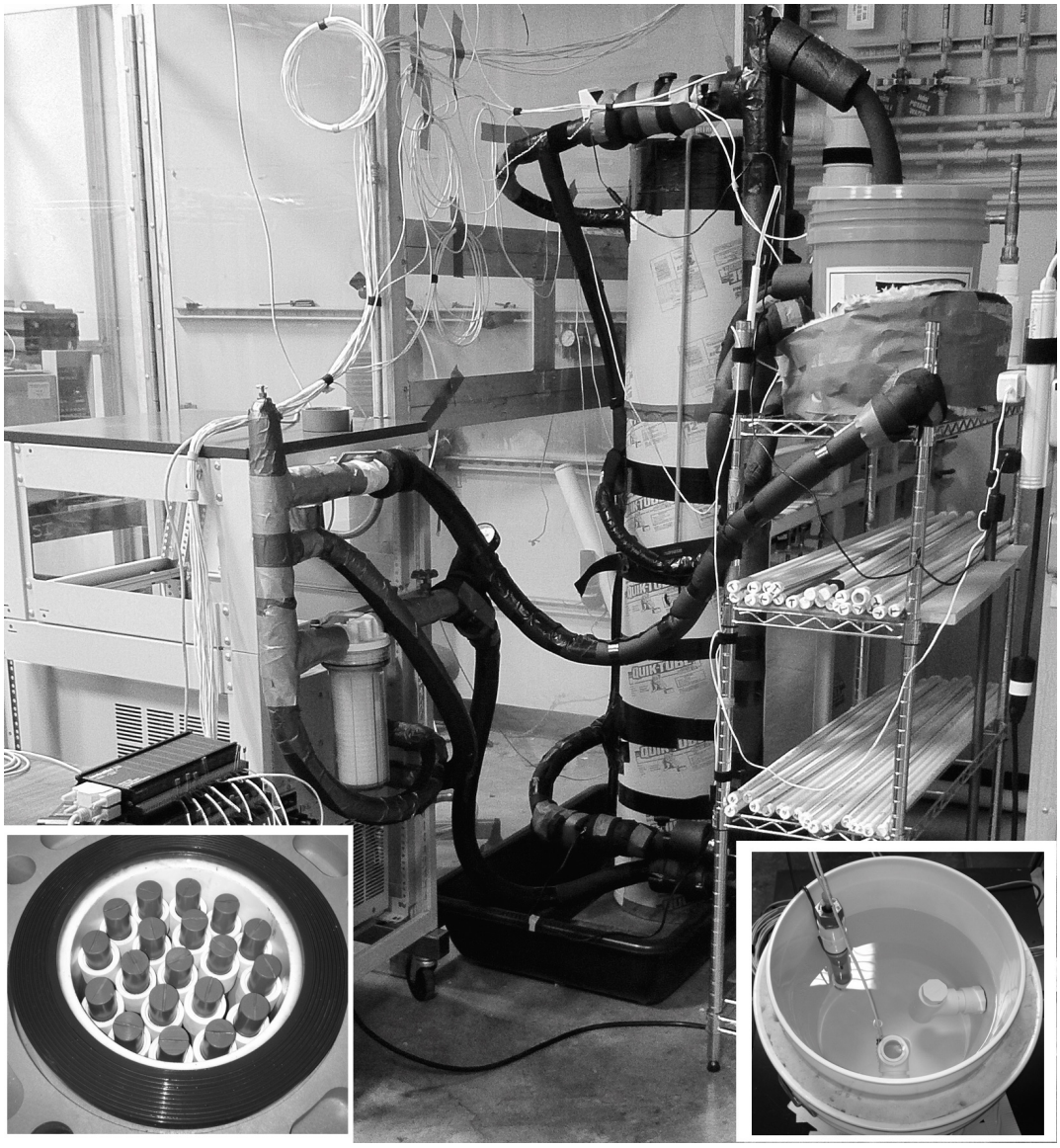

Figure A3: This picture of the apparatus shows the chiller, thermal store, and the return tank (see Figure 5 for more information). The chiller supplies the heat transfer fluid loop, which terminates in the return tank located on the wire rack. The thermal store draws chilled water from the loop, either to the bottom (charge cycle) or top (discharge cycle) of the tank and outputs it to the return tank, where the flow rate can be measured and used to calibrate to the flow meters before and after each run. The inset on the right shows the water bath tank; the inset on the left shows the 9-tube packing arrangement.

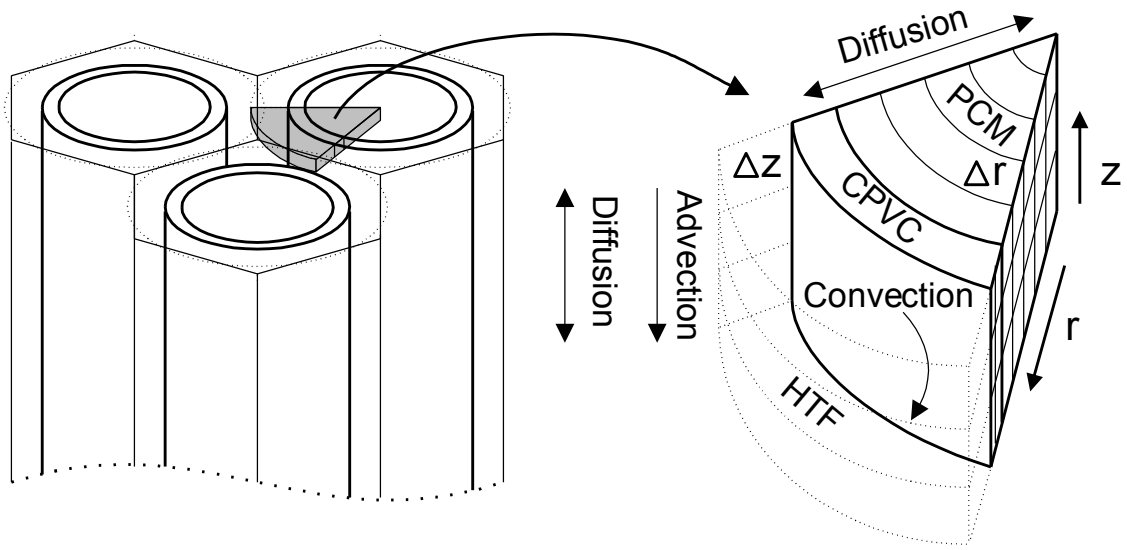

Figure A4: Elements, dimensions, and heat transfer considerations of the initial numeric model. PCM is encapsulated in CPVC tubes, which are then packed into a larger containment tank at regular spacing intervals. The tube count, radius, spacing and length all affect thermal performance of the store. Note that the hexagonal annular cylinder is replaced by an equivalent cylindrical form, the radius of which is based on the number of tubes and the total cross-sectional free area of the tank.

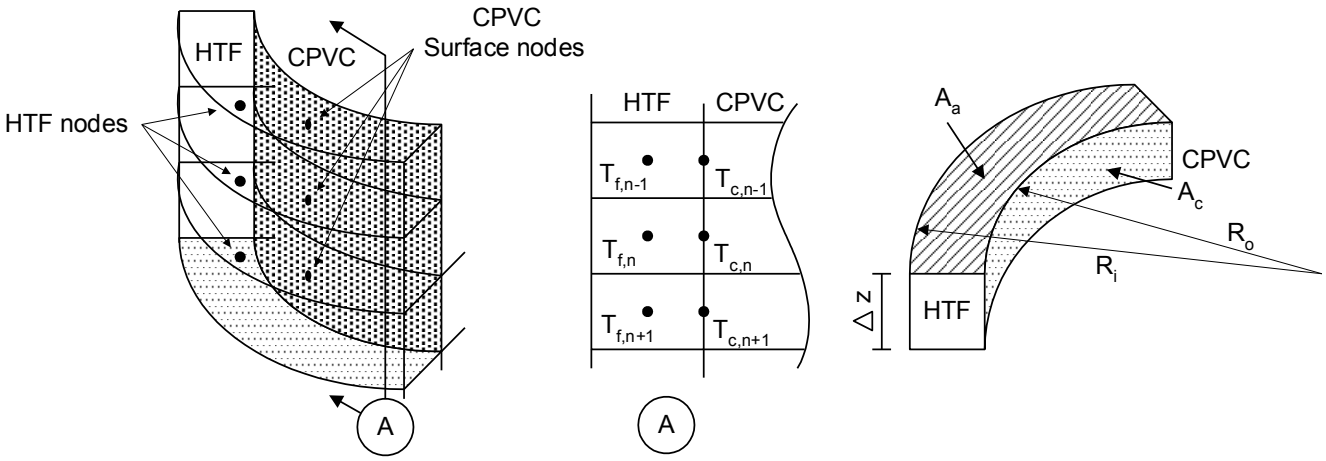

Figure A5: Geometry and nodes for advection-convection-diffusion energy balance equations. This represents advection due to HTF flow, forced convection between the HTF and the surface of the CPVC encapsulation tubes, and vertical diffusion in the HTF.

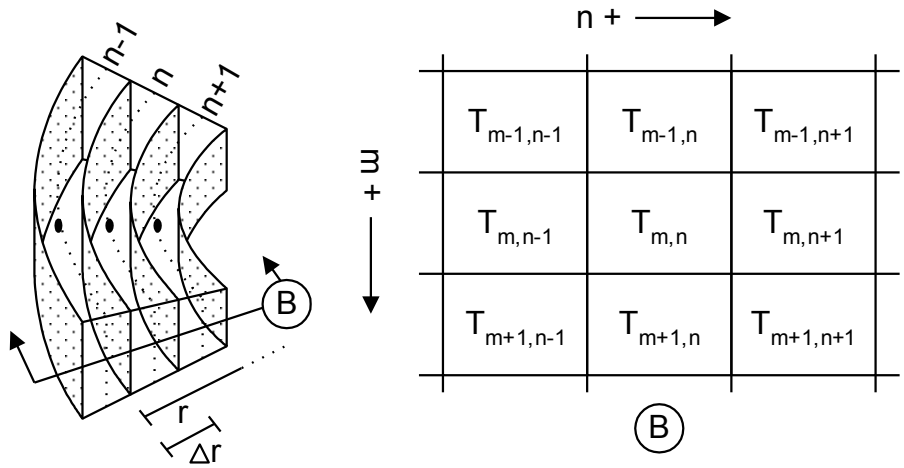

Figure A6: Internal conduction nodes and numbering scheme. This represents the system of nodes used to calculate the temperature and energy exchange within the PCM and encapsulation tubes due to diffusion through the materials.

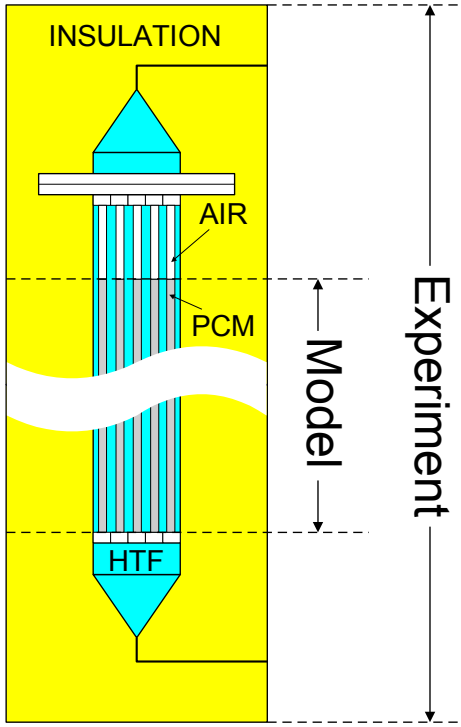

Figure A7: Schematic of the experimental apparatus vs. the numeric model. Note that the basic numeric model does not include the water pools at the top or bottom of the experiment, nor does it include the thermal mass of the PVC tank shell or fixtures. The basic numeric model is only concerned with the portion of the thermal store that contains PCM-filled CPVC tubes and the surrounding HTF. The portion of the encapsulation tubes that contain air is also excluded from the basic numeric model.

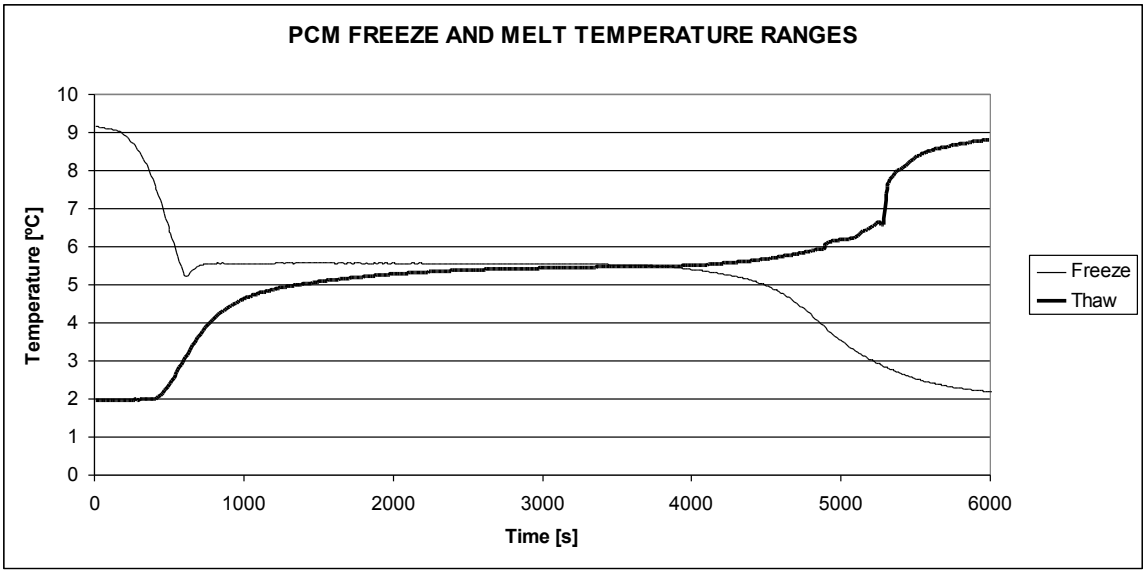

Figure A8: Freeze/melt performance of 99% Tetradecane. The freeze curve is nearly flat, with freeze occurring between 5.6 and 5.4ºC. Note the sub cooling to 5.2ºC before freezing occurs. The melt cycle occurs over a wider temperature range of between 4.5 and 6.5ºC. Water bath temperatures are 2ºC and 9ºC for the freeze and melt cycles, respectively.

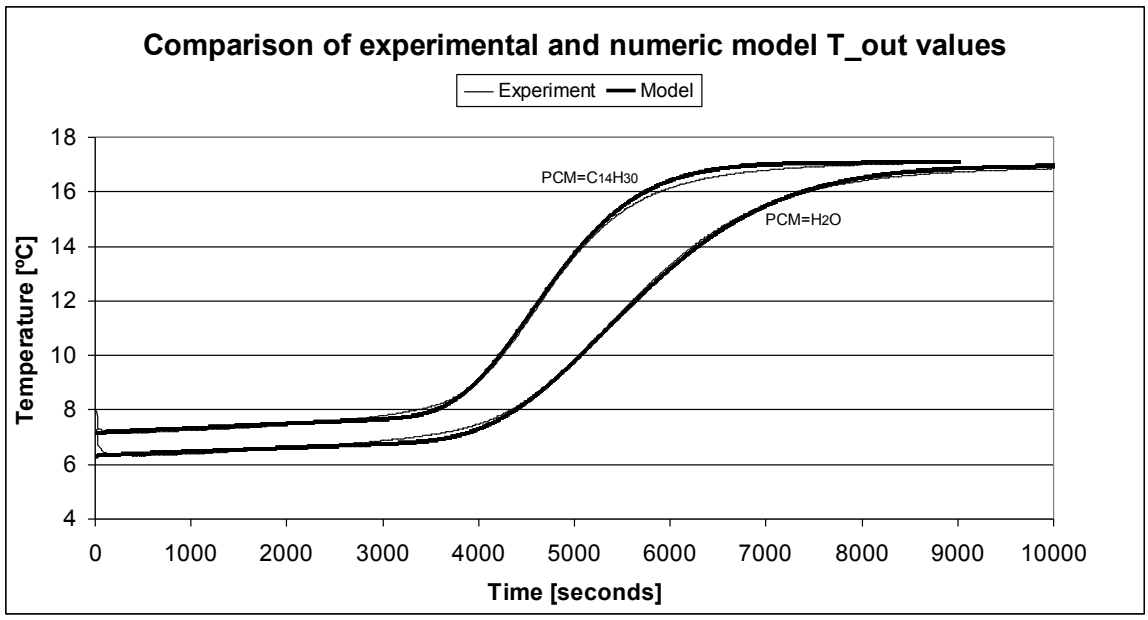

Figure A9: Comparison of experimental and model output temperatures in sensible storage mode. Both water and tetradecane filled encapsulation tubes were used for these results. The Nusselt number was set at 2.5 to generate the numeric model data. Corrections are applied to the numeric model as detailed in the Methods section to compensate for the fundamental differences between the idealized model and the actual experiment.

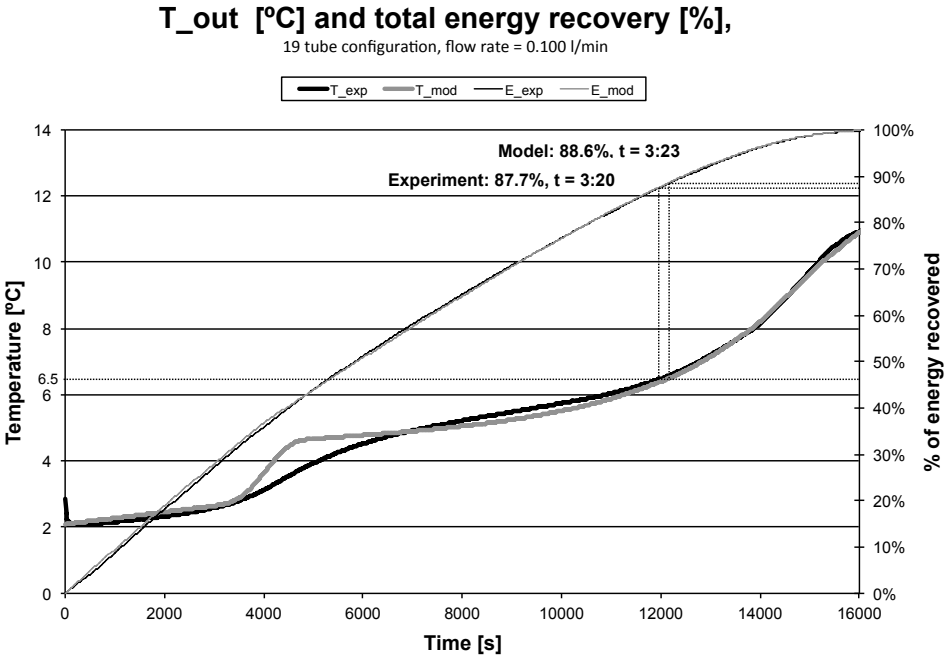

Figure A10: Output temperature and energy recovery with respect to time for both the experiment and numeric model at a flow rate of 100ml/min. The percentage of total energy recovered while the output temperature is less than or equal to 6.5ºC is identified. Total energy recovered includes losses, which can be captured through the use of higher insulation levels.

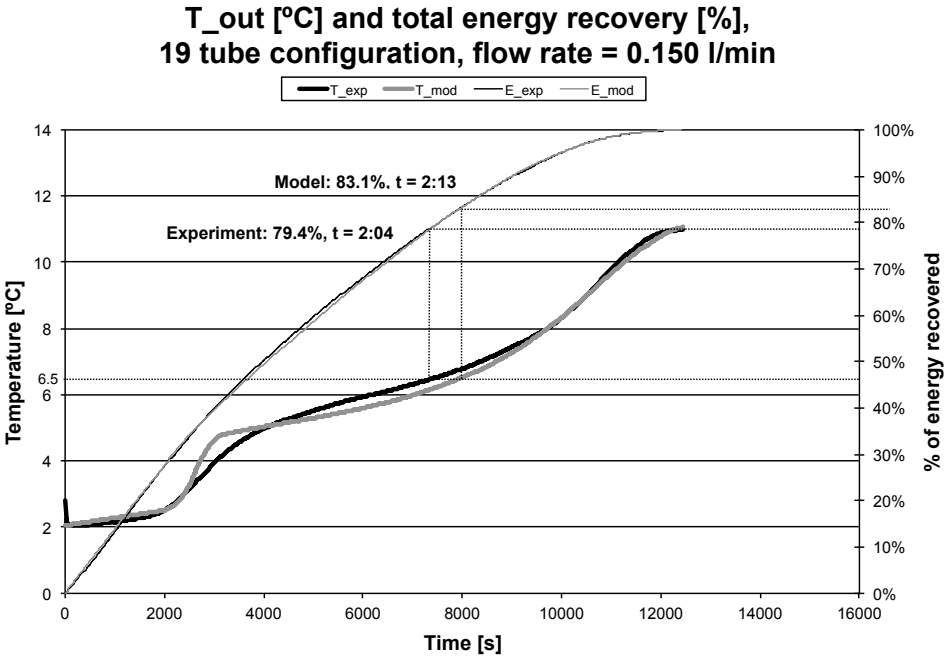

Figure A11: Output temperature and energy recovery with respect to time for both the experiment and numeric model at a flow rate of 150ml/min.

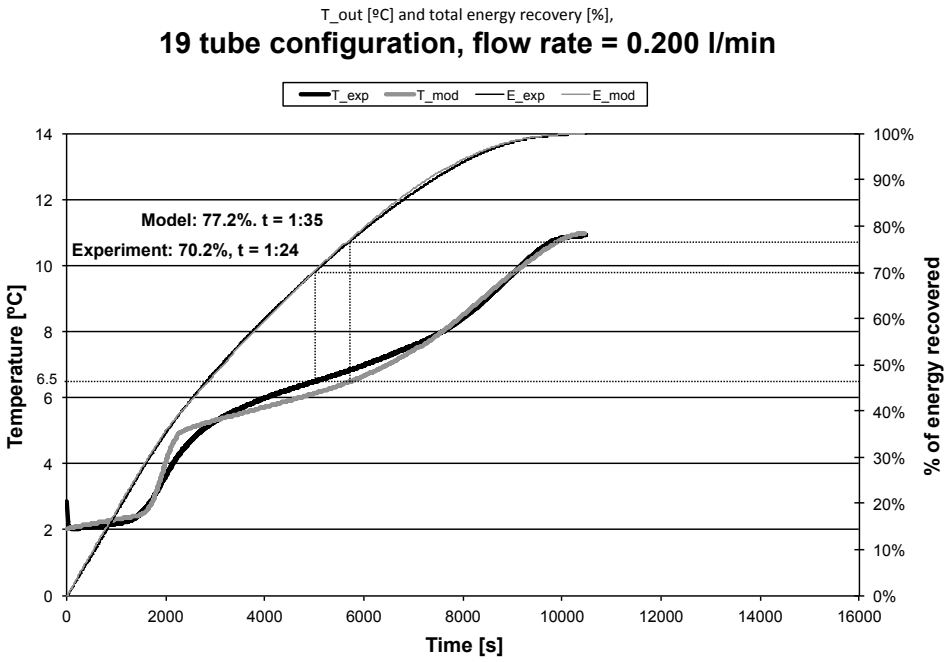

Figure A12: Output temperature and energy recovery with respect to time for both the experiment and numeric model at a flow rate of 200ml/min.

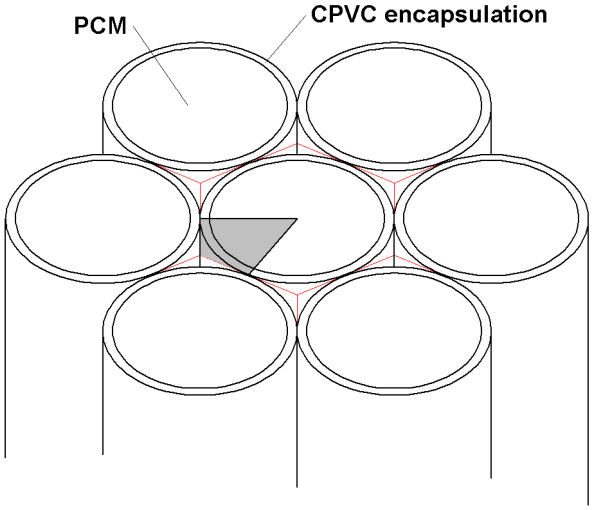

Figure A13: An example of the high-density hexagonal packed PCM encapsulation tube arrangement. Note that the 60º element of the numeric model (in gray) still applies for this configuration. Also note the triangular-shaped HTF flow paths formed by the confluence of the PCM encapsulation tubes.

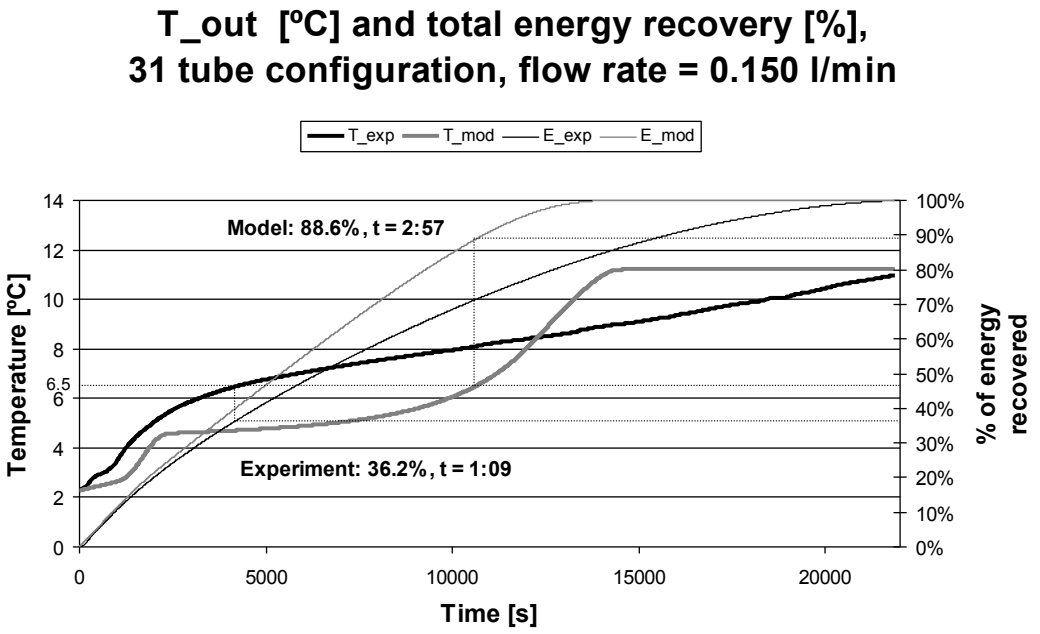

Figure A14: This plot shows the difference between the experiment and numeric model data for a high-density hexagonal packed configuration of 31 PCM encapsulation tubes. Note the large discrepancy between the temperature and energy plots, indicating that the numeric model breaks down as the encapsulation tubes become more closely spaced. Future research will investigate the minimum spacing required to support the annular ring assumption of the numeric model.

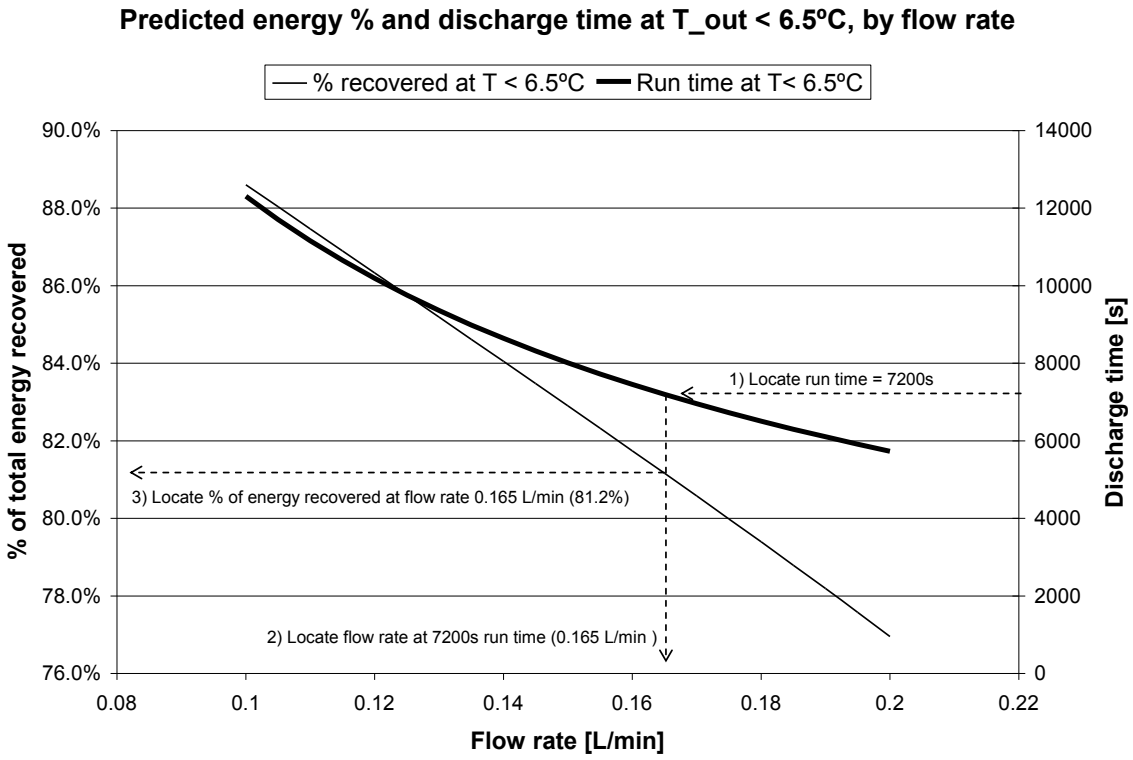

Figure A15: Performance for full discharge cycles, as predicted by the numeric model. This figure shows how the maximum energy recovery (as a percentage of total recoverable energy) relates to flow rate and run time. The plots here can be used to determine optimal run parameters. For example, for a run time of 2 hours (7200 seconds) the optimal flow rate is 0.165 L/min, which results in a predicted energy recovery of 81.2% of total recoverable energy.

Property	Value	Test condition	Source
Freezing temperature	5.5ºC	N/A	Hale et al, 1971
Density (solid)	825 kg/m^3	4ºC	
Density (liquid)	771 kg/m^3	10ºC	
Latent heat	226 (kJ/kg)	(Based on liquid density)	
Conductivity	0.15 W/(m ºK)	20ºC	Kousksou, 2010
Heat capacity (solid)	1.68 kJ/(kg ºK)	-20 to 0ºC	
Heat capacity (liquid)	2.18 kJ/(kg ºK)	25ºC	
Heat capacity (T-avg)	1.99 kJ/(kg ºK)	2ºC – 11ºC	(calculated)

Table A1: Properties of pure Tetradecane

Property	Value	Conditions	Source
Density	1000 kg/m^3	12ºC	Incropera, 2007
Conductivity	0.590 W/(m ºK)		
Heat capacity	4.189 kJ/(kg ºK)		

Table A2: Properties of distilled water at 12ºC

Description	Symbol	Value or range	Error	Relative*	Units	Source
Temp	T	2 - 11 °C	0.1	1.5%	C	Supplier
Ambient Temp	T_{amb}	23	1	4.0%	C	Measured
T_{in} - T_{out}	ΔT	0 - 9 °C	0.14	3.1%	C	Calculated
Flow rate	F_{lpm}	0.100 - 0.200	0.003	2.0%	L/min	Measured
Density, HTF	ρ_w	1036	3	0.3%	kg/m^2	ASHRAE
Heat capacity, HTF	C_w	3750	50	1.3%	J(kg K)	
Loss rate	LR	0.2 - 0.3	0.05	20.0%	W/K	Measured
Overall (energy calculations)				4.0%		

* The relative error for parameter values given as a range is calculated at the median value.

Table A3: Experimental uncertainty values

Appendix B

PAPER 2: IMPROVED PERFORMANCE IN TUBE-ENCAPSULATED PHASE CHANGE THERMAL ENERGY STORES FOR HVAC APPLICATIONS

Stephen Bourne, Atila Novoselac (graduate advisor)

(Published in Building and Environment, 2015: DOI 10.1016/j.buildenv.2015.12.023)

ABSTRACT

Thermal energy stores can be used to shift building peak electric loads for cooling to off-peak hours. Compact, high-density thermal storage solutions are required for buildings that may not have the space necessary for typical thermal storage systems, such as chilled water tanks. Previous studies show that latent thermal stores using polymer tube-encapsulated paraffin-based phase change materials (PCM) yield acceptable thermal performance at low to moderate encapsulation tube packing densities, but that thermal performance falls as tube packing densities climb due to increasingly restricted heat transfer fluid (HTF) flow paths. This paper reports the experimental results found when using a highly conductive encapsulation material to redistribute the thermal energy around the PCM, mitigating the effect of the restricted HTF flow paths and enabling maximum encapsulation tube packing densities. These experiments show a more than two-fold increase in the percentage of recoverable thermal energy over a similar polymer tube based system, providing thermal performance comparable to that of a low density polymer tube encapsulation system while increasing PCM capacity by 111%. Test results are provided in a format suitable for estimating design criteria for larger thermal stores, and a design parameter – the resistance ratio – is proposed to assist in optimizing encapsulation tube parameters.

Keywords: phase change material (PCM), thermal storage, encapsulation

LIST OF SYMBOLS

Symbols

A	*Area (general) [m²]*
A_c	*Surface area associated with convection [m²]*
A_t	*Cross-sectional area associate with conduction along the encapsulation tubes [m²]*
A_p	*Area associated with conduction between the encapsulation tube and the PCM [m²]*
Bi	*Biot number*
C	*Constant associated with the geometry of hexagonal packed cylinders*
C_f	*Specific heat of heat transfer fluid [J/(kg ·ºK]*
D_h	*Hydraulic diameter (four times the area divided by the wetted perimeter) [m]*
E_{lat}	*Total latent energy in the thermal store [J]*
E_{rec}	*Fraction of total (latent and sensible) energy recovered during a discharge cycle*
E_{sen}	*Total sensible energy in the thermal store [J]*
k	*Conductivity (general) [W/(m · °K)]*
k_f	*Conductivity of the heat transfer fluid (35% propylene glycol and water) [W/(m · °K)]*
k_p	*Conductivity of the PCM (tetradecane) [W/(m · °K)]*
k_t	*Conductivity of the encapsulation tube material [W/(m · °K)]*
K_r	*Dimensionless ratio of the net effective conductivity between adjoining materials*
h	*Thermal convection coefficient [W/(m² · ºK]*
L	*Arbitrary length constant [m]*
L_k	*Characteristic length of conduction into a cylinder; used for Biot number [m]*
L_p	*Length constant associated with conduction into a cylinder (r/2) [m]*
Lt	*Length constant associated with conduction around the cylinder (rø) [m]*
m	*Mass flow rate [kg/s]*
Nu	*Nusselt number*
r_i	*Inside radius of the encapsulation tubing [m]*
r_o	*Outside radius of the encapsulation tube [m]*
R_c	*Resistance of convection between the HTF and the encapsulation tube [ºK/W]*
R_k	*Resistance to conductivity in a cylinder (Biot number example) [ºK/W]*
R_p	*Resistance of conduction between the PCM and the encapsulation tube [ºK/W]*
R_r	*Ratio of the average radius of the encapsulation tube to the tube wall thickness*
R_t	*Resistance of conduction around the encapsulation tube over length L_t [ºK/W]*
Q	*Volume flow rate of heat transfer fluid [liters/min]*
t	*Time [s]*
T	*Temperature (general) [ºC or ºK]*
T_p	*Average (expected) temperature of the frozen PCM [ºC]*
T_∞	*Free-stream temperature of the HTF [ºC]*
T_{amb}	*Ambient temperature [ºC or ºK]*
T_{avg}	*Time-averaged output temperature*

Subscripts

p	*PCM parameter*
f	*Heat transfer fluid (HTF) parameter*
t	*Encapsulation tube parameter*

Chapter B1: Introduction

Commercial and residential buildings consume more than 40% of the primary energy used in the United States, including 70% of all U.S. electricity [1]. Overall, 11% of electricity is used for environmental cooling applications in the U.S. [2]. The amount of electricity used for environmental cooling in

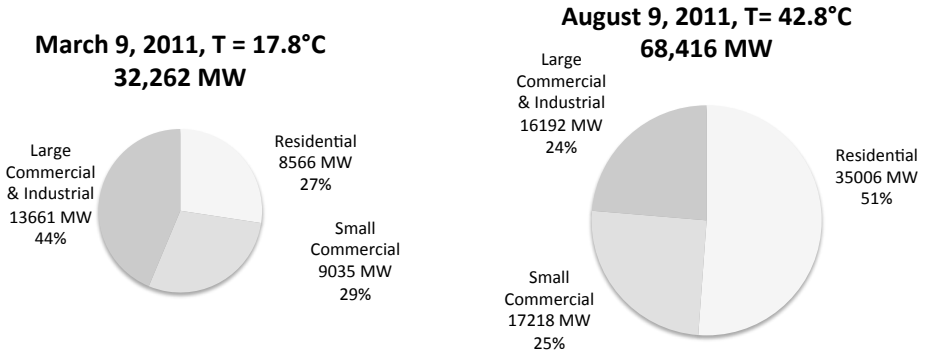

Figure B1: Extrapolated impact of weather on peak electric loads in Texas [Doggett, 2013]. T = outdoor temperature in °C. Note that the increase in peak power use resulting from weather-sensitive load is primarily due to an increase in energy use by residential customers, ostensibly associated with HVAC use.

the warmer southern climates of the U.S. can rise substantially above this average; it has been estimated that more than 20% of the annual electric consumption for residential buildings in the southern census region of the United States is used for cooling applications, and can go as high as 27% of annual electric load in the hot and humid climate of Florida [3]. As shown in Figure B1, when concentrated into the summer cooling season weather-sensitive loads such as these can exceed 50% of peak summer electric demand [4]. Furthermore, the demand for residential and commercial cooling is expected to increase due to an ongoing shift in population towards warmer regions of the country [5].

The ability to shift peak cooling loads to off-peak periods, when existing

underutilized base load generation capacity is available, can reduce the cost of electric power and improve returns on electric generation capital equipment investments [6]. Shifting of these cooling loads to periods of renewable energy availability can also mitigate the uncertainty in power generation accompanied by the increased use of intermittent renewable energy sources such as wind and solar power, while making better use of these renewable energy systems [7].

Actively-controlled thermal energy stores can provide the means to time-shift building cooling loads. An active thermal storage system works like a thermal battery, charging during periods of low electricity costs or high availability and discharging when electricity is scarce or expensive. These storage systems can be particularly effective at reducing peak energy demand and overall building energy costs for environmental systems when utility peak demand and/or time-of-day electric rates are in place [8,9]. A properly-sized thermal storage system can also reduce the required size and peak capacity of environmental cooling equipment, and thus reduce capital equipment costs, since the capacity of the equipment need only meet average rather than peak demand rates [10].

Water-glycol mixtures are a popular material used to store thermal energy in sensible form (as a change in temperature of a storage medium) since it has a relatively high heat capacity of between 3.7 and 4.2kJ/(kg*K) depending on composition [11]. In addition, Water-glycol based hydronic cooling systems are common [12], making integration of this type of thermal store with existing cooling systems simple and cost effective. However, the necessary chilled water tanks are large; while new buildings can be designed around such tanks, existing buildings may not have the space necessary to add a sensible chilled water thermal storage system. Given the long lifespan of existing residential and commercial structures (the median age of residential and commercial buildings in the U.S. is approximately 37 and 28 years, respectively [13,14]), the ability

to retrofit thermal storage to existing buildings must be considered. For these retrofit applications, smaller, more compact high-density thermal stores may be required.

Such high density thermal stores can be developed using materials that store thermal energy in latent form, during a change in phase - for instance, from liquid to solid or gas to liquid - instead of in sensible form. Latent energy storage is characterized by a large enthalpy change at a constant (or with only a small change in) temperature. The result is that latent (phase change) systems can store thermal energy at a density an order of magnitude greater than that of a sensible (temperature change) system. For example, a chilled water system using a 35% propylene glycol to water ratio operating over a 9°C temperature range can store approximately 32.1 kJ/kg, while a water-based ice thermal storage system can store upwards of 330kJ/kg at a near-constant temperature of 0°C [15].

Many materials can be used for latent thermal energy storage. These materials are collectively known as PCMs, or phase change materials. Typical PCMs suitable for use in environmental control thermal storage applications are generally restricted to liquid-solid phase changes for volumetric efficiency and ease of use [16]. While some liquid-gas phase transitions have high gravimetric thermal capacity, their volume changes and required operating pressures make them difficult to utilize [17]. Common liquid- solid phase PCMs include water (ice), organics such as paraffins or fatty acids, and salt hydrates [18-21].

Water as ice has successfully been used for years as a phase change thermal storage medium (i.e., the “icebox” from years past). However, water expands when frozen making containment difficult during phase cycling. In addition, water freezes at a temperature significantly lower than the 5-12°C typically used for HVAC systems, requiring a separate chiller system for ice-based thermal storage and increasing overall HVAC system installation and operation costs [22,23]. Salt hydrates are caustic, tend to

need subcooling (a requirement that they be cooled below their freezing point before crystallization is initiated), and suffer from phase segregation over repeated freeze-thaw cycles that limit their useful lifespan [24]. Paraffins and fatty acid hydrocarbons offer relatively high heats of fusions (~200kJ/kg), chemical stability, no subcooling (self-nucleating), do not degrade with thermal cycling, are available in temperature ranges suitable for HVAC applications, and are compatible with most encapsulation materials [25-28]. They also tend to have poor thermal conductivity and are somewhat flammable, but these issues can be mitigated by thermal system design. The paraffin compound tetradecane shows promise for use in active cold thermal storage systems, as it has a phase change temperature suitable for environmental cooling use of between approximately 5.5 and 5.8°C and a heat of fusion of approximately 215kJ/kg [20,29].

A previous study has demonstrated that latent thermal stores constructed of tube-encapsulated paraffin-based PCMs show improved thermal storage densities over conventional sensible chilled water tanks [30]. Tube encapsulation is selected because it allows for a greater PCM density than spherical encapsulation; cylinders have a maximum packing density of 90.7% versus only 74.0% for spheres. In these experiments CPVC encapsulation tubes containing tetradecane as a PCM are packed into a tank in a pseudo-annular ring configuration, where the tubes are spaced such that each is surrounded by HTF (heat transfer fluid) that flows longitudinally along the vertically oriented encapsulation tubes. This configuration results in two dimensional heat transfer, in the r and z directions, within the encapsulation tubes and PCM. The study found that - when using laminar HTF flow at moderate encapsulation tube densities, where the cross sectional area of the encapsulation tubes equaled approximately half of the cross sectional area of the tank - this configuration allowed for approximately 80% of thermal store capacity to be recovered over a two hour period at an output temperature of < 6.5°. This

performance level is acceptable for reducing peak cooling loads, which typically occur over a 2 to 6 hour period.

However, as the packing density of the CPVC PCM encapsulation tubes reaches their maximum and the tubes assume a hexagonal-packed configuration, the annular flow path is reduced to six shared roughly triangular-shaped flow paths around each tube as shown in Figure B2. While Nusselt number correlations exist for triangular pipe flow, these are average values; the convective heat transfer is not the same everywhere along the surface of the tubes due to the restricted fluid flow near the apexes of each triangular flow path. This causes the HTF flow to be unevenly distributed around each encapsulation tube, resulting in uneven thermal energy distribution to and into the encapsulation tubes. This forces the encapsulation tube material and PCM to redistribute the thermal energy around and into the PCM. Both the CPVC and PCM used by Bourne and Novoselac [30] have poor thermal conductivity, resulting in unacceptable thermal performance for the hexagonal packed configuration.

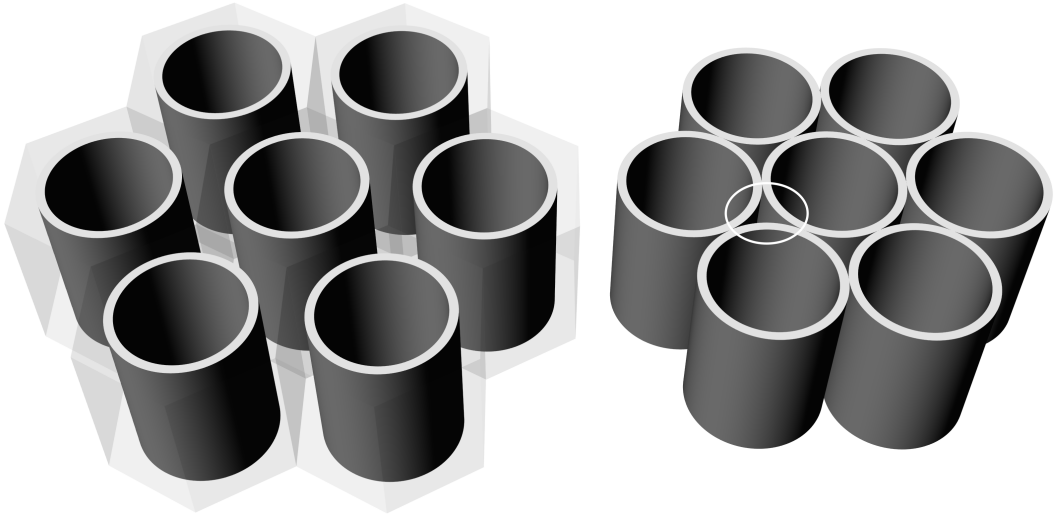

Figure B2: Spaced vs. hexagonal-packed encapsulation tubes. The concentric hexagonal cylinders surrounding the spaced tubes represent the area available for HTF flow. For the hexagonal packed tubes, the area for HTF flow is limited to the indicated triangular-like areas formed by the confluence of the tubes.

One method for resolving the poor performance of the hexagonal packed configuration is through the use of PCM conductivity enhancements. Previous studies have investigated the use of internal PCM conductivity enhancements, such as metallic foam or stainless steel lessing rings, to improve the effective conductivity of the PCM [31-33]. However, these methods add cost and reduce the PCM capacity of the thermal storage system by between 10 and 20%. In addition, the experiments of Bourne and Novoselac [30] indicate that the paraffin PCM Tetradecane does have sufficient conductivity for the intended application, so long as the thermal energy is evenly distributed around small encapsulation tubes. This suggests that another potential solution is the use of a highly conductive encapsulation shell material to redistribute the thermal energy around the PCM and restore the two-dimensional (in r and L) heat transfer paradigm of the evenly-spaced pseudo annular ring packing configuration.

This study investigates the use of a highly conductive tube material as a means to redistribute thermal energy around the encapsulation tubes and into the PCM, restoring the even thermal distribution of the pseudo annular ring configuration while allowing for a higher-density hexagonal-packed configuration. A design parameter based upon a modified Biot number is proposed as a means of confirming the necessary physical properties for the PCM encapsulation tubes (size, thickness, and thermal conductivity), which can be used by designers to optimize the performance and cost of thermal stores of this type. Experiments are conducted using a densely-packed configuration of metallic encapsulation tubes, and the results compared to a previous study that used CPVC encapsulation.

The Methods section describes the development of the design parameter for encapsulation tube specifications. This section also describes the heat transfer fluid (HTF) and PCM used, the encapsulation tube type, the thermal store tank into which the

encapsulation tubes are packed, the ancillary equipment and materials used for the thermal store apparatus, and the procedure used for testing. Test results, as well as a comparison to previous tests using CPVC encapsulation tubes [30], are given in the Results section. Recommendations for application of this store design, typical parameters, and future research are given in the Discussion section.

Chapter B2: Methods

An experimental thermal store design is constructed utilizing a PCM encapsulated in metallic cylindrical tubes and loaded into an insulated PVC tank in a dense hexagonal-packed configuration. The physical properties of the encapsulation tubes are chosen so as to meet the conditions prescribed by a design parameter proposed herein. The thermal performance of this configuration is tested by charging and discharging the thermal storage unit while monitoring the temperature of the HTF (heat transfer fluid) as it passes in and out of the thermal store. The results are compared to previous experiments that used the same PCM & tank design but a different encapsulation material.

B2.1 PHASE CHANGE MATERIAL (PCM)

The PCM used in these experiments is Tetradecane, a paraffin. The properties of pure Tetradecane, taken from the literature (as referenced in the table), are shown in Table B1.

Property	Value	Condition	Source
Freezing temperature	5.5ºC	N/A	
Density (solid)	825 kg/m^3	4ºC	
Density (liquid)	771 kg/m^3	10ºC	Hale et al, 1971 [20]
Latent heat	226 (kJ/kg)	(liquid)	
Conductivity	0.15 W/(m ºK)	20ºC	
Heat capacity (solid)	1.68 kJ/(kg ºK)	-20 to 0ºC	Kousksou et al. 2010 [34]
Heat capacity (liquid)	2.18 kJ/(kg ºK)	25ºC	
Heat capacity (T-avg)	1.99 kJ/(kg ºK)	2ºC – 11ºC	(calculated)

Table B1: Properties of pure Tetradecane

A laboratory grade product of approximately 99% purity is selected over a technical grade product of 95% due to previous experiments, conducted by Bourne and Novoselac [35], that suggested a lowering of the freeze point to an unacceptable level was due to impurities in the technical grade product. This observation is supported by a previous studies [10] [36] conducted by using binary mixtures of tetradecane and

hexadecane, which showed that a few percent of hexadecane in tetradecane could drop the freeze point by several degrees.

Paraffin-based PCMs can melt over a temperature range, rather than at a distinct fixed temperature [37]. Previous experiments by Bourne and Novoselac [30] utilizing 99% tetradecane as a PCM in a similar thermal store design have determined that the melting temperature range in this application is between approximately 4.5 and 6.5°C. This is an important consideration when designing a PCM-based thermal store; if the necessary output temperature is too low, then the thermal store may not fully cycle. This can reduce the effective capacity of the thermal store.

B2.2 HEAT TRANSFER FLUID

The HTF (heat transfer fluid) is a mix of distilled water containing 35% by volume propylene glycol. The pertinent properties of the HTF, evaluated at the mean thermal store operating temperature of 6.5°C, are shown in Table B2.

Property	Value	Units	Source
Density	1038	kg/m^3	ASHRAE Fundamentals 2009 [11]
Kinematic viscosity	$6.73x10^{-6}$	m^2/s	
Conductivity	0.394	$W/(m \cdot °K)$	
Heat capacity	3735	$J/(kg \cdot °K)$	

Table B2: Properties of 35% by volume propylene glycol in water at 6.5°C

The discharge cycle flow rates are selected such that the thermal store can be discharged over a two to six hour period while maintaining a useable output temperature for as much of the discharge cycle as possible. A useable discharge temperature for chilled water HVAC applications is < 6.5°C. Charge cycle flow rates are set at the maximum flow tested for the discharge cycle. HTF flow rates tested are constant during each test, but vary between runs at between 100ml/min and 300 ml/min in 50ml/min

increments; charge cycles are all at 300ml/min.

The Reynolds number for these flows, using this tank configuration, HTF, and a characteristic length based on the hydraulic radius of the flow paths, is on the order of one. This means that a laminar flow regime is maintained throughout the tests. While higher flow rates would produce turbulent flow, the required flow velocity through the tank would be at least 3 orders of magnitude greater than during these tests. This would result in a higher heat transfer rate, but would also result in little change to the temperature of the HTF as it passes through the store. Since an express purpose of the thermal store is to change the temperature of the HTF as it passes through the store, the flow rate must be restricted to flows such that the HTF residence time is high enough to affect the HTF temperature. Note that due to the small hydraulic diameter of the flow paths (~0.21 times the encapsulation tube radius), the heat transfer rates are high enough for the intended purpose, even with laminar flow.

B2.3 PCM ENCAPSULATION DESIGN PARAMETER – TUBING RESISTANCE RATIO

An encapsulation tube design parameter, the tubing resistance ratio, is proposed as a means to predict whether or not the physical properties and parameters of the encapsulation tube are capable of producing a well-distributed thermal condition around the PCM when a hexagonal packed configuration of encapsulation tubes is used. This parameter is modeled after a Biot number, but differs in that it compares the resistance of the encapsulation tube to redistribute thermal energy around itself to that of the resistance of passing the energy between both the HTF and the PCM. The physical basis and mathematical formula for this parameter is explained below.

Typical Biot number calculations compare the resistance of external convection with the resistance of internal conduction; for example, in the case of convection to a

solid cylinder. Since the areas of convection and conduction are initially the same (at the surface of the cylinder), the area components cancel and the Biot number becomes a ratio of conductive to convective resistance, as shown in Equation B1, where L_k is the characteristic length of conduction in the cylinder. When the Biot number is much less than 1 (by an order of magnitude) then it is assumed that the temperature within the conductive component does not vary with position, simplifying transient thermal problems [15]. This also suggests that temperature is well distributed throughout the conductive material in question.

$$R_c = \frac{1}{hA}, \quad R_k = \frac{L_k}{kA}, \quad Bi = \frac{R_k}{R_c} = \frac{hL_k}{k} \tag{B1}$$

However, heat transfer to a body is not always the result of convection; heat transfer by conduction of adjacent materials is also possible. As a result, this calculation cannot be limited solely to applications involving the ratios of convective and conductive resistances; any combination of convective or conductive heat transfer must be considered. In addition, the areas associated with heat transfer to the surface of a material and conduction within it, based on tube geometry, may not always be the same. In such cases a modified form of the Biot number can be used. Such a modified form is used for the analysis of the needed physical properties of the encapsulation tubes in this study to insure that the thermal energy is well distributed around the encapsulated PCM.

The design parameter of resistance ratio is based on the numeric modeling element shown in Figure B3. Each modeling element is comprised of a $\pi/3$ rad segment of an encapsulation tube (including the associated HTF, encapsulation material, and PCM), with a height equal to an arbitrary vertical step L. The outermost vertical

interfaces of these elements are adiabatic, being in contact with identical surfaces of identical elements; however, horizontal faces are not adiabatic as there is a vertical temperature gradient between elements when the thermal store is operating. The physical basis for the development of the resistance ratio will be one half of the PCM and encapsulation tube of this numeric modeling element, as divided by the plane of symmetry for the element as shown in Figure B4 (which for clarity does not show the HTF portion of the element).

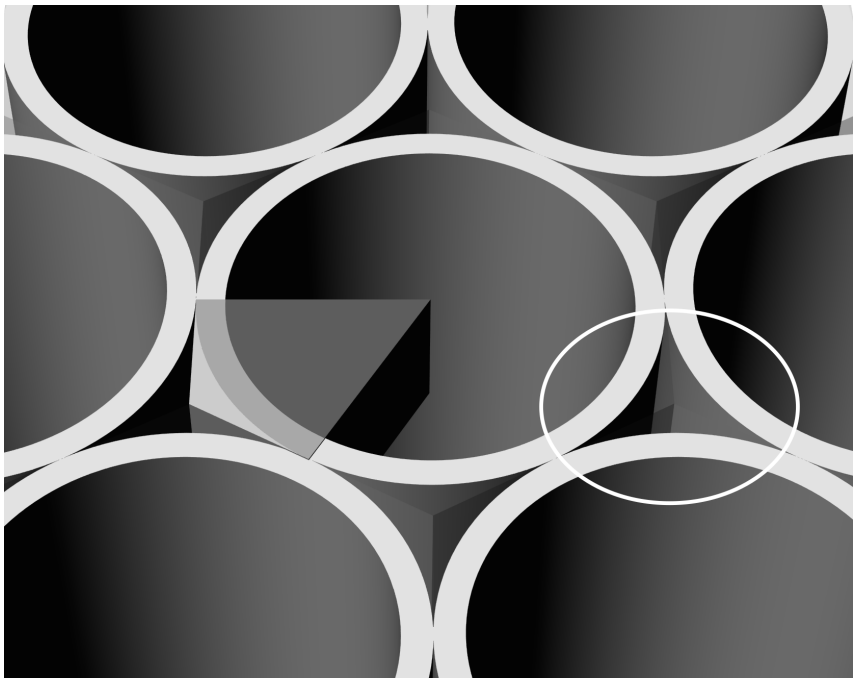

Figure B3: The hexagonal packed tube configuration and the resulting triangular-like flow paths (example circled). The partial segment shown in the center tube represents a numeric modeling element whose external vertical interfaces are adiabatic boundaries; this element forms part of the basis for the modified Biot number.

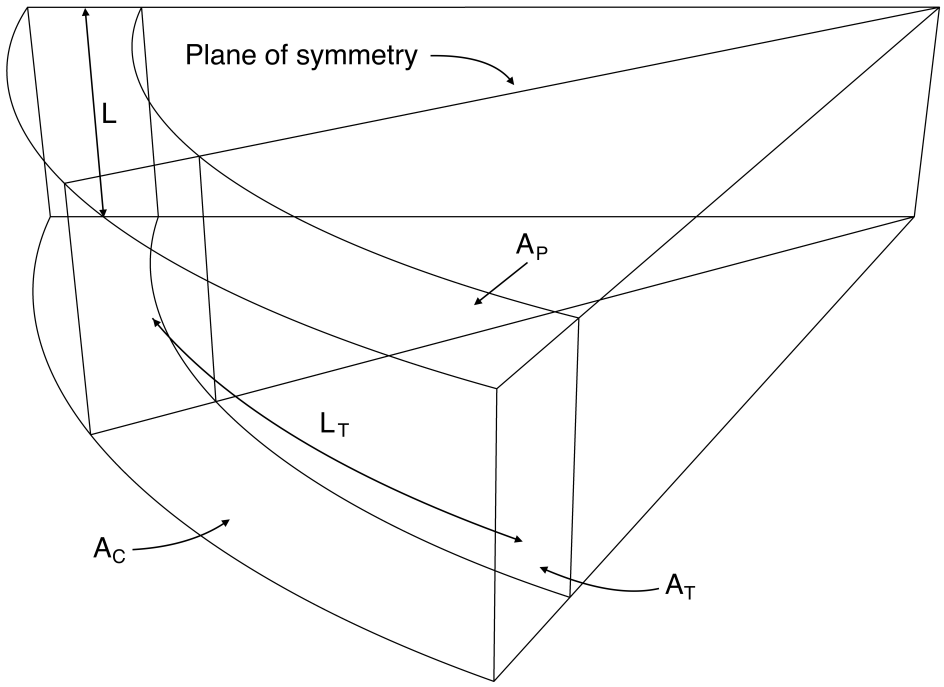

Figure B4: Dimensional parameters used for the calculation of the resistance ratio: L = arbitrary vertical step; L_t = characteristic length of conduction in the encapsulation material; A_c , A_t , A_p = areas associated with convection, conduction in the encapsulation tube, and conduction in the PCM respectively.

To develop the resistance ratio we must first calculate the thermal resistances for heat transfer in each of the mediums - convection from the HTF to the encapsulation tube, conduction within the PCM, and conduction around the encapsulation tube. Equation B2 shows the calculation for the thermal resistance of convection to the encapsulation tube for a symmetry section of the numeric model segment. It is assumed that the thermal resistance for convection is based on the relevant surface area of the encapsulation shell and an average Nusselt number. The Nusselt number is estimated as 2.5, which corresponds to the Nusselt number for laminar flow in an equilateral triangular pipe [38]. The hydraulic diameter is calculated as four times the cross sectional area of the triangular-like HTF flow path divided by its wetted perimeter. Due to the relationship

between hydraulic diameter and the convection surface area of the encapsulation tube in the hexagonal packed configuration, tube dimensional parameters cancel out and the resulting resistance is a constant function of the Nusselt number, HTF conductivity k_f, and an arbitrary length constant L (corresponding to the height of the modeling element).

$$R_c = \frac{1}{hA_c} = \frac{D_h}{Nu\,k_f A_c} = \frac{\frac{4\left(\sqrt{3}-\frac{\pi}{2}\right)r_o^2}{\pi r_o}}{Nuk_f \frac{\pi}{6} r_o L} = \frac{12\left(2\sqrt{3}-\pi\right)}{\pi^2}\frac{1}{Nu\,k_f L} \tag{B2}$$

The resistance of the PCM section is determined as it would normally be for a typical Biot number calculation involving a cylinder, with the characteristic length L_p set equal to $r_i/2$ (the volume of the an infinite cylinder divided by its surface area [15]). Note that due to the relationship between the characteristic length L_p and the area of conduction A_p, the tube dimensional parameters cancel out and the resulting resistance is a constant function of the PCM conductivity k_p and the arbitrary length constant L. The resulting thermal resistance calculation is shown in Equation B3.

$$R_P = \frac{L_p}{k_p A_p} = \frac{\frac{r_i}{2}}{k_p \frac{\pi}{6} r_i L} = \frac{3}{\pi}\frac{1}{k_p L} \tag{B3}$$

It has been assumed that the thermal energy convected to the encapsulation tube surface is based on the surface area of the encapsulation shell and an average Nusselt number, but its distribution across the face of the encapsulation shell is unknown. Since our goal is to verify that the encapsulation shell can effectively redistribute the thermal energy around the PCM under the worst-case, most conservative conditions, it will further be assumed that the all of the convected energy enters the encapsulation shell at

the line of symmetry and is conducted around the encapsulation shell. The characteristic length for conduction within the encapsulation tube L_t is thus taken as the distance between the center of the encapsulation tube wall at the plane of symmetry and the center of the encapsulation tube wall at the edge of the modeling unit, where the apex of the triangular flow paths are formed by the intersection of the tubes. This conservative position also requires that the cross-sectional area of the tube segment A_t be used for the area of conduction, since conduction is now assumed to be along the horizontal cross-section of the tube. The result is a calculation for the conservative (highest) resistance of the encapsulation tube shell as shown in Equation B4. Note that this is the only resistance calculation that retains encapsulation tube dimensional parameters.

$$R_t = \frac{L_t}{k_t A_t} = \frac{\frac{\pi}{6}\left(\frac{r_o + r_i}{2}\right)}{k_t\left(r_o - r_i\right)L} = \frac{\pi}{6}\frac{\left(r_o + r_i\right)/2}{\left(r_o - r_i\right)}\frac{1}{k_t L} \tag{B4}$$

These resistances can be thought of as representing a steady-state thermal circuit between the free-stream temperature of the HTF T_∞, and the frozen PCM T_p, as shown in Figure B5. If the resistance along the encapsulation tube R_t is much less than that of either the resistance to convection R_c or the resistance to the conduction into the PCM R_p (when R_t/R_c and $R_t/R_p << 1$) , then the temperature differential across R_t is small and the temperature will be well-distributed in the encapsulation material.

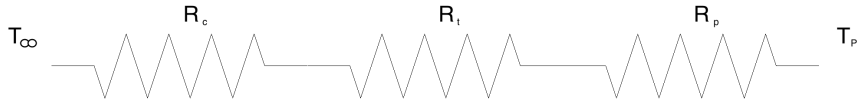

Figure B5: A representation of a steady-state thermal circuit, consisting of three resistances (convection from the HTF, conduction through the encapsulation tube, and conduction in the PCM) between two driving temperatures.

The resulting resistance ratios R_t/R_c (between the encapsulation tube and the HTF) and R_t/R_p (between the encapsulation tube and the PCM) are shown in Equations B5 and B6. Both of these ratios must be << 1 for the temperature to be considered even throughout the encapsulation tube. Note that both of these equations resolve to the product of a dimensionless constant multiplier C based on the hexagonal packing geometry, a dimensionless geometry variable R_r describing the ratio of the average tube radius to its wall thickness, and a dimensionless conductivity variable K_r describing the conductivity ratio of the adjoining materials (including any Nusselt number modifier). These dimensionless quantities are summarized in Table B3.

$$\frac{R_t}{R_c} = \frac{\pi^3}{72\left(2\sqrt{3}-\pi\right)} \frac{\left(r_o + r_i\right)/2}{\left(r_o - r_i\right)} \frac{Nu\, k_f}{k_t} \tag{B5}$$

$$\frac{R_t}{R_p} = \frac{\pi^2}{18} \frac{\left(r_o + r_i\right)/2}{\left(r_0 - r_i\right)} \frac{k_p}{k_t} \tag{B6}$$

Resistance Ratio	C	R_r	K_r
R_t/R_c	$\frac{\pi^3}{72\left(2\sqrt{3}-\pi\right)}$	$\frac{\left(r_o + r_i\right)/2}{\left(r_o - r_i\right)}$	$\frac{Nu\, k_f}{k_t}$
R_t/R_p	$\frac{\pi^2}{18}$		$\frac{k_p}{k_t}$

Table B3: Dimensionless quantities C, R_r and K_r for R_t/R_c and R_t/R_p

Existing convention for Biot number calculations require a resistance ratio of less than 0.1, which is the criterion accepted here as well. The Nusselt number for flow in the

roughly triangular flow paths is estimated at 2.5 as discussed previously. For the metallic tubes tested in this study, the two ratios compute to $R_t/R_c = 0.035$ and $R_t/R_p = 0.002$. For the CPVC tubes tested in the previous study the two ratios compute to $R_t/R_c = 38$ and $R_t/R_p = 2.4$. Note that of the two encapsulation tube types compared here, both of which have the same external radius, only the metallic tubes meet the criterion of 0.1 or less for the resistance ratios.

B2.4 EXPERIMENTAL APPARATUS

The PCM encapsulation system tested consists of a set of copper tubes. These are standard ½" (12.7mm) type M thin-wall rigid copper tubes commonly used in plumbing systems. These tubes are selected to address availability and cost concerns, as well as for compliance with the resistance ratios < 0.1 requirement. The pertinent physical properties of these tubes are shown in Table B4.

Property	Value	Units	Source
Outside radius	0.007938	m	ASTM B88-14
Inside radius	0.007227	m	
Conductivity	403	W/(m·°K) at 6.5°C	Incropera 2007
Heat capacity	385	J/(kg·°K)	

Table B4: Properties of ½" (12.7mm) type M thin-wall copper tubing

The encapsulation tubes are cut to a total finished length of 1.14m , including end caps. This length is arbitrarily chosen so as to maintain a manageable size for the test apparatus. Each tube is filled with 0.150ml of PCM to a height of 0.908m. The completed tubes contain approximately 0.232m of clear space above the liquid PCM to minimize internal pressure changes due to the expansion/contraction of the PCM during phase cycling.

The tank is constructed of standard 4 inch (0.102m) schedule 40 PVC pipe. The

top and bottom of the tank utilize a combination of PVC and brass fittings to allow for water flow and instrumentation. A PVC pipe flange is installed near the top of the tank to facilitate disassembly, which allows for the installation and exchange of the PCM tubes. The main body of the tank is placed into a 0.305m diameter cardboard form tube and supported by 0.102m of polyurethane insulation board at its base. The remaining space around the tank is filled with polyurethane spray foam insulation. The upper portion of the tank is manually insulated with polyurethane foam batting and rigid foam insulation cut to size, then covered by a 0.305m diameter cardboard cylinder.

A total of 31 encapsulated PCM tubes are placed in the thermal storage tank in a hexagonal packed configuration. Where this packing configuration meets the walls of the tank, gaps form between the tubes and tank. The total area of the gaps is large when compared to the free area between the tubes, and so to minimize their impact on HTF flow the larger gaps are plugged using 5/8 inch flexible vinyl tubing with sealed ends.

The temperature of the incoming and outgoing HTF is measured using Omega Engineering epoxy-encapsulated thermistors, part number 44033. These thermistors are positioned directly in the flow path of HTF to insure consistent measurements. The thermistors are connected to GW Instruments iNet-100 A/D data acquisition hardware using a precision 4.7kohm resistor that provides excitation current. The resistor has an accuracy of +/- 0.025%-20ppm/°C. This configuration has a temperature measurement accuracy of +/-0.1°C. Temperature data is recorded at 10 second intervals during each test run.

HTF flow rates are measured using Omega Engineering Pelton-type turbine wheel flow meters, model number FLR1009, with a range of 50 to 500 ml/min. These produce a linear output voltage signal of 0 to 5 VDC corresponding to the flow rate. These devices have a repeatability of 0.2% of full scale flow within their allowed operating range. One

flow meter is used for each of the inputs, but since the meters are unidirectional only one is in use during each test as needed by the test cycle (charge or discharge); the unused flow meter is bypassed. To improve accuracy of the flow measurements, the flow meters are calibrated at each use by directly measuring the output flow and comparing it to the reported flow rate at the beginning and end of each test run.

A Polyscience 5706T portable chiller unit supplies chilled water to the thermal storage tank through a high-flow-rate supply loop adjacent to the thermal store. The high-flow-rate loop prevents changes in the temperature of the supply due to residence time in the loop. Short, small diameter polyethylene tubing connects the thermal store inputs/outputs to the supply loop. The output from the thermal store is switched between the top and bottom of the tank, depending on mode (charge or discharge), with the output going to an intermediate tank to permit flow rate verification before returning to the Polyscience chiller. All tubes are insulated with foam rubber insulation to minimize losses. A schematic of the tank and its connections is shown in Figure B6.

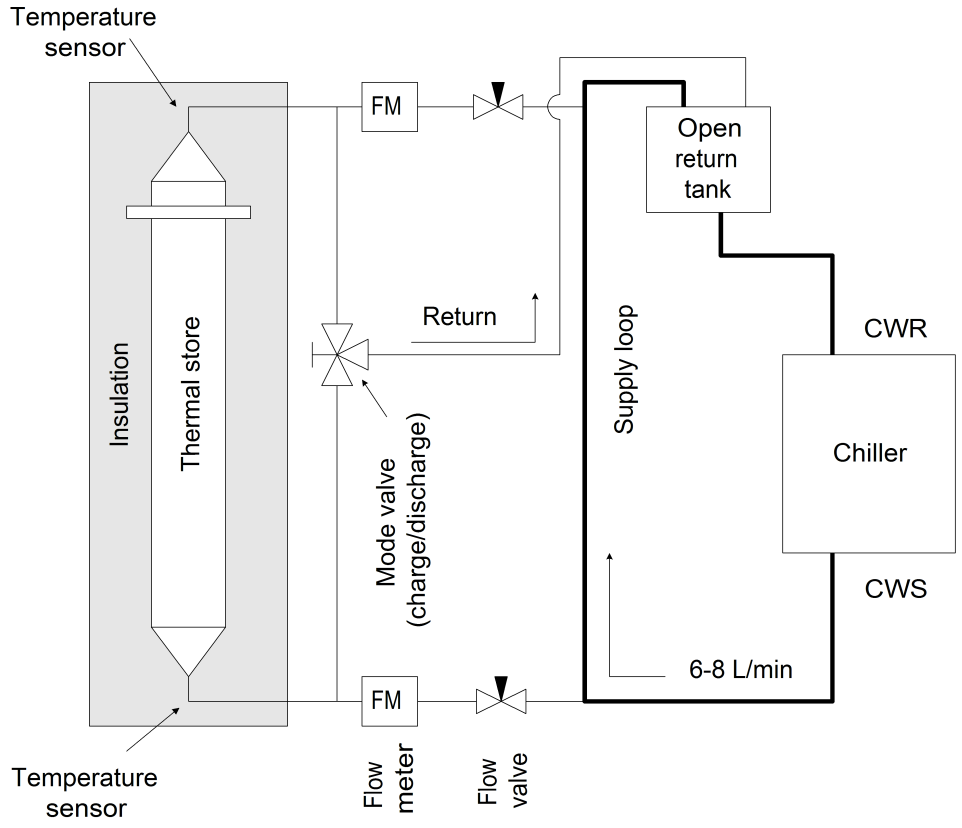

Figure B6: Experiment schematic. The high flow supply loop provides chilled water at a stable temperature to the tank inlets. The loop allows the low-flow inlet tubes to be as short as possible to limit heat gain from the environment. The open return tank allows for flow rate confirmation during each test.

B2.5 EXPERIMENTAL PROCEDURE

During the charge cycle, HTF at approximately 2◦C is pumped into the bottom of the tank to freeze the PCM; in this mode the HTF warms as it passes from the bottom to the top of the tank. During the discharge cycle, chilled water at approximately 11◦C is pumped into the top of the tank to melt the PCM; in this mode the HTF cools as it passes from the top to the bottom of the tank. The 2◦C charge temperature is selected as low enough to fully freeze the PCM while still being within the capability of typical chilled water systems. The 11◦C temperature for the discharge cycle is selected as representative of a typical cooling coil chilled water return temperature.

By changing the direction of HTF flow depending on the cycle, a negative temperature gradient (measured from top to bottom) in the tank is preserved. This minimizes buoyancy-driven effects so as to prevent short-circuit flows through the tank. It also serves to encourage stratification within the tank.

At the end of each discharge cycle the system is allowed to attain a steady-state condition where the incoming water is at ~11°C while the output temperature is slightly higher. The increase in water temperature results from thermal gains through the tank shell and insulation. These gains are calculated with respect to the overall tank in terms of W/°K, with °K being the number of degrees kelvin difference between the average temperature in the tank and the ambient temperature. This rate is used to estimate losses through the tank during run time based on average tank and ambient temperatures. Losses are considered recoverable energy, since they can be prevented (and thus made available for recovery) through better insulation; in other words they are the result of insulation specification not the PCM, encapsulation, or internal tank design.

B2.6 EXPERIMENTAL ERROR ANALYSIS

The values used in the experimental calculations and their uncertainties are shown in Table B5. The relative uncertainty for values that operate over a range is determined using the median value of that range. Temperature uncertainty is taken directly from thermistor manufacturer data (based on NIST certification), while energy flow uncertainty is calculated from the relevant parameters. While the relative uncertainty of the loss rate is highest (LR in Table B5), the loss rate portion of the total energy calculation is small and contributed very little to the uncertainty of the total energy calculations.

Description	Symbol	Value or range	Absolute error	Relative error*	Units	Source
T_{in} - T_{out}	ΔT	0 - 9 °C	0.14	3.1%	C	Calculated
Flow rate	F_{lpm}	0.100 - 0.300	0.003	1.5%	L/min	Measured
Density, HTF	ρ_f	1036	3	0.3%	kg/m²	ASHRAE
Heat capacity, HTF	C_f	3735	50	1.3%	J(kg K)	
T_{amb} - T_{avg}	ΔT_{amb}	12 - 21°C	1	6.1%	C	Calculated
Loss rate	LR	0.2 - 0.3	0.05	20.0%	W/K	Measured
Overall (energy calculation)				3.7%		

- The relative error for parameter values given as a range is calculated at the median value.

Table B5: Experimental uncertainty values

Chapter B3: Results/Discussion

Tests are performed on the thermal store with copper encapsulation tubes using multiple flow rates representative of expected loads on a per-unit basis. The results are compared to previous results using CPVC encapsulation tubes. Design guidelines are provided for similarly constructed thermal storage systems.

B3.1 THERMAL STORE TEST RESULTS

The test results for the thermal store using copper encapsulation tubes are summarized in Figures B7 through B9. Figure B7 gives the output temperature of the experimental thermal store and the net % of recovered energy with respect to time for flow rates between 100 and 300ml/min in 50ml/min increments (note that recovered energy includes losses through the tank wall, since it is possible to recover these losses with better insulation). The results show that for a usable output temperature of equal to or less than 6.5°C (a minimum delta T of 4.5°C), approximately 73% to 93% of total recoverable thermal storage capacity (sensible and latent) can be recovered depending on flow rate. These flow rates correspond to operating times of between 5.4 and 1.8 hours for 100ml/min and 300ml/min respectively, commensurate with a two to six hour peak power demand window.

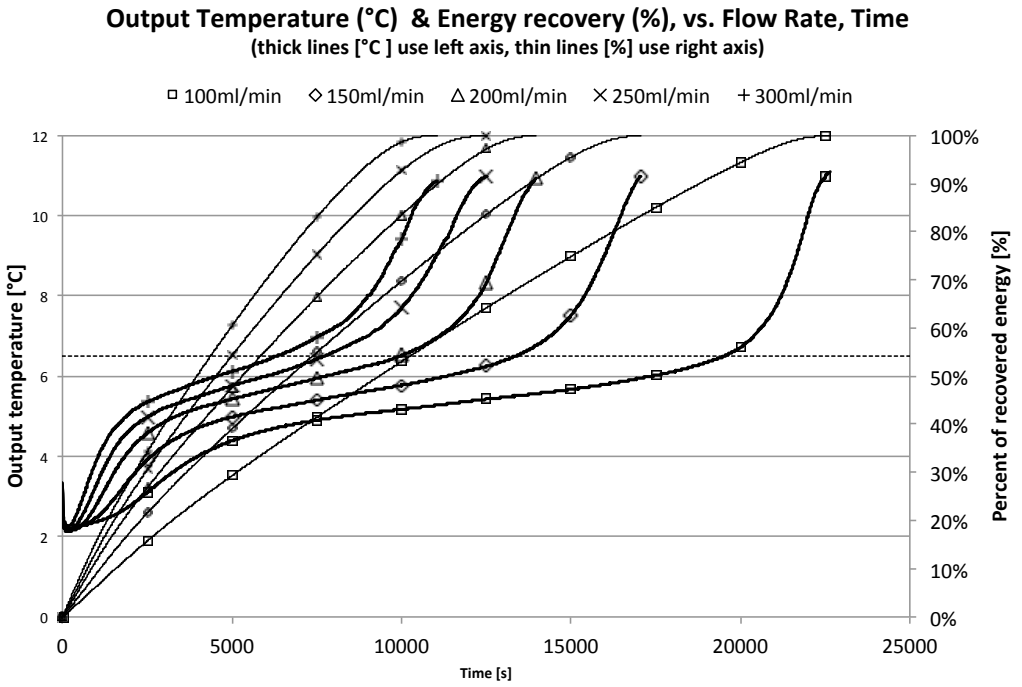

Figure B7: Energy recovery vs. output temperature. A reference output temperature of T <= 6.5C is provided by the dashed line, but the data can be used for any output temperature. To use this graph, find where a temperature plot for a specific flow rate crosses the desire reference temperature, them move up to the corresponding energy line and read the recovery percent on the right axis.

Figure B8 gives the percent of energy recovered based on the desired maximum output temperature and HTF flow rate. The output temperature range is restricted to temperatures greater than the melting range of the tetradecane PCM, which has been previously measured as between 4.5 and 6.5°C [30]. Selecting an output temperature lower than the upper bound of PCM melting range will limit energy recovery and reduce the effectiveness of the thermal store. The flow rate range was selected to obtain discharge periods of between two and six hours, suitable for peak HVAC cooling load mitigation.

The data in Figure B8 indicates that a greater percentage of energy can be recovered when higher output temperatures are allowed; this is due to the thermal store

being able to run longer at any given flow rate before the higher maximum output temperature is reached. Lower flow rates are also shown to allow for more energy recovery because longer HTF residence times within the thermal store work to keep the output temperature lower further into the discharge cycle.

The energy recovery rate can be approximated by a linear equation of flow rate for each output temperature, as shown in Figure B8, when limited to the tested flow rate range. However, it is expected that the energy recovery rates for all output temperatures will approach 100% as the flow rate approaches zero, and will asymptotically approach a small static value equal to the thermal energy stored in the HTF present in the tank as the flow rate approaches its maximum. As a result, while a linear equation may be capable of representing the energy recovery rate over the examined flow rates, it is not linear over the full range of possible flow rates.

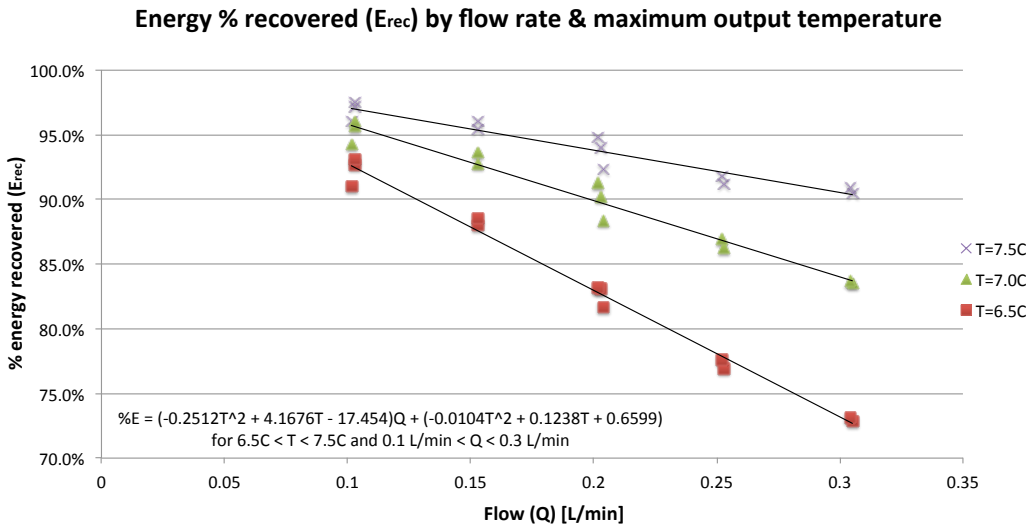

Figure B8: Energy recovery rate as a function of flow rate and maximum allowed output temperature. The equation shown, based on a regression of the linear equations, is accurate to +/- 2% when compared to experimental results.

Figure B9 gives the run time in hours based on the example maximum output temperatures (between 6.5° and 7.5°C) and HTF flow rates (between 0.1 and 0.3 L/min). Like the data in Figure B8, this data shows that run times increase with higher allowed output temperatures and lower flow rates. We can explain the data in Figure B9 by considering an energy balance between the HTF flow and the thermal store capacity, as shown in Equation B7.

$$mC_f\left(T_{in}-T_{avg}\right)t=\left(E_{sen}+E_{lat}\right)E_{rec} \quad \rightarrow \quad t=\frac{\left(E_{sen}+E_{lat}\right)E_{rec}}{mC_f\left(T_{in}-T_{avg}\right)} \tag{B7}$$

For the purposes of the energy balance we can assume that the input temperature (T_{in}) is fixed, as it has been in our experiments. T_{avg} is defined as the time-averaged output temperature of the thermal store over the discharge run. E_{sen} and E_{lat} are the total sensible and latent thermal energy in the store, while E_{rec} is the fraction of total thermal energy recovered during the discharge run. C_f and m are the specific heat and mass flow rate (density times volume flow rate) of the HTF respectively. Reorganizing the equation as shown in Equation B7 demonstrates that the run time t is proportional to the energy recovery rate and inversely proportional to the mass flow rate and time-averaged output temperature.

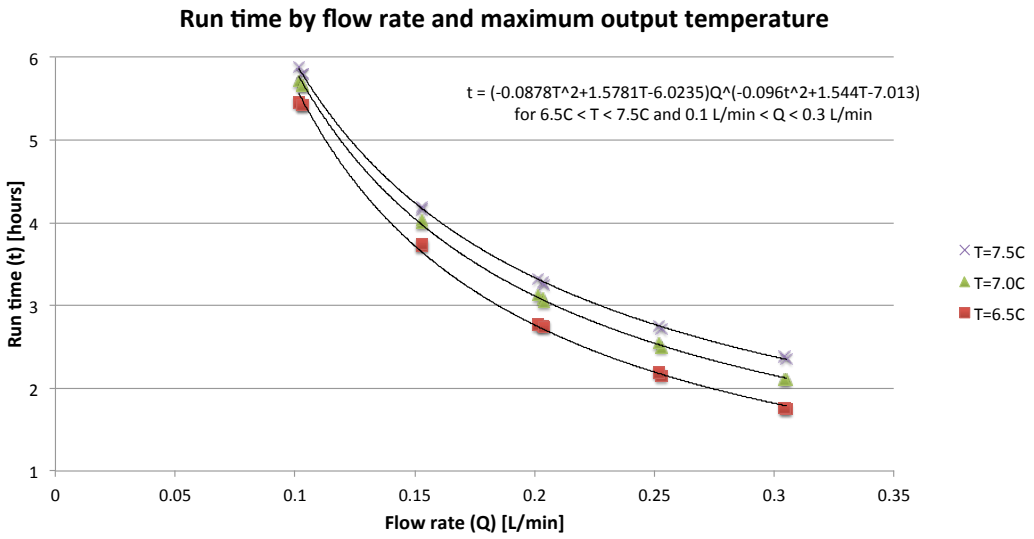

Figure B9: Run time as a function of flow rate and maximum allowed output temperature for the experimental thermal storage tank. The equation shown, based on a regression of the power equations, is accurate to +/- 3% when compared to experimental results.

Note that E_{rec} has been shown in Figure B8 to be an approximately linear function of the flow rate over the range of flow rates tested. Also, note from Figure B7 that as flow rates increase so do output temperatures, indicating that T_{avg}. is also a function of flow rate. Given the placement of E_{rec} , T_{avg} , and m in Equation B7 and the fact that they are all functions of the flow rate, this suggests that run time is a power function of flow rate. A regression of the test data in Figure B9 shows that run time can be approximated by a power function of flow rate for each maximum output temperature and flow rate range considered in these experiments.

The data in Figure B8 can also be used to predict the recovery rate for thermal storage tanks of larger diameter than the experimental tank, so long as the same type and length of PCM and encapsulation tubes are used. This is possible because the hexagonal packing produces a near-constant cross-sectional ratio of PCM to tank area. Increasing the cross-sectional area of the tank (and thus the corresponding encapsulation tube count

and cross-sectional area) will increase the allowed flow rate for each specific temperature and recovery rate. The increase in allowed flow rate is based on the ratio of the tank cross-sectional area to that of the experimental tank. For instance, doubling the cross-sectional area of the tank will allow for twice the volumetric flow rate for any given output temperature and recovery rate. However, these values should be considered conservative estimates due to an increase in packing efficiency (the ratio of total encapsulation tube cross-sectional area to the cross sectional area of the thermal store) as the tank becomes larger. The experimental store has a packing efficiency, when the filler rods are considered, of 86.7%, while hexagonal packed circles in an infinitely large plane can reach a 90.7% overall packing efficiency [39]. As the tank diameter becomes larger the packing efficiency will have a tendency towards, but never quite reach, this theoretical limit.

Figures B8 can also be used to conservatively predict energy recovery rates for taller tanks that utilize the same PCM and encapsulation tube size. Adding height to the top of the tank provides capacity that will be discharged before the lower portion of the tank, thus increasing the overall recoverable capacity of the thermal store without adding unrecoverable capacity. This results in recovery rates that will always be at least as high as those for the experimental tank for any taller tank. Similarly, conservative estimates for run times can be made in the same manner utilizing the data from Figure B9.

A multivariable regression method [40] is used to develop the empirical equations shown in Figures B8 and B9. These equations are functions of maximum output temperature ($6.5°C \leq T \leq 7.5°C$) and flow rate ($0.1\ L/min \leq Q \leq 0.3\ L/min$), and provide either the recovered energy percentage or run time as indicated.

Table B6 summarizes the flow rate, energy recovery, and run time results for copper tubes, and also includes this data from previous experiments involving CPVC

encapsulation for comparison [30].

Encapsulation material	# of tubes	Flow rate [ml/min]	Net energy recovered (T<6.5°)	Run time [hours] (T<6.5°C)
Copper	31	100	93%	5.4
Copper	31	150	88%	3.7
Copper	31	200	83%	2.8
Copper	31	250	77%	2.1
Copper	31	300	73%	1.8
CPVC	31	100	43%	2.0
CPVC	19	100	88%	3.3

Table B6: Flow rate, energy recovery, and run time for copper, CPVC tubes

B3.2 COMPARISON TO PREVIOUS RESULTS

Previous results [30] are based on CPVC encapsulation tubes packed into a nearly identical tank. These experiments used both a high-density and low-density configuration of encapsulation tubes. The high density configuration consisted of 31 CPVC tubes in a hexagonal packed configuration, which is the highest density supported in the tank and is represented by the packing shown on the right in Figure B2. The high density configuration is identical to the 31 tube packing for the copper tubes utilized in the current experiments, as the copper and CPVC tubes have the same outside diameter, and results in tube packing density (cross sectional area of tubes compared to the free cross sectional area of the tank) of ~ 87%. The low density configuration consisted of 19 tubes evenly spaced in the tank using tube-mounted spacer rings. This produces the pseudo annular ring packing as represented by the packing shown on the left of Figure B2, and results in a tube packing density of ~46%. It should be noted that the CPVC tubes, due to their thicker walls, contain less PCM than the copper tubes of the current experiment (116ml versus 150ml/tube), and thus have a lower thermal storage density. A comparison of the results between these two sets of experiments is shown in Figure B10 and with data organized in Table B6.

The previous study found that the high-density configuration of CPVC tubes performed poorly, allowing only 43% of the stored thermal energy to be recovered at a useable (<6.5°C) temperature. The copper encapsulation tubes with the same configuration and flow rate presented in this study allowed recovery of up to 93% of stored thermal energy, more than double that of the CPVC tubes. Also, the thinner walls of the copper tubes provided a 29% increase in PCM capacity.

The previous study also found that the low density CPVC configuration, where the pseudo annular ring packing allowed the HTF to flow evenly around the encapsulation tubes, had acceptable thermal performance but at a lower PCM density. Up to 88% of the thermal energy could be recovered in this configuration. The hexagonal packed copper tubes used in the current study performed in a similar manner, recovering up to 93% of stored thermal energy while increasing PCM capacity by 111% over the CPVC tube pseudo annular ring configuration. This demonstrates that highly conductive encapsulation tubes can mitigate the effects of the restricted HTF flow paths resulting from the hexagonal packed configuration, providing pseudo annular ring performance at hexagonal packed thermal storage densities.

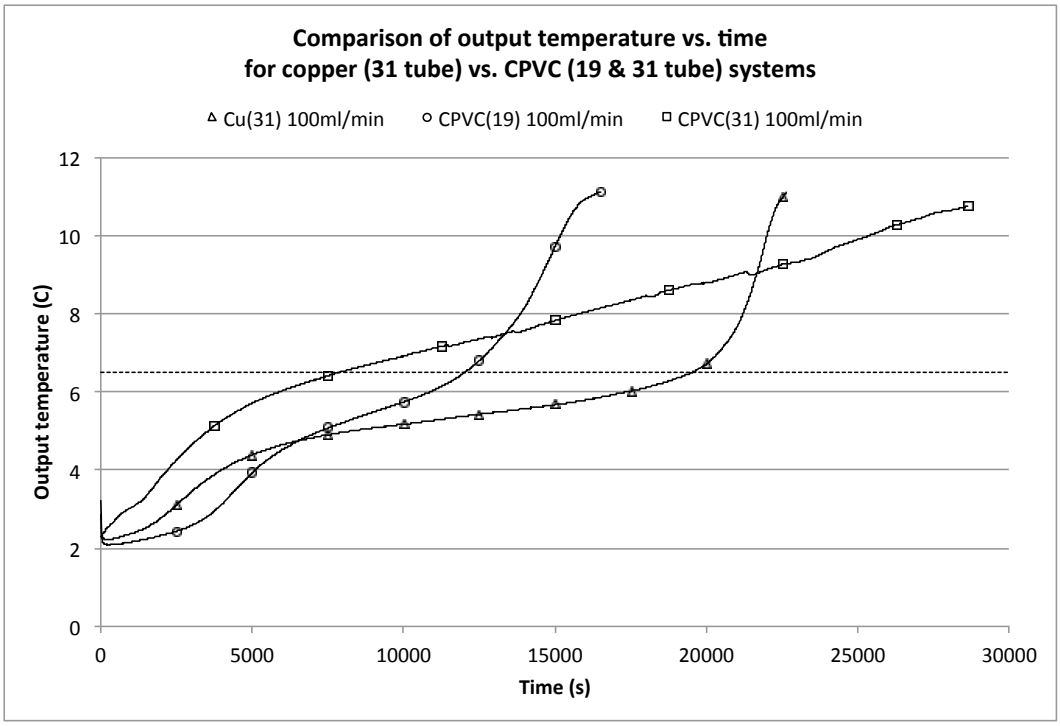

Figure B10: A comparison of performance between CPVC and copper encapsulation tubes. Note that both the 19 tube CPVC and 31 tube copper encapsulation tubes produced acceptable results with 88% and 93% of energy recovered, although the 31 tube copper system offered a much higher thermal capacity.

B3.3 DISCUSSION ON OPTIMIZED ENCAPSULATION

Similarly sized encapsulation tubes that meet the requirements of the resistance ratio defined herein (copper tubes) performed better in tests than those that did not (CPVC tubes). However, the copper tubes tested are based on readily available components that do not optimize the resistance ratio. Minimizing the wall thickness of the encapsulation tubes while maintaining compliance with the resistance ratio requirements will minimize material costs and maximize the thermal storage density of the system. In addition, other encapsulation materials may provide a lower-cost option than the copper tubes tested in these experiments.

Larger diameter tubes will also reduce encapsulation costs on a per PCM volume

basis (by reducing the tube count per unit of PCM), but will also increase the time required to discharge the PCM due to the increased resistance to heat transfer through the deeper inner layer of poorly-conducting PCM. This will also limit flow rates for acceptable heat recovery levels and output temperatures. Additional tests or modeling will be required to determine the range of tubing sizes that have the capability to produce acceptable performance levels. However, encapsulation tube sizes on the order of those used in these experiments have shown to be capable of acceptable heat transfer and recovery rates for time-shifting of environmental cooling loads. The analysis here will be limited to encapsulation tubes of the same outside diameter as used in these experiments.

When the resistance ratios, as defined in their dimensionless form (Table B3), are required by definition to be less than 0.1 for acceptable performance, inequalities can be defined as shown in Equation B8.

$$0.1 > C R_r K_r \quad \rightarrow \quad R_r < \frac{0.1}{C K_r} \tag{B8}$$

These inequalities can be solved for the maximum permissible value of Rr as a function of C and Kr for both Rt/Rc and Rt/Rp using the values found in Table B3. Rr can then be solved for ri based on ro. For example, performing this calculation using the same 35% propylene glycol HTF, 99% tetradecane PCM, and copper tubing material results in required Rr values of less than 30.6 and 490 for Rt/Rc and Rt/Rp respectively. Solving for ri using r0 = 0.007938m (the outside diameter of both the copper and CPVC encapsulation tubes) gives values of 0.007683m and 0.007921m, with the controlling value being the smaller inside radius of 0.007684m (which corresponds to the thicker encapsulation shell). This results in an encapsulation wall thickness less than 1/3 of that used in the copper tubes tested in this study, increasing PCM mass by 13%. Repeating

these calculations for an alternative encapsulation material, such as aluminum (Ke = 237 W/(m·°K) [15]) gives an inside radius of 0.007509m, increasing PCM mass by 8% over the tested copper tubes. A similar analysis for CPVC tubes indicate that it is not possible to meet the resistance ratio requirements with the same outside radius as the copper tube used in this study. However, this may be possible with smaller diameter tubes.

Future studies should investigate the use of different tube sizes to optimize thermal efficiency, performance, and encapsulation costs for use in environmental cooling applications, and to provide additional validation for the dimensionless design parameter developed in this study.

Chapter B4: Summary

This study has investigated methods to improve the storage density and performance of tube-encapsulated PCM-based thermal systems. Experiments are performed using a highly-conductive encapsulation tube material designed to improve thermal energy distribution around the encapsulated PCM, thus allowing for higher tube densities. The results show that performance issues, such as low recovery rates and long run times, resulting from a dense hexagonal packing of polymer encapsulation tubes can be mitigated by properly sizing the tubes and by constructing the tube shells of conductive materials that are capable of redistributing the thermal energy around the encapsulated PCM. The use of this method prevents the need to apply internal conductivity enhancements to the PCM, which would increase costs and reduce the capacity of the thermal store.

A comparison of performance between ASTM-standard 1/2 inch copper and CPVC tube encapsulation systems shows a more than two-fold increase in recoverable energy at comparable tube densities, or an increase of up to 111% in PCM capacity while maintaining comparable thermal performance, for the copper tubes used in this study. The tests also show that this thermal store design, when using encapsulation tubes having an approximate outside diameter of 0.625 inches [~ 15mm), can provide a performance level suitable for use in building cooling load applications, allowing the recovery of between 73% and 93% of stored energy over a 1.8 to 5.4 hour time window. Design guidelines are provided for scaling of the test configuration to various storage system capacities, using the same type and size of encapsulation tubes as utilized here.

In addition, a dimensionless design parameter - the resistance ratio - is proposed as a means of determining the necessary conductivity and dimensional parameters of

encapsulation tubes. The resistance ratio parameter provides design guidance to allow for acceptable thermal store performance while optimizing thermal store capacity and minimizing encapsulation costs.

While the performance results are specific to thermal stores utilizing 1/2 inch CPVC and copper pipes meeting ASTM standards [41,42], the resistance ratio may be applied to other encapsulation tube configurations to optimize the performance of similarly constructed thermal stores.

B4.1 ACKNOWLEDGEMENTS

This work was made possible in part by funding from Pecan Street Inc. (a 501(c)3 non- profit public-private partnership in Austin, Texas), the American Society for Heating, Refrigeration and Air Conditioning Engineers through their Graduate Student Grant-In-Aid Award Program, and by the University of Texas at Austin.

References

[1] U.S. Energy Information Administration. 2015a. "Monthly Energy Review - Energy Information Administration." Accessed September 1. http://www.eia.gov/totalenergy/data/monthly/index.cfm#consumption.

[2] U.S. Energy Information Administration. 2015b. "Use of Electricity - Energy Explained, Your Guide To Understanding Energy - Energy Information Administration." Accessed September 1. http://www.eia.gov/energyexplained/index.cfm?page=electricity_use.

[3] U.S. Energy Information Administration. 2015c. "Residential Energy Consumption Survey (RECS) - Data - U.S. Energy Information Administration (EIA)." Accessed September 1. http://www.eia.gov/consumption/residential/data/2009/index.cfm?view=consumption.

[4] Doggett, Trip. 2013. "ERCOT - A Strategic View of the Future." presented at the Gulf Coast Power Association Fall Annual Conference, October 2. http://www.ercot.com/content/news/presentations/2013/GCPA - 02 Oct 2013 FINAL.pdf.

[5] U.S. Energy Information Administration. 2015d. "Annual Energy Outlook 2015 with Projections to 2040." DOE/EIA-0383(2015). Washington, D.C.: U.S. Energy Information Administration. http://www.eia.gov/forecasts/aeo/.

[6] Bentley, W. G., and John C. Evelyn. 1986. "Customer Thermal Energy Storage a Marketing Opportunity for Cooling off Electric Peak Demand." *Power Systems, IEEE Transactions on* 1 (4): 57–61.

[7] Hermanns, Holger, and Holger Wiechmann. 2009. "Future Design Challenges for Electric Energy Supply." In *Emerging Technologies & Factory Automation, 2009. ETFA 2009. IEEE Conference on*, 1–8. http://ieeexplore.ieee.org/xpls/abs_all.jsp?arnumber=5347150.

[8] Hajiah, Ali, and Moncef Krarti. 2012. "Optimal Control of Building Storage Systems Using Both Ice Storage and Thermal Mass – Part I: Simulation Environment." *Energy Conversion and Management*, April. doi:10.1016/j.enconman.2012.02.016.

[9] Hajiah, Ali, and Moncef Krarti. 2012. "Optimal Controls of Building Storage Systems Using Both Ice Storage and Thermal Mass – Part II: Parametric Analysis." *Energy Conversion and Management* 64 (December): 509–15. doi:10.1016/j.enconman.2012.02.020.

[10] He, Bo, E. Mari Gustafsson, and Fredrik Setterwall. 1999. "Tetradecane and Hexadecane Binary Mixtures as Phase Change Materials (PCMs) for Cool Storage in District Cooling Systems." *Energy* 24 (12): 1015–28.

[11] American Society of Heating, Refrigerating and Air-Conditioning Engineers. 2009. *2009 ASHRAE Handbook: Fundamentals*. American Society of Heating, Refrigeration and Air-Conditioning Engineers.

[12] Kuehn, Thomas H., James W. Ramsey, and James L. Threlkeld. 1998. *Thermal Environmental Engineering*. 3rd ed. Upper Saddle River, NJ: Prentice-Hall.

[13] U.S. Census Bureau. 2013. "American Housing Survey for the United States: 2011." H150/11. U.S. Government Printing Office. https://www.census.gov/content/dam/Census/programs-surveys/ahs/data/2011/h150-11.pdf.

[14] U.S. Energy Information Administration. 2006. "Commercial Building Energy Consumption Survey." U.S. Energy Information Administration. http://www.eia.gov/consumption/commercial/about.cfm.

[15] Incropera, Frank, David Dewitt, Theodore Bergman, and Adrienne Lavine. 2007. *Fundamentals of Heat and Mass Transfer*. 6th ed. Hoboken, NJ: John Wiley and Sons.

[16] Regin, A. Felix, S.C. Solanki, and J.S. Saini. 2008. "Heat Transfer Characteristics of Thermal Energy Storage System Using PCM Capsules: A Review." *Renewable and Sustainable Energy Reviews* 12 (9): 2438–58. doi:10.1016/j.rser.2007.06.009.

[17] Mehling, Harald, and Luisa F. Cabeza. 2008. *Heat and Cold Storage with PCM: An Up to Date Introduction Into Basics and Applications*. Berlin: Springer.

[18] Abhat, A. 1983. "Low Temperature Latent Heat Thermal Storage: Heat Storage Materials." *Solar Energy* Vol 30 (4): 313–32.

[19] Agyenim, Francis, Neil Hewitt, Philip Eames, and Mervyn Smyth. 2010. "A Review of Materials, Heat Transfer and Phase Change Problem Formulation for Latent Heat Thermal Energy Storage Systems (LHTESS)." *Renewable and Sustainable Energy Reviews* 14 (2): 615–28. doi:10.1016/j.rser.2009.10.015.

[20] Hale, D, M Hoover, and M O'Neill. 1971. "Phase Change Materials Handbook." NASA CR-61363. Huntsville, AL: Lockheed Missles and Space Company. http://hdl.handle.net/2060/19720012306.

[21] Humphries, William, and Edwin Griggs. 1977. "A Design Handbook for Phase Change Thermal Storage Control and Energy Storage Devices." National Aeronautics and Space Administration Scientific and Technical Information Office. http://hdl.handle.net/2060/19780007491.

[22] Li, Gang, Yunho Hwang, and Reinhard Radermacher. 2012. “Review of Cold Storage Materials for Air Conditioning Application.” *International Journal of Refrigeration* 35 (8): 2053–77.

[23] Dimaano, Maria Natalia R., and Takayuki Watanabe. 2002. “The Capric–lauric Acid and Pentadecane Combination as Phase Change Material for Cooling Applications.” *Applied Thermal Engineering* 22 (4): 365–77.

[24] Farid, Mohammed M, Amar M Khudhair, Siddique Ali K Razack, and Said Al-Hallaj. 2004. “A Review on Phase Change Energy Storage: Materials and Applications.” Energy Conversion and Management 45 (9-10): 1597–1615. doi:10.1016/j.enconman.2003.09.015.

[25] Feldman, D., M. M. Shapiro, and D. Banu. 1986. “Organic Phase Change Materials for Thermal Energy Storage.” *Solar Energy Materials* 13 (1): 1–10.

[26] Feldman, D., M. M. Shapiro, D. Banu, and C. J. Fuks. 1989. “Fatty Acids and Their Mixtures as Phase-Change Materials for Thermal Energy Storage.” *Solar Energy Materials* 18 (3): 201–16.

[27] He, B, V Martin, and F Setterwall. 2004. “Phase Transition Temperature Ranges and Storage Density of Paraffin Wax Phase Change Materials.” *Energy* 29 (11): 1785–1804. doi:10.1016/j.energy.2004.03.002.

[28] Baetens, Ruben, Bjørn Petter Jelle, and Arild Gustavsen. 2010. “Phase Change Materials for Building Applications: A State-of-the-Art Review.” *Energy and Buildings* 42 (9): 1361–68. doi:10.1016/j.enbuild.2010.03.026.

[29] Lide, David R. 2001. *Handbook of Chemistry and Physics*. 82nd ed. Boca Raton, FL: CRC Press LLC.

[30] Bourne, Stephen, and Atila Novoselac. 2015. “Compact PCM-Based Thermal Stores for Shifting Peak Cooling Loads.” *Building Simulation*, July. doi:10.1007/s12273-015-0243-6.

[31] Fan, Liwu, and J. M. Khodadadi. 2011. “Thermal Conductivity Enhancement of Phase Change Materials for Thermal Energy Storage: A Review.” Renewable and Sustainable Energy Reviews 15 (1): 24–46.

[32] Chun-Long Chen, and Nihad Dukhan. 2012. “Metal-Foam Enhanced PCM Storage System: The Cylinder-in-Cylinder Geometry.” *ASHRAE Transactions*.

[33] Velraj, R., R. V. Seeniraj, B. Hafner, C. Faber, and K. Schwarzer. 1999. “Heat Transfer Enhancement in a Latent Heat Storage System.” *Solar Energy* 65 (3): 171–80.

[34] Kousksou, T., A. Jamil, T. El Rhafiki, and Y. Zeraouli. 2010. “Paraffin Wax Mixtures as Phase Change Materials.” *Solar Energy Materials and Solar Cells* 94 (12): 2158–65.

[35] Bourne, Steve, and Atila Novoselac. 2014. “Compact Phase Change Based Thermal Storage: Experimental Apparatus, Methodology, and Results.” *ASHRAE Transactions* 120 (1): 1–8.

[36] Choi, Eunsoo, Young I. Cho, and Harold G. Lorsch. 1992. “Thermal Analysis of the Mixture of Laboratory and Commercial Grades Hexadecane and Tetradecane.” *International Communications in Heat and Mass Transfer* 19 (1): 1–15.

[37] He, Bo, and Fredrik Setterwall. 2002. “Technical Grade Paraffin Waxes as Phase Change Materials for Cool Thermal Storage and Cool Storage Systems Capital Cost Estimation.” *Energy Conversion and Management* 43 (13): 1709–23.

[38] Cengel, Yunus A., Robert H. Turner, and John M. Cimbala. 2008. *Fundamentals of Thermal-Fluid Sciences*. 3rd ed. New York, NY: McGraw Hill.

[39] Bezdek, Andréas, and Wlodzimierz Kuperberg. 1990. “Maximum Density Space Packing with Congruent Circular Cylinders of Infinite Length.” *Mathematika* 37 (01): 74–80.

[40] Stoecker, W.F. 1989. *Design of Thermal Systems*. 3rd ed. McGraw-Hill.

[41] ASTM. 2014a. “Standard Specification for Seamless Copper Water Tube.” ASTM International.

[42] ASTM. 2014b. “Standard Specification for Chlorinated Poly(Vinyl Chloride) (CPVC) Plastic Hot- and Cold-Water Distribution Systems.” ASTM.

Appendix C

PAPER 3: DESIGN GUIDELINES FOR HIGH-DENSITY THERMAL STORAGE SYSTEMS UTILIZING HEXAGONAL PACKED TUBE ENCAPSULATED PCM

Stephen Bourne, Atila Novoselac (graduate advisor)

(Submitted to Building and Environment)

ABSTRACT

HVAC cooling loads can be a large part of peak electric demand, particularly in hot and humid climates. Overall, 13% of electricity consumption is used for building HVAC operations in the U.S., but can account for as much as 27% of electricity use for residences in hot and humid climates. The ability to time-shift these cooling loads to off-peak hours, or to periods when intermittent energy generation is available, can reduce the cost of electric power and make better use of renewable energy resources. Local thermal energy stores for HVAC cooling load applications can be used for this purpose; however, a compact high-density solution is required for retrofit applications where large sensible energy thermal storage units are impractical.

This study investigates a latent thermal energy store using tube-encapsulated phase change material, densely packed using a hexagonal scheme within a larger containment tank, as a solution for high-density thermal storage for retrofit HVAC cooling load applications. A numerical model is developed and validated against existing test data, and a parametric analysis is performed to determine the impact of encapsulation tube radius, length, and quantity on thermal store performance and capacity. Guidelines are provided for engineers seeking to implement this design for specific applications, and an example of using the parametric data for this purpose is provided. A "stack and pack" variant of this system is proposed to reduce costs and encourage adoption of this thermal storage system.

LIST OF SYMBOLS

Symbols

α_f	Thermal diffusivity of the heat transfer fluid [m2/s]
A	Area (general) [m2]
A_a	Area associated with advection [m2]
A_c	Area associated with convection [m2]
A_k	Area associated with conduction [m2]
a	Constant (general)
C_f	Specific heat of the heat transfer fluid
D_h	Hydraulic diameter [m]
ε_p	PCM fraction of cross sectional area of thermal store [%]
ε_r	Energy recovery fraction [%]
H(t)	Latent enthalpy of a model volume element at time t
Hf	Heat of fusion [J]
h	Thermal convection coefficient [W/(m2 · ºK]
k	Conductivity (general) [W/(m · °K)]
k_{eff}	Conductivity, effective (general) [W/(m · °K)]
L	Length (general) [m]
Nu	Nusselt number [ ]
ϱ_f	Density of heat transfer fluid [kg/m3]
P_r	Prandtl number [ ]
r	Radius [m]
Re	Reynolds number [ ]

Reo	Outside radius of the encapsulation tube(s) [m]
Rei	Inside radius of the encapsulation tube(s) [m]
T	Temperature (general) [ºC or ºK]
T_m	Temperature at which PCM begins to melt [C]
T_s	Temperature at which PCM begins to solidify
t	Time (general) [s]
Δt	Time step interval [s]
V_f	Volume associated with a HTF node [m3]
w	Vertical heat transfer fluid velocity [m/s]
z	Vertical dimension (general) [m]
z_R	Reference vertical dimension (for graph); 1, 2, or 3m
Δz	Vertical step dimension or change in vertical height [m]

Subscripts

p	PCM parameter
f	Heat transfer fluid (HTF) parameter
s	Surface of encapsulation tube
t	Encapsulation tube parameter
m	Row identifier
n	Column identifier

Superscripts

t	time parameter [s]

Chapter C1: Introduction and background

HVAC cooling loads can be a large part of peak electric demand, particularly in hot and humid climates. For example, 13% of electricity consumption is used for building HVAC operations in the U.S. [1], but can account for as much as 27% of electricity use for residences in some southern tropical areas, such as Florida [2]. During the summer season, HVAC cooling loads can rise dramatically; the Energy Reliability Council of Texas (ERCOT) reports that up to 53% of their peak electric load during the summer can be attributed to weather-sensitive HVAC operation [3]. Small commercial and residential applications make up the largest share of this weather sensitive load.

The shifting of peak cooling loads to off-peak hours can reduce the cost of electric power by allowing baseload generation equipment to operate more economically, both by increases in operating efficiency and by improved returns on capital equipment investments [4]. The ability to shift peak cooling loads can also be used as a demand management tool to direct electric load towards periods when intermittent renewable energy resources are available. This can mitigate the uncertainty in power generation accompanied by the increased use of intermittent wind and solar power sources, while making better use of these renewable resources [5]. The ability to use demand-management tools to shift peak electric load associated with HVAC operation will become increasingly important as intermittent renewables comprise a larger and growing share of electric supply. In addition, residential and small commercial HVAC cooling demand is expected to increase in the U.S. due to a shift in population towards warmer regions of the country [6], increasing the demand for HVAC cooling. These are strong incentives for generators to look for utility-scale or distributed energy storage opportunities.

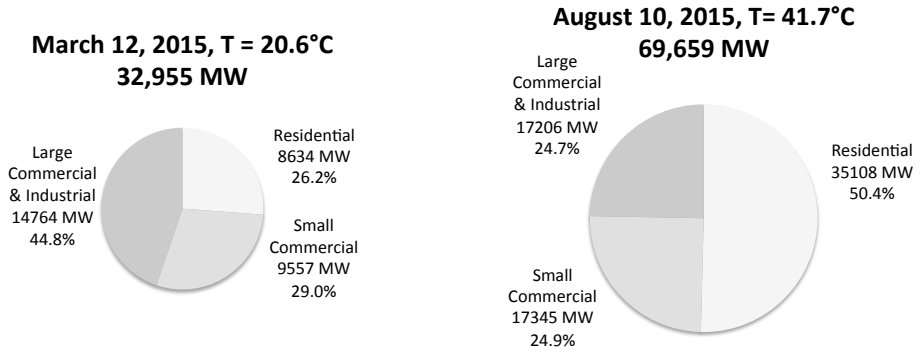

Figure C1: The impact of weather-sensitive HVAC operations on total electric demand, as determined by ERCOT [Wattles 2013]. T = outdoor temperature in °C. Note that the increase in peak power use resulting from weather-sensitive load is primarily due to residential and small commercial customers.

Local, actively-controlled thermal energy stores can be used to time-shift peak cooling loads. These systems store "cold" during off-peak electric hours, which is then used during peak hours to supplement or replace compressor-based HVAC operations. A common method of thermal energy storage used with hydronic-based HVAC systems utilizes large tanks of chilled secondary coolants, or heat transfer fluids (HTF), such as solutions of water and anti-freeze plus corrosion inhibiting components. Sensible thermal energy is stored in the system as a change in temperature of the storage medium. Water-based thermal storage systems have thermal storage densities typically on the order of 5.8 to 8.1 kWh (thermal)/m^3 of HTF, based on a 5 to 7 °C change in temperature of a water-based fluid as it passes through an HVAC system. Newer systems are capable of operating over a larger temperature change of up to 13 degree C, increasing the thermal storage density to 15.3kWh/m^3. However, these systems require the use of specialized chillers designed to run at a lower temperatures [7].

Due to their storage density, sensible water-based thermal storage systems tend to be quite large. While new buildings can be constructed to allow for these large sensible

thermal stores, existing buildings may not have the free space necessary for the coolant storage tanks. The average age of residential and commercial buildings in the U.S. is 37 and 28 years respectively [8.9], which underscores the need develop retrofittable thermal storage systems for these applications. For existing buildings, a solution that can operate at a higher storage density to minimize the size of the thermal store is required. In addition, the thermal store should be compatible with existing or typical chiller and cooling coil equipment so that the chiller supporting the existing HVAC system can also charge the thermal store.

An alternative method of thermal storage utilizes the latent heat resulting from a change in phase, most commonly between solid and liquid forms to minimize volumetric and pressure changes in the system. Materials used in this manner are termed "phase change materials", or PCMs. PCM-based thermal storage systems are characterized by large changes in enthalpy at small or no change in temperature. Common solid-liquid PCMs suitable for cold storage are water, paraffins, and fatty acids, and salt hydrates [10-15]. Of these, paraffins show promise as a thermal storage PCM due to their high latent energy capacity (~220kJ/kg), lack of a subcooling requirement to initiate freezing, compatibility with common encapsulation materials, and chemical stability over many thermal cycles [14, 16-18]. Paraffins are hydrocarbon alkanes available in a wide range of compositions and freezing temperatures, with longer carbon chains having higher melting temperatures [Hale, Humphries].

To be used in a thermal storage application, the PCM must be isolated from the HTF used in the HVAC system. One method to isolate the PCM is through the use of a shell-and-tube design, where the PCM occupies the shell and tubes carrying HTF run through the shell [19]. This design has an advantage in that the shell-and-tube heat exchanger configuration is well understood. However, the tubes running through the shell

complicate plumbing and increase costs, and also occupy space that would otherwise contain PCM and thus lowers overall system capacity.

Alternatively, the PCM can be macro-encapsulated into cylindrical, rectangular or spherical containers [20]. The encapsulated modules of PCM are then placed into a larger tank and exposed to a flow of HTF to store or recover latent thermal energy. Spherical encapsulation containers, while having the greatest surface area, pack poorly; hexagonal close-packing of spheres results in a maximum density of only ~74% [21]. Rectangular encapsulation can be packed to 100% density, but this leaves no room for the HTF to flow; this encapsulation system must be mechanically spaced to allow HTF flow, increasing the cost and complexity of the thermal store. Cylinder (tube) encapsulation, on the other hand, self-packs into a hexagonal arrangement to a maximum 90.7% density [22] while leaving small triangular-like flow paths for HTF distributed evenly around each tube. The base performance and cost per unit of a thermal store constructed with hexagonal-packed tubes is configurable by altering the diameter of the cylinders, while the capacity is scalable by increasing the height and number of cylinders.

Previous studies have shown that this hexagonal-packed cylinder configuration can provide acceptable performance and improved thermal storage densities for HVAC applications if the thermal encapsulation shell meets certain conditions defined by the thermal properties of the encapsulation material, PCM, HTF, and cylinder dimensional parameters [23,24]. A thermal storage system for HVAC cooling load applications, utilizing the PCM tetradecane ($C_{14}H_{30}$) and a hexagonal-packed array of encapsulation tubes, can have a thermal storage density of between 3 and 7 times that of advanced conventional chilled water storage systems. Future improvements in PCMs may yield even higher densities. However, generally applicable design guidelines for engineers wishing to implement this thermal store design are lacking.

The objective of this study is to provide design guidance for the hexagonal-packed tube encapsulated PCM-based thermal storage systems proposed by Bourne and Novoselac [23-26]. The study investigates the affect of encapsulation tube radius, length, and quantity on system performance and provides guidelines necessary for the use of this design in specific applications. In addition, a modular "stack and pack" method of design and construction is proposed that will facilitate the mass manufacture of this system, reducing costs and enabling wider adoption of the design.

Chapter C2: Methods

A finite volume numeric model is developed for the hexagonal-packed tube encapsulated thermal store design. The numeric model is validated against existing data, and a parametric analysis is performed based on various encapsulation tube lengths and radii.

C2.1 Numerical Model

A linear numerical model based on a finite volume method is selected for maximum flexibility. The finite volume method permits multiple phase fronts (as well as non-distinct, "mushy" phase fronts [27]) that might occur during interrupted charge/discharge cycles of paraffin compounds, and also permits the variable or intermittent flow rates typically encountered in hydronic-based HVAC systems. In addition, this model type allows for thermal re-reorganization in the store due to conduction during periods of zero HTF flow, which can occur from repeated intermittent cooling demand calls between charge sessions. Finally, this method allows for a combined vertical and radial conduction scheme, which is required for the highly conductive encapsulation shells needed for this design. The model takes as input matrices representing the previous time step temperature and latent energy values for each node (latent energy is set to 0 for surface and non-PCM nodes), HTF input temperature and flow rate, as well as physical parameters and constants for the model. It returns a set of matrices representing the current time step temperature and latent energy values. Successive iterations can be used to model operation over any time interval. The default time step is one second.

The finite volume numerical model of the thermal store is based on a method previously developed for annular flow around closely-spaced cylinders of encapsulated

PCM [24]. This model is modified for the hexagonal-packed cylinder-encapsulated PCM-based thermal store design by allowing for the HTF flow paths created by the intersection of the encapsulation tubes, as shown in Figure C2, to be treated as triangular pipes. Nusselt number correlations exist for average heat transfer in triangular pipes; however, these correlations represent an average heat transfer effect that is not uniform across the pipe surface. This is because HTF flow is restricted at the apex of the triangles, reducing heat transfer in these areas. To eliminate this concern, the model incorporates the "resistance ratio" design parameter proposed by Bourne and Novoselac [23] in the specification of the encapsulation tubes. When applied, this design parameter ensures that the conductivity around the shell of the encapsulation cylinder is an order of magnitude higher than the conductivity either to or from the PCM or HTF. This makes possible the assumption that the thermal load and temperature are well distributed and uniform around the surface of the encapsulation cylinder ($dT/d\theta = 0$) making thermal transfer in the encapsulation cylinder and PCM axisymmetric. This simplifies modeling by reducing the model to two dimensions (r and z). Note that because the resistance ratio parameter defines the relationship of the outside radius of the encapsulation tube and material to the encapsulation wall thickness, only the outside radius and material of the encapsulation tube are specified for the model.

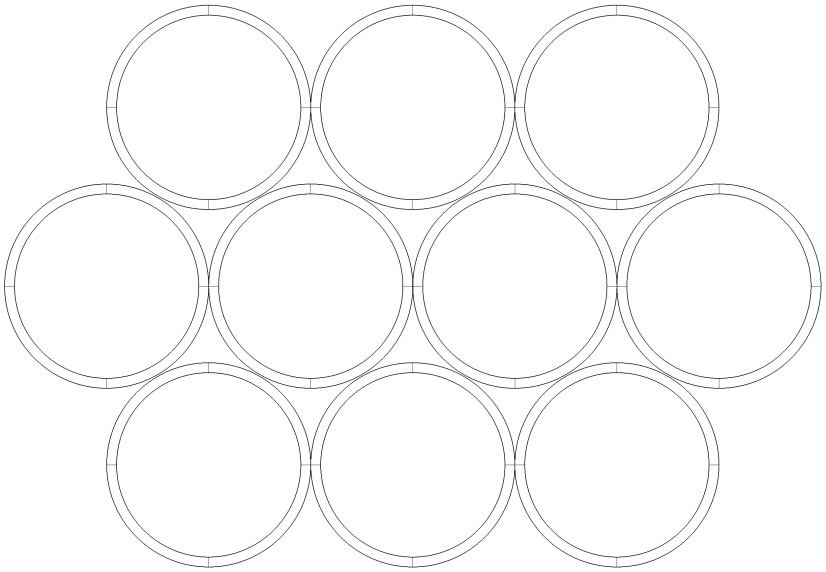

Figure C2: The packing scheme used in the thermal store. Note the triangular-like flow paths for the HTF that result from the intersection of the encapsulation cylinder surfaces.

Figure C3 shows an element that is the basis for the numerical model. This element represents a 60° ($\pi/3$ radian) section of an encapsulation cylinder with arbitrary step height Δz, including its surrounding HTF and enclosed PCM, spanning between the contact points of the adjoining encapsulation cylinders. The vertical surfaces of the element are adiabatic, based on the assumptions that $dT/d\theta = 0$ (axisymmetric) in the PCM and encapsulation shell, and that HTF stratification in the tank results in a uniform temperature for all HTF cells at the same vertical location in the tank. However, horizontal surfaces are subject to the temperature gradient in the tank and are therefor not adiabatic. These two assumptions (vertical interfaces are adiabatic, horizontal interfaces are not) allow the thermal store to be modeled as a stack of these elements.

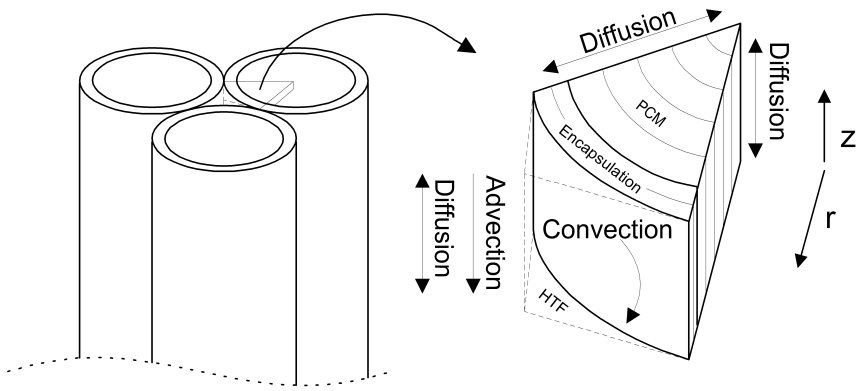

Figure C3: An element of the numerical model, which consists of components representing the HTF, encapsulation cylinder, and PCM. The model combines a vertical stack of these elements.

Each element consists of volumes representing the HTF, encapsulation material, and PCM, and each volume contains a node. In addition, some surface nodes are assigned where dissimilar materials or heat transfer mechanisms occur. Volume nodes are used to track temperature, and thus accumulate sensible energy. Volume nodes in the PCM are also used to track latent energy. Surface nodes track temperature, but do not accumulate thermal energy; they act only as transfer agents between volume nodes. An example representation of the nodes and volumes use in the model is shown in Figure C4.

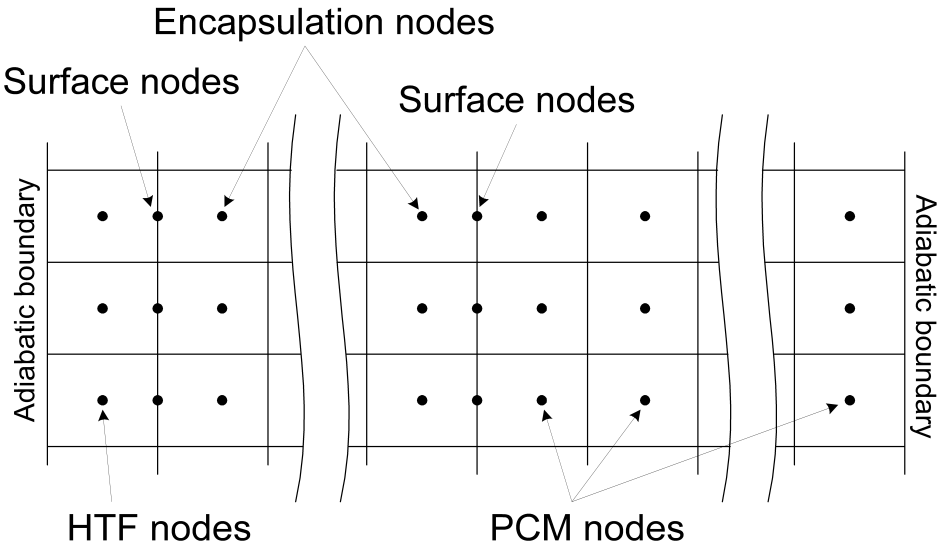

Figure C4: Example node breakdown for different elements of the model. HTF, encapsulation, PCM, and boundary surface nodes are depicted. The number of PCM and encapsulation nodes are configurable for each model run.

The model considers advection of HTF flow, vertical diffusion in the HTF, convection from the HTF to the surface of the encapsulation surface, as well as vertical and radial conduction within the encapsulation material and PCM. Changes in sensible energy are calculated by temperature differences between time steps and the specific heat of the material associated with each volume node; changes in latent energy are calculated by the net energy exchanged during phase transition at each time step.

A natural temperature gradient in the tank is maintained to insure that the tank remains stratified and that buoyancy-driven, short-circuit HTF flows are avoided. To accomplish this goal, the direction of HTF flow is made dependent on the cycle type (charge or discharge). During the charge cycle, cold supply HTF is pumped into the bottom of the thermal store and warms as it rises in the tank, absorbing energy from the solidifying PCM; during the discharge cycle, warm return HTF is pumped into the top of

the tank and is cooled as it descends in the tank. Maintaining tank stratification minimizes the potential for buoyancy-driven free convection in the HTF, and so this potential is ignored. Only conductivity is considered in the PCM, regardless of phase; any buoyancy-driven convection effects in the PCM are assumed to be included in the effective conductivity of the PCM, k_c.

Thermodynamic properties associated with the HTF and the encapsulation material are considered constant over the temperature range of the thermal store; these properties are evaluated at the mean operating temperature. Thermodynamic properties of the fully solid or fully liquid PCM are set dependent on phase state.

If the PCM has different conductivity parameters for each phase (liquid, solid) then the conductivity during phase change is set as a linear interpolation of the solid and liquid values based on phase state. In addition, since adjacent cells of PCM may be in different states of phasing and therefore have different conductivity values, the net effective conductivity between adjoining nodes is calculated before each iteration of the model; this allows for the use of larger model elements, reducing node counts and improving model computational run-times. This calculation equates the sum of the thermal resistances to heat flow for the applicable portion of the each element to the net total effective resistance; simplifying and inverting the result yields the effective conductivity between the nodes. Figure C5 and Equation C1 demonstrate this calculation for horizontally adjoining nodes/cells; the same procedure is applied for vertically adjoining cells.

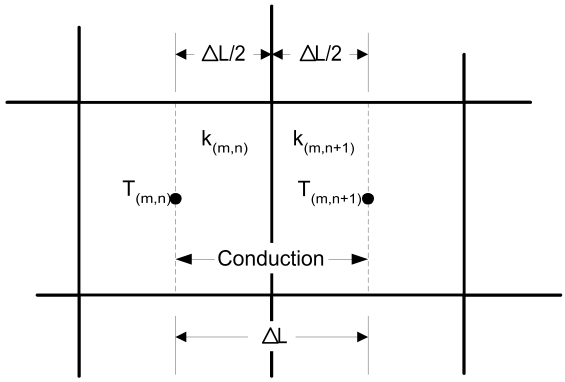

Figure C5: The physical basis for calculating the effective conductivity value k with respect to heat transfer between adjoining cells with different conductivities.

$$\frac{\Delta L/2}{k_{m,n}A_k}+\frac{\Delta L/2}{k_{m,n+1}A_k}=\frac{\Delta L}{k_{eff}A_k} \quad \rightarrow \quad k_{eff}=\frac{2k_{m,n}k_{m,n+1}}{k_{m,n}+k_{m,n+1}} \tag{C1}$$

Heat transfer associated with the HTF is modeled using a single HTF node at each vertical step in the model. Advection and vertical diffusion is modeled between HTF nodes, and convection is modeled between the HTF nodes and the surface nodes of the encapsulation cylinder. For convection purposes, the spaces formed between the encapsulation cylinders are modeled as a set of triangular pipes. The flow rates from experiments using this design [23,24] show that velocities are very low. Reynolds numbers are on the order of 1, ensuring laminar flow. A Nusselt number for laminar flow in triangular pipes of 2.5 is used for convection purposes [28]. Each HTF node volume is assumed well mixed at the beginning of each time step, with uniform temperature. The geometry and node configuration is shown in Figure C6, with the formula used to describe the energy balance and heat transfer with respect to the HTF given in Equation C2.

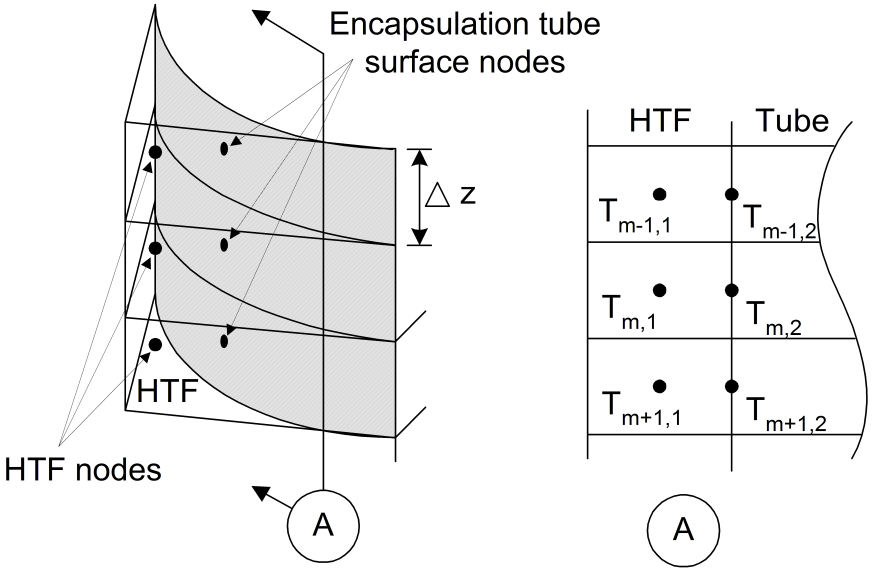

Figure C6: Geometry and node configuration for heat transfer in the HTF. This figure shows the HTF and convection surface nodes considered during the convection, advection, and diffusion modeling of the HTF. Flow is vertical (top to bottom) during the discharge cycle.

$$V_f \rho_f C_f \left(T_{m,1}^{t} - T_{m,1}^{t-\Delta t}\right) = A_c h \left(T_{m,2} - T_{m,1}\right)\Delta t + A_a k_f \left(\frac{T_{m-1,1} - T_{m,1}}{\Delta z} - \frac{T_{m,1} - T_{m+1,1}}{\Delta z}\right)\Delta t + A_a w \rho_f C_f \left(T_{m-1,1} - T_{m,1}\right)\Delta t \quad \text{(C2)}$$

This equation collapses to the differential form found in Equation C3.

$$\frac{\partial T}{\partial t} = \frac{A_c}{V_f}\frac{h}{\rho_f C_f}\left(T_s - T_f\right) + \alpha_f \frac{\partial^2 T}{\partial z^2} - w\frac{\partial T}{\partial z} \quad \text{(C3)}$$

The hydrodynamic entry length can be estimated with Equation C4 using the hydraulic diameter of the triangular-like flow paths and an estimated expected Reynolds number on the order of 1, and the thermal entry length can also be estimated using Equation C5 and the mean Prandtl number of the HTF [28]. The results indicate that the hydrodynamic entry length is on the order of 1mm, and as a result the flow is assumed hydrodynamically fully developed everywhere in the tank. The results also indicate that the thermal entry length is short relative to the length of the tank, on the order of 16mm.

It should be noted that the thermal entry length calculation is predicated on a constant wall temperature, which is not present in this design. However, the rate of change of wall temperature in the tank during operation is small, and as a result we will assume that the thermal entry acts as if the wall temperature is constant over the time and length interval of interest for each model element, and that the flow is fully thermally developed everywhere in the tank with respect to the model elements.

$$L_{fd,h} = 0.05\mathrm{Re}_{D_h} D_h \tag{C4}$$

$$L_{fd,t} = 0.05\mathrm{Re}_{D_h} D_h \mathrm{Pr} \tag{C5}$$

Heat transfer within the encapsulation cylinders and the PCM considers conduction only, in both the r and z directions, regardless of whether the PCM is solid, changing phase, or liquid. The geometry and node configuration is shown in Figure C7. Note that the surface nodes used between the PCM and the encapsulation material are not shown here.

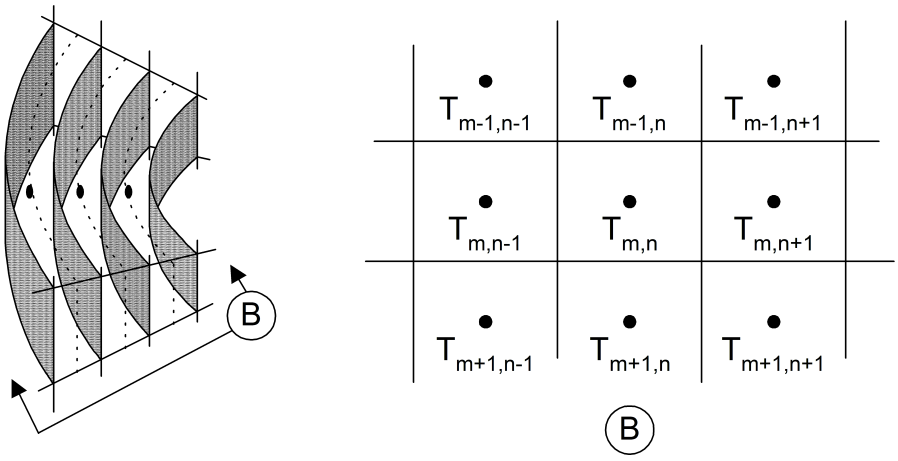

Figure C7: The node configuration for radial and vertical conduction in the encapsulation and PCM.

Figure C7 is used to develop Equation C3 to solve for unknown temperatures at each time step.

$$V_{(m,n)}\rho_{(m,n)}C_{(m,n)}\frac{T^{t}_{(m,n)}-T^{t-\Delta t}_{(m,n)}}{\Delta t}=$$
$$\left[k_{(m,n)}A_{o(m,n)}\frac{T_{(m,n-1)}-T_{(m,n)}}{\Delta r}-k_{(m,n)}A_{i(m,n)}\frac{T_{(m,n)}-T_{(m,n+1)}}{\Delta r}\right]+ \qquad \text{(C6)}$$
$$\left[k_{(m,n)}A_{h(m,n)}\frac{T_{(m-1,n)}-T_{(m,n)}}{\Delta z}-k_{(m,n)}A_{h(m,n)}\frac{T_{(m,n)}-T_{(m+1,n)}}{\Delta z}\right]$$

This equation assumes that adjacent nodes have the same heat capacity and conductivity, which is not true at the interface between the encapsulation tube and the PCM; however, surface nodes are used there to differentiate between the materials and eliminate this concern. The PCM conductivity values shown in Equation C6 are replaced with the calculated effective conductivity values at run time. This equation collapses to the heat equation (assuming k = constant) in cylindrical coordinates for the r and z dimensions:

$$\frac{\partial T}{\partial t}=\frac{\alpha}{r}\frac{\partial}{\partial r}\left(r\frac{\partial T}{\partial r}\right)+\alpha\frac{\partial^2 T}{\partial z^2} \qquad \text{(C7)}$$

To improve the performance and accuracy of the model, a log-mean value is used for conduction calculations involving radial areas represented in Equation C6. This is based on the idea that radial conduction between volumetric temperature nodes can be thought of as conduction between two surface nodes of a cylindrical mass. In this case the integration of Fourier's law gives an effective area for heat transfer equal to the log mean area of the two surfaces involved [29]. This log mean area is used for conduction between radial nodes to maintain model accuracy while allowing larger radial steps.

While the general heat equation still applies during phase transition, its use must be modified to account for the phase change process. During phase change the PCM

absorbs or releases a large amount of energy; for an idealized pure PCM, the temperature would be constant during that change. A model for this process would fix the PCM temperature during phase change and then solve for the remaining surrounding temperatures, energy exchanges and net enthalpy change associated with the phase transition. After the PCM element had received or released all the necessary energy to complete phasing, the model would return to representing the PCM element using fixed thermodynamic properties for the PCM in liquid or solid form. However, the PCM modeled here is not ideal.

Previous experiments [24] have shown that the 99% tetradecane PCM utilized melts over a temperature range estimated to be between 4.5°C and 6.5°C, rather than at a single temperature. Differential scanning calorimeter (DSC) testing on other paraffins show similar characteristics, and also that the heat absorption rate during phase change is not constant with temperature [30]. This precludes the use of an alternative constant specific heat capacity value for use during PCM phase change (the heat of fusion divided by the temperature range over which the phase change occurs). Instead, a latent enthalpy tracking method is used to determine the temperature of a phasing PCM node at each time step based on its current phase state. Note that this method is used only for determining the temperature of PCM nodes undergoing phase change; otherwise, the temperatures are found by simultaneously solving for them with the remaining node temperatures.

The area under the curve shown in Figure C8 represents an estimate of the latent enthalpy change in the PCM with respect to temperature over the phase change temperature range. The basic curve shape is based on heat flow rate curves for similar paraffins undergoing DSC testing using a slow temperature ramp rate [30,31], and the knowledge that the DSC heat flow rates are proportional to instantaneous specific heat

during phase change [31]. The curve is estimated as a square function of temperature, with the requirement that the integral of the curve represent the total heat of fusion of the PCM element (Equation C8). This leads to Equation C9, which solves for the temperature of the PCM node based on the cube root of the fractional phase state of the node.

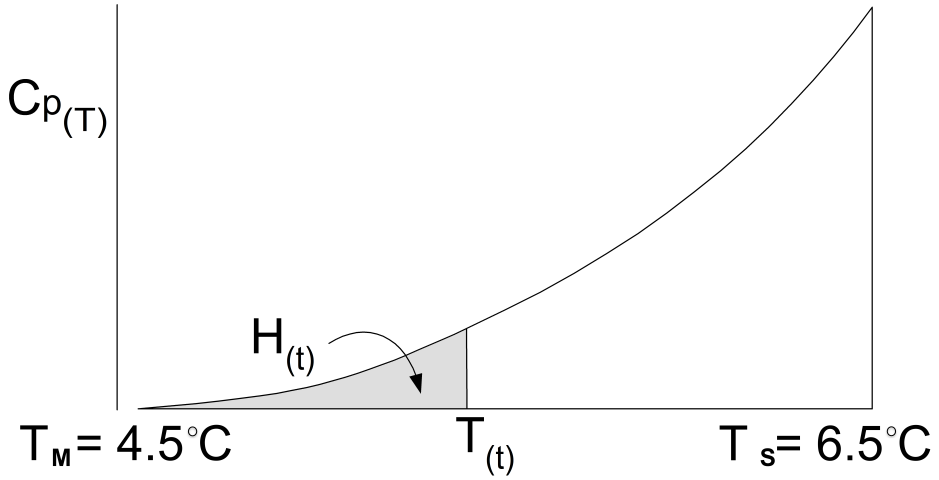

Figure C8: This curve is used to find the temperature of a PCM node only while it is undergoing phase change. T_m and T_s are the low and high temperatures (4.5 and 6.5°C respectively) of the phase change process, and the area $H_{(t)}$ represents the total enthalpy contributing to phase change at time t and temperature T(t).

$$H_f = \int_0^{T_s - T_m} aT^2\,dT = \frac{a}{3}\left(T_s - T_m\right)^3 \quad \rightarrow \quad a = \frac{3H_f}{\left(T_s - T_m\right)^3} \tag{C8}$$

$$H(t) = \int_0^{T - T_m} aT^2\,dT = H_f \frac{\left(T(t) - T_M\right)^3}{\left(T_S - T_M\right)^3} \quad \rightarrow \quad T(t) = T_M + \left(T_S - T_M\right)\sqrt[3]{\frac{H(t)}{H_f}} \tag{C9}$$

The temperature of a phasing PCM element is set at the beginning of each time step iteration based on the current phase state, and the remaining unknown model node

temperatures are resolved. The current enthalpy of the phasing PCM element is then updated using the resolved node temperatures and general conduction equations. In this way the temperature of a PCM node undergoing phase transition is held constant during the time step, as with a perfect PCM, but is updated to a new constant value for the next time step based on the updated phase enthalpy. Small time steps (1 sec) minimize error using this method.

C2.2 MODEL VALIDATION/CALIBRATION

The model data is compared to previous test data [23] to validate the model. However, there are some fundamental differences between the idealized model and the actual experiments from which the validation data was obtained. To make the model comparable to the test data, adjustments are made to the model as described in the following paragraphs. All adjustments to the model are removed for the parametric study; these adjustments are only used for model validation purposes.

The experimental apparatus has an additional volume of HTF at the top and bottom of the tank. A pre-processor is added to the model to account for the time shift and thermal diffusion that occurs as a result of these pools.

The numerical model assumes a perfect insulation system (no losses through the shell). The actual experiment has limited insulation resulting in some losses through the shell, and due to the small diameter of the shell these losses are iportant (large surface area to volume ratio). To account for the losses, a separate loss calculation is added to the model based on the measured loss rate of the experiment. The measured loss rate is based on a measured steady-state loss rate; typical loss rates noted are between 0.2 and 0.3 W/°K over the surface of the tank, where °K is the difference between the ambient and tank temperature. This adjustment is applied directly to the HTF in the tank during the

model run.

The PVC shell of the experiment accounted for approximately 5% of the total thermal capacity of the thermal store, while the model assumes no mass in the shell. To compensate for this the sensible thermal capacity of the shell is proportionally added to the sensible capacity of the PCM.

A finite amount of time is required set up the experimental apparatus for each run, resulting in a small thermal gain through the shell of the tank. This results in a partial tank stratification, causing a small temperature differential between the top and bottom of the tank. An adjustment is made in the temperatures of the model to duplicate the 0.2°C gradient in the tank before each model run to compensate for this gain.

A validation/calibration run is made at temperatures above the freezing point of the PCM. This allows calibration of the PCM liquid state conductivity, and validation of the model for sensible energy conditions. Note that only the PCM conductivity is adjusted during calibration; all other properties of the materials used in the thermal store are taken from the literature as shown in Tables C1 through C3. For this comparison the thermal store is stabilized at a temperature slightly above 7°C (above the melting temperature of the PCM), then 17°C HTF is input to the store at a normalized rate of approximately 30L/(min m^2 of PCM) until the temperature stabilizes in the tank stabilizes. The model and experimental data are then compared, as shown in Figure C9. The best fit resulted when using a conductivity value for the PCM in its liquid state of 0.15 W/(m °K), and results in the model data beings almost indistinguishable from the experimental data. This value also agrees with published data [12].

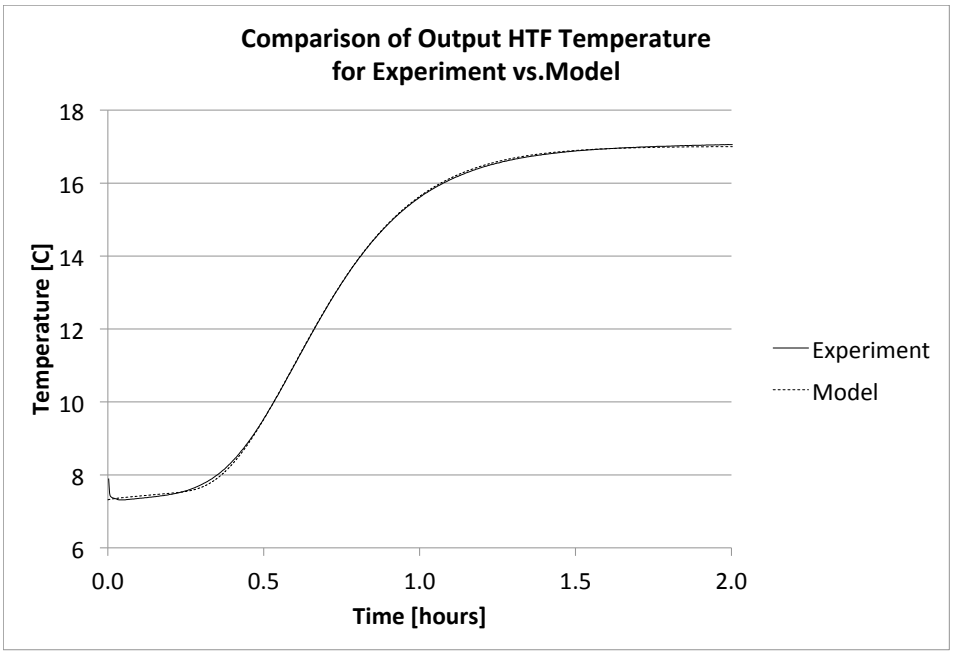

Figure C9: A comparison of the model to experimental data. The experimental thermal store is preconditioned to 7°C, then 17°C water is input until the thermal store stabilizes at the new temperature. This temperature range is chosen to ensure sensible thermal changes only are considered. The experiment and model show good agreement.

A second validation run is made at temperatures below the minimum freezing point of the tetradecane PCM. This allows calibration of the solid state PCM conductivity, and validation of the model under a second sensible energy condition. In this case the thermal store was conditioned to a temperature of approximately -4°C, then HTF at a temperature of 3.5°C is input to the store until the temperature stabilizes at the new value. The model and experiment data are compared in Figure C10.

In this case no single value of conductivity for the solid PCM allowed for a match over all of the data. However, visual inspection of a clear PVC tube containing frozen tetradecane noted a separation of the PCM from around the partial inside perimeter of the tube. The PCM has a higher density when solid, which indicates that the PCM shrinks when frozen. The observation and density data suggest that a high-resistance interface

may be formed at the inside surface of the encapsulation tube due to the PCM shrinking and pulling away from the surface of the tube during the freeze cycle. To compensate for this the model utilizes a two-step conductivity value for the solid state PCM. The node adjacent to the tube surface is given a conductivity a value of 0.06 W/(m °K), while all other solid PCM nodes are assigned a conductivity for the solid PCM value equal to that of the liquid phase, or 0.15 W/(m °K). The interface discontinuity only exists while the node is fully solid; as soon as the melting process starts in a node it is assumed that the melted PCM will fill in the discontinuity, and so at that point the PCM node is reassigned the standard solid phase conductivity value of 0.15 W/(m °K). These values provide a reasonable match to the experimental data up to the point where the output temperature climbs above 1.5°C.

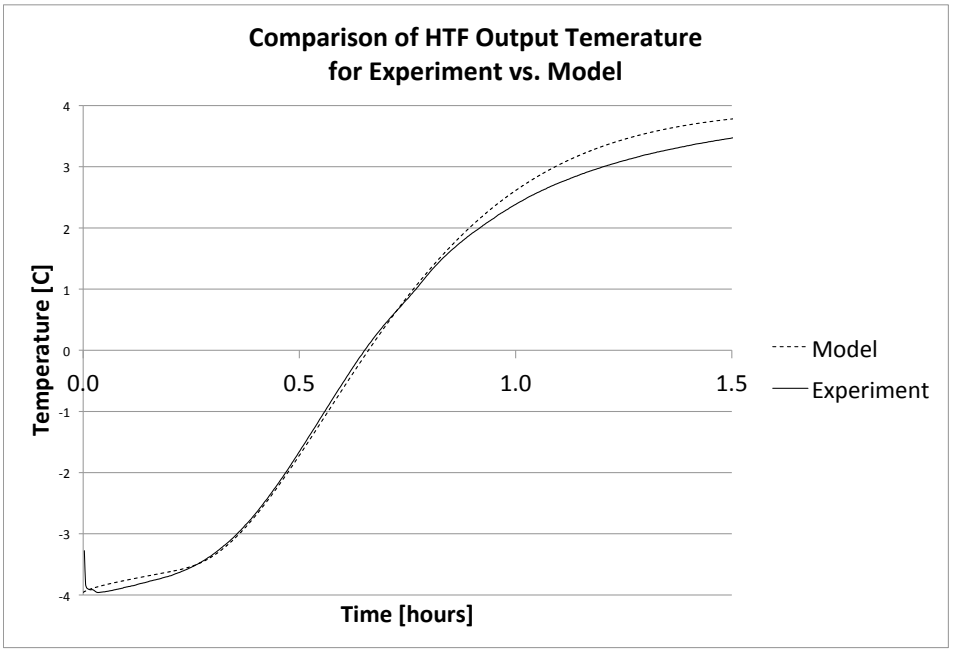

Figure C10: A comparison of the output HTF temperature between the model and the experiment. Using a two-stage conductivity value provides good agreement up to ~2°C. The remaining differences are attributed to early onset phase transition.

After 0.8 hours (output temperature above 1.5°C) the model and experimental

data diverge significantly. However, a sensible energy analysis of the model and experiment does not account for the additional energy absorption of the experiment. A possible reason for this discrepancy is that an early-onset portion of the phase transition is absorbing part of the energy. Since the additional energy cannot be accounted for in a sensible energy balance, we will assume that an early phase transition is the cause of the divergence.

A latent heat value for the PCM is found using an energy balance method to be 215kJ/kg for the 99% tetradecane during the original experiments. This value is in the range of published values for tetradecane (211 – 227 kJ/kg) [12,13,32], and is used here as well for compatibility.

A comparison between the model and the experiment over a phase transition is also performed using the calibrated model information. The comparison includes both output temperature and energy recovery as a percent of total energy in the thermal store. The results of that comparison are shown in Figure C11. The results shows greater variance due to the unknowns associated with the thermal properties of the PCM during phase transition, however, the energy recovery as percent of total thermal store energy and HTF output temperature are in good agreement. When the particular value of interest for this study – the percent of total energy recovered at $T_{out} < 6.5°C$ – is compared between the model and the experimental data, it shows an average error of approximately +/-4%. This value is similar to the expected error reported for the experimental measurements, given as 3.7% [23]. This shows that the model is sufficiently accurate for its intended purpose.

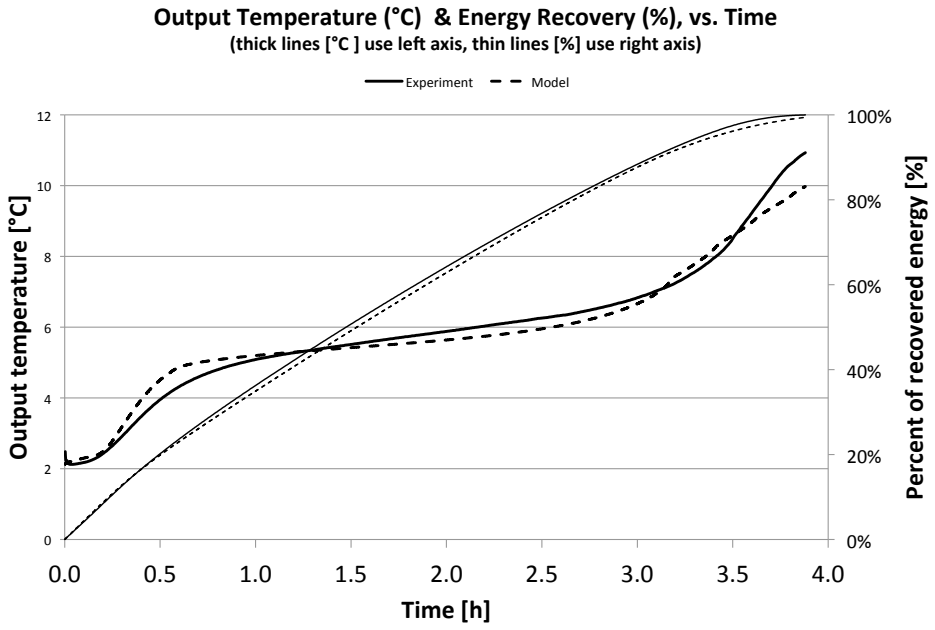

Figure C11: A comparison of experimental to model data shows good agreement. This plot shows both recovery rate as a percent of total thermal capacity and output temperature of the HTF. The discrepancies are likely due to the unknown thermal properties of the PCM as it undergoes a phase transition.

C2.3 PARAMETRIC ANALYSIS

The model is run for a series of encapsulation tube outside radius dimensions ranging from 0.007m to 0.016m [0.007, 0.010, 0.013, and 0.016m] and heights of 1 to 3 meters in 1 meter increments. Aluminum is modeled for the encapsulation tube material to minimize costs (for instance, by capitalizing on existing knowledge held by the soft drink and canning industry in the manufacture, filling, and protection of aluminum containers). The selected PCM is tetradecane, $C_{14}H_{30}$, in a lab-grade (99%) configuration. The HTF is a 35% solution of propylene glycol in distilled water. The tank shell thermal mass is ignored, and the tank is also assumed to be perfectly insulated (no tank wall losses). The thermodynamic properties of the HTF, aluminum encapsulation material, and PCM are given in Tables C1 through C3.

Property	Value	Units	Source
Density	1038	kg/m^3	ASHRAE Fundamentals 2009 [33]
Kinematic viscosity	$6.73x10^{-6}$	m^2/s	
Conductivity	0.394	$W/(m \cdot ^\circ K)$	
Heat capacity	3735	$J/(kg \cdot ^\circ K)$	

Table C1: Properties of 35% (by volume) propylene glycol in water at 6.5°C

Property	Value	Units	Source
Density	2700	kg/m^3	Lide,2001 [34]
Conductivity	236	$W/(m \cdot ^\circ K)$	
Heat capacity	881	$J/(kg \cdot ^\circ K)$	

Table C2: Properties of Aluminum at 6.5°C

Property	Value	Condition	Source
Freezing temperature	5.5ºC	N/A	Hale et al, 1971 [12]
Density (solid)	825 kg/m^3	4ºC	
Density (liquid)	771 kg/m^3	10ºC	
Latent heat	211 to 226 (kJ/kg)	(liquid)	
Conductivity	0.15 W/(m ºK)	20ºC	
Heat capacity (solid)	1.68 kJ/(kg ºK)	-20 to 0ºC	Kousksou et al. 2010 [35]
Heat capacity (liquid)	2.18 kJ/(kg ºK)	25ºC	

Table C3: Properties of Tetradecane

Flow rates are normalized per cross-sectional area [m^2] of PCM, based on the encapsulation tubes being vertical in the tank and the cross sectional area a horizontal plane through the store. These flow rates of 20 to 60 liters/(min m^2 of PCM) [20, 30, 40, 40, 50, and 60 L/(min m^2 of PCM)] are proportional to those used in previous studies of this thermal store design [23].

The initial state of the store is fully charged at 2°C, and the incoming HTF is set at a fixed 11°C. A temperature of 6.5°C is assumed to be the upper limit of usable output temperature, and is used for comparison purposes between different configurations and run parameters.

Chapter C3: Results/discussion

Model runs are performed for each of the possible tube sizes and flow rate values under consideration. Calculations pertaining to thermal store capacity are normalized so that each store, regardless of encapsulation tube size, has a PCM cross-sectional area of $1m^2$ and utilizes tubes of 1, 2, or 3m in length. Figure C12 shows an example of output temperature and cumulative energy recovery as a percent of store capacity.

Figures C13 shows the percent of total energy (sensible and latent) recovered at an output temperature of less than than 6.5°C for aluminum encapsulation tubes by tube radius, length, and flow rate. Flow rates are normalized per square meter of PCM, as examined by a horizontal cross section through the thermal store. These results show that smaller tube diameters allow for greater total energy recovery at any flow rate, but that larger diameter tubes can be used where taller tanks, lower flow rates, or lower total energy recovery values can be tolerated. Larger tubes can reduce costs associated with PCM encapsulation per unit of storage.

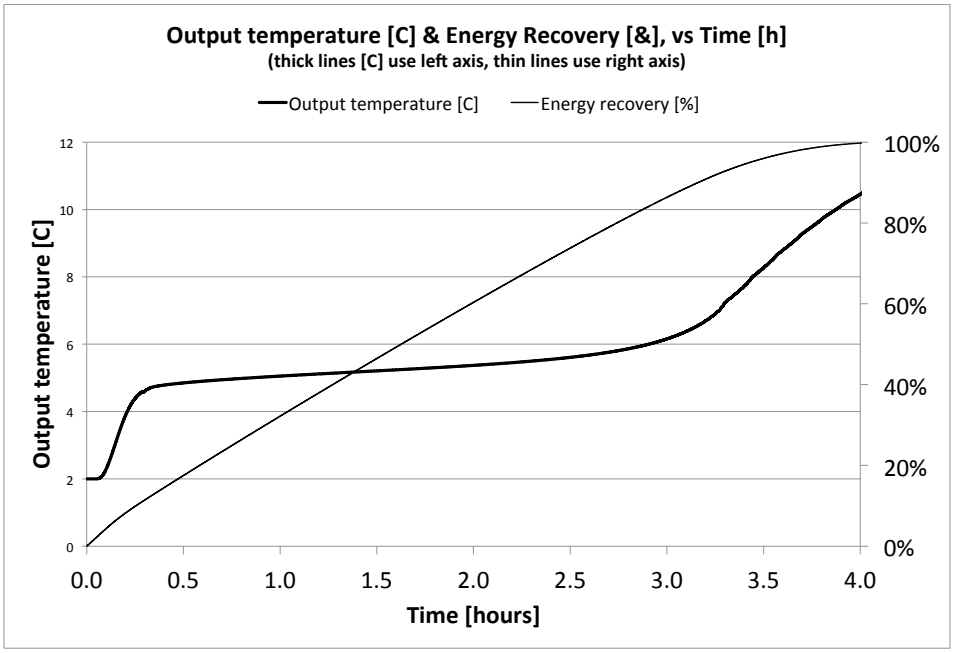

Figure C12: Example output from the model showing the temperature out and energy recovery as a percentage of total capacity with respect to time for 0.007m readius encapsulation tubes and a 40L/(min*m^2 PCM) flow rate of incoming 11°C HTF. Find the time where the temperature reaches the maximum permissible output temperature and then move up to find the percent of energy recovered.

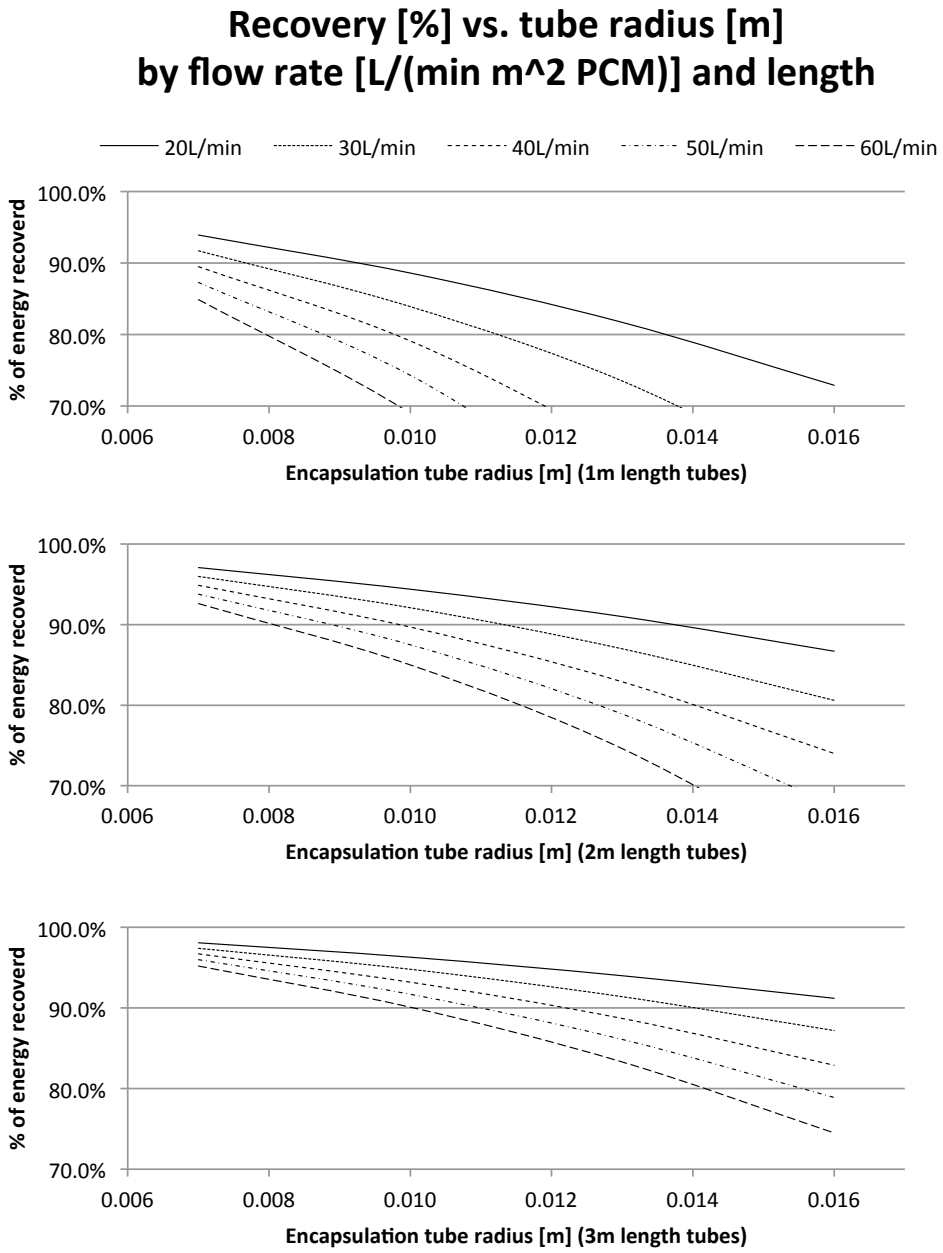

Figure C13: The recovery rate as a percentage of total thermal store capacity is plotted for various encapsulation tube radii by flow rate per m^2 of PCM cross-sectional area, for 1,2,and 3m long tubes, where the input temperature is 11°C and the output temperature is <6.5°C. The results show that as tube radius increases, flow rates must be slowed or the tubes lengthened to maintain a high recovery rate.

Understanding how the performance of this system will be altered as a result of diameter, height, or material changes in the thermal store can extend the use of this parametric data. For example, since the flow rate of the model is based on the cross sectional area of PCM, adding diameter to the tank provides an increase in flow rate and capacity proportional to the increased cross-sectional area of the store while maintaining the recovery rate and run times predicted for the smaller unit. For example, a thermal store with a PCM cross-sectional area of $2m^2$ would allow for a flow rate of 40L/min while following the energy recovery projection for a 20L/(min m^2 of PCM) flow rate as shown in Figure C13. This same procedure can also be used to design smaller thermal stores.

Taller encapsulation tubes can add capacity and performance as well, but have a different impact on recovery/flow rate performance. A further analysis of the store shows that as the system is operated a temperature gradient is formed in the thermal storage tank. Once established, the temperature gradient maintains a relatively stable slope and length as it moves down the tank during the discharge cycle until it meets the tank output, after which the output temperature rises quickly. This is demonstrated in Figure C14, which shows snapshots of the tank HTF temperature with respect to vertical position within the tank at ½ hour time intervals. This indicates that, so long as the length of the thermal store is longer than the final temperature gradient formed in the tank at the point the maximum acceptable output temperature is reached, any length added to the thermal store encapsulation tubes will add capacity that is completely recoverable.

As a result, an increase in height will add capacity and improve the energy recovery fraction ε_r of the thermal store at any given configuration and flow rate. The

change in energy recovery resulting from a height increase over the reference heights of 1, 2, and 3 meters can be estimated using Equation C7. In this equation, $\varepsilon_{r'}$ is the adjusted energy recovery percent, ε_r is the recovery percent taken from the appropriate graph in Figure C13, z_R is the reference height of the graph used in Figure C13, and Δz is the height added above the reference height. All of the tested configurations, when recovery was above 70%, met the requirement for thermal gradient length necessary use of Equation C7.

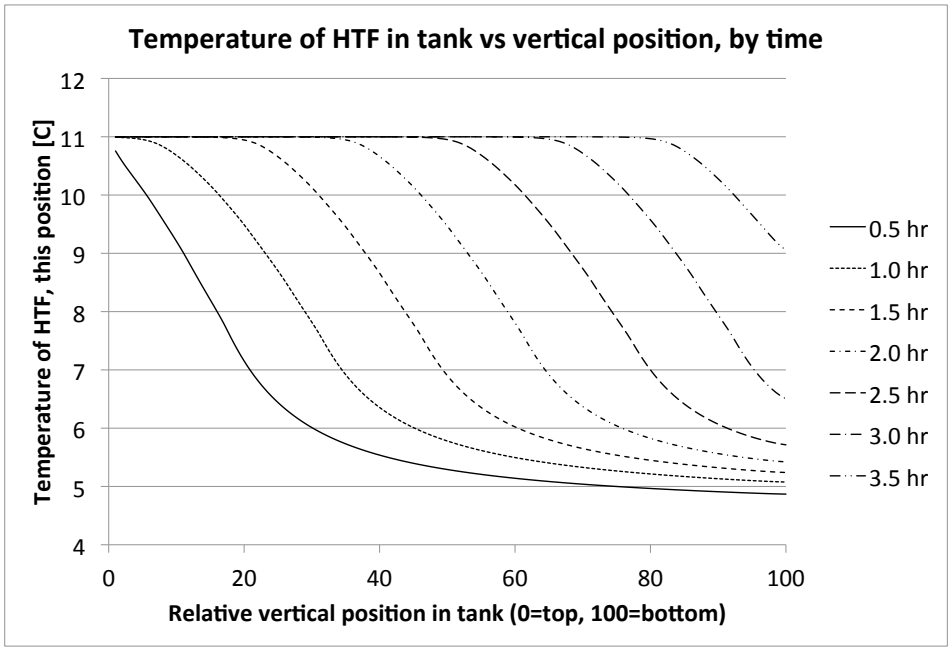

Figure C14: The temperature gradient initially formed in the tank is pushed down the tank as it discharges. In this case (0.007m radius encapsulation tubes, 40L/(min*m^2 of PCM flow rate) the gradient profile is fully developed by the one-hour mark. Once established the gradient travels down the tank until it reaches the tank exit, after which the output temperatures begin to rise quickly.

$$\varepsilon_{r'} = \frac{\varepsilon_r z_R + \Delta z}{z_R + \Delta z} \tag{C10}$$

The use of the resistance ratio [23] to set the inside radius of the encapsulation

tubes, coupled with the hexagonal packing of the encapsulation tubes, results in a constant ratio of PCM packing ε_p (the ratio of PCM cross-sectional area to tank cross-sectional area, or PCM volume to tank volume) for any given encapsulation material, HTF, and PCM. For 35% propylene glycol HTF and tetradecane PCM encapsulated in copper tubes this ratio is 0.849, while it is 0.811 for aluminum. However, even though the copper tubes have a higher PCM density, a thermal store consisting of $1m^3$ of PCM will require more aluminum tubes than copper tubes. This results in a larger overall thermal store size but also greater surface area and thus heat transfer rate for the aluminum tubes. These ε_p values can be used to determine the overall uninsulated size of a given storage capacity, or the storage capacity from the maximum uninsulated size of the tank.

The model results also show that, for the aluminum tubes modeled, the ratio of latent to total thermal energy is approximately 0.90; this can be used to estimate the total energy available in the store using the known volume of PCM in the system.

It is possible to specify a thermal store for a particular application using the data provided in this section, as shown by the following example. Let's assume that a residential-scale thermal store is required. The operating parameters are a capacity of 60kWh(thermal) with peak demand rate of 9kW, and a desired recovery rate as a percent of total capacity of 80%. Lets also assume that space is limited for this residential unit, and that the uninsulated diameter of the base can be no more than 1m (radius = 0.5m). The steps to design this thermal store are as follows:

9. Divide the thermal store desired capacity by the desired recovery percent; this gives the actual needed capacity of the thermal store: 75kWh.
10. Find the cross-sectional area of the PCM in the thermal store, based on the allowed size (radius = 0.5m, area = $0.79m^2$) multiplied by the packing ratio parameter for aluminum tubes of 0.811; this gives a PCM cross-

sectional area of 0.64 meters.

11. Calculate the necessary HTF flow rate to meet the demand rate using an average temperature change between HTF supply and return of 5.5°C, and the specific heat property for the HTF as given in Table C3. This application requires a flow rate of 26 L/min.
12. Divide the required flow rate by the PCM cross sectional area to obtain the flow rate normalized to a $1m^2$ cross sectional area of PCM, as used in the graphs of Figure C13. This gives a normalized flow rate of 40L/(min m^2 of PCM).
13. Multiply the required thermal capacity by the typical ratio of latent to total thermal energy (0.90), and then divide this value by the latent capacity of the PCM and PCM density to estimate the total PCM volume needed. For this case the total PCM volume required is $1.5m^3$ of PCM.
14. Divide the total PCM required by the PCM cross sectional area to obtain the minimum height of the thermal store, in this case 2.4 meters..
15. Using Equation C10, calculate the actual recovery percentage ε_r from the desired recovery percentage ε_r, using a reference height of 2m (because we will use the 2m chart in Figure C13) and an actual height of 2.4m; for this design the value comes to 75%.
16. Using the chart for a 2m tall thermal store in Figure C13, locate the tube size where the 40 L/min flow rate crosses a horizontal line drawn corresponding to a 75% recovery rate; any tube radius equal to or smaller than the identified radius will function in this application. In this case the 40 L/min flow rate line does not go below 75% at the largest tube radius listed, (0.016m radius) so any tube radius this size or smaller is acceptable.

The overall thermal density of this storage system design can also be estimated in a similar fashion. For aluminum encapsulation tubes, the thermal density is estimated as 41.5kWh/m^3; this is 2.7 to 7.2 times that of typical chilled water storage systems.

As an alternative, using pre-manufactured encapsulation tubes of fixed lengths (for example, in 0.5m increments) enables a thermal store of to be constructed using a "stack and pack" method. The height and radius of the thermal store can be selected based on the data provided in this parametric analysis so that the needed design operating parameters are met. Such a method of construction would facilitate the mass manufacturing of this design, reducing costs and enabling wider adoption of these thermal storage systems.

Chapter C4: Summary

This study investigates the design and operation of a high capacity thermal store consisting of aluminum cylinders containing tetradecane as a PCM, which are densely packed in a hexagonal pattern into a larger tank. A numerical model of the design is validated against existing test data, then used for a parametric analysis of encapsulation tube radius, height, and HTF flow rate on the performance of the thermal store.

The results show that this design is capable of providing acceptable storage capacities and recovery rates for use in HVAC cooling applications, providing 2.7 to 7.2 times the storage density of chilled water systems. The parametric data also shows that smaller diameter encapsulation tubes provide faster recovery rates and higher overall recovery efficiency, but that larger tubes can also provide suitable performance when lower flow rates or taller encapsulation tubes are permitted. The data provided by this study provides guidance for the development of thermal stores of varying size and performance using this design, and an example of the process for specifying a thermal store from this data is provided.

The thermal store modeled makes a number of assumptions as to the thermal properties of the PCM as it undergoes phase change. These assumptions may account for the remaining discrepancies between the experimental data and the model predictions. More research is needed into the properties of the PCM during phase change, which may have non-linear components that affect model compliance. Specifically, the instantaneous heat capacity with respect to temperature and the conductivity during phase transition both need further investigation. In addition, the possibility of internal convection heat transfer by the melting PCM should also be investigated.

References

[1] U.S. Energy Information Administration. 2015b. "Use of Electricity - Energy Explained, Your Guide To Understanding Energy - Energy Information Administration." Accessed September 1. http://www.eia.gov/energyexplained/index.cfm?page=electricity_use.

[2] U.S. Energy Information Administration. 2015c. "Residential Energy Consumption Survey (RECS) - Data - U.S. Energy Information Administration (EIA)." Accessed September 1. http://www.eia.gov/consumption/residential/data/2009/index.cfm?view=consumption.

[3] Wattles, Paul. 2016. "ERCOT-IGERT Presentation 2/8/16." presented at the IGERT group presentation, University of Texas, February 8.

[4] Bentley, W. G., and John C. Evelyn. 1986. "Customer Thermal Energy Storage a Marketing Opportunity for Cooling off Electric Peak Demand." *Power Systems, IEEE Transactions on* 1 (4): 57–61.

[5] Hermanns, Holger, and Holger Wiechmann. 2009. "Future Design Challenges for Electric Energy Supply." In *Emerging Technologies & Factory Automation, 2009. ETFA 2009. IEEE Conference on*, 1–8. http://ieeexplore.ieee.org/xpls/abs_all.jsp?arnumber=5347150.

[6] U.S. Energy Information Administration. 2015d. "Annual Energy Outlook 2015 with Projections to 2040." DOE/EIA-0383(2015). Washington, D.C.: U.S. Energy Information Administration. http://www.eia.gov/forecasts/aeo/.

[7] Andrepont, John S. 2012. "Applications of Low Temperature Fluid (LTF) in Thermally Stratified Thermally Stratified Thermal Energy Energy Storage (TES)." *ASHRAE Transactions* 118: 487.

[8] U.S. Census Bureau. 2013. "American Housing Survey for the United States: 2011." H150/11. U.S. Government Printing Office. https://www.census.gov/content/dam/Census/programs-surveys/ahs/data/2011/h150-11.pdf.

[9] U.S. Energy Information Administration. 2006. "Commercial Building Energy Consumption Survey." U.S. Energy Information Administration. http://www.eia.gov/consumption/commercial/about.cfm.

[10] Abhat, A. 1983. "Low Temperature Latent Heat Thermal Storage: Heat Storage Materials." *Solar Energy* Vol 30 (4): 313–32.

[11] Agyenim, Francis, Neil Hewitt, Philip Eames, and Mervyn Smyth. 2010. "A Review of Materials, Heat Transfer and Phase Change Problem Formulation for

Latent Heat Thermal Energy Storage Systems (LHTESS)." *Renewable and Sustainable Energy Reviews* 14 (2): 615–28. doi:10.1016/j.rser.2009.10.015.

[12] Hale, D, M Hoover, and M O'Neill. 1971. "Phase Change Materials Handbook." NASA CR-61363. Huntsville, AL: Lockheed Missles and Space Company. http://hdl.handle.net/2060/19720012306.

[13] Humphries, William, and Edwin Griggs. 1977. "A Design Handbook for Phase Change Thermal Storage Control and Energy Storage Devices." National Aeronautics and Space Administration Scientific and Technical Information Office. http://hdl.handle.net/2060/19780007491.

[14] Baetens, Ruben, Bjørn Petter Jelle, and Arild Gustavsen. 2010. "Phase Change Materials for Building Applications: A State-of-the-Art Review." *Energy and Buildings* 42 (9): 1361–68. doi:10.1016/j.enbuild.2010.03.026.

[15] Sharma, Atul, V.V. Tyagi, C.R. Chen, and D. Buddi. 2009. "Review on Thermal Energy Storage with Phase Change Materials and Applications." *Renewable and Sustainable Energy Reviews* 13: 318–45.

[16] Feldman, D., M. M. Shapiro, and D. Banu. 1986. "Organic Phase Change Materials for Thermal Energy Storage." *Solar Energy Materials* 13 (1): 1–10.

[17] Feldman, D., M. M. Shapiro, D. Banu, and C. J. Fuks. 1989. "Fatty Acids and Their Mixtures as Phase-Change Materials for Thermal Energy Storage." *Solar Energy Materials* 18 (3): 201–16.

[18] He, B, V Martin, and F Setterwall. 2004. "Phase Transition Temperature Ranges and Storage Density of Paraffin Wax Phase Change Materials." *Energy* 29 (11): 1785–1804. doi:10.1016/j.energy.2004.03.002.

[19] Trp, Anica. 2005. "An Experimental and Numerical Investigation of Heat Transfer during Technical Grade Paraffin Melting and Solidification in a Shell-and-Tube Latent Thermal Energy Storage Unit." *Solar Energy* 79 (6): 648–60. doi:10.1016/j.solener.2005.03.006.

[20] Regin, A. Felix, S.C. Solanki, and J.S. Saini. 2008. "Heat Transfer Characteristics of Thermal Energy Storage System Using PCM Capsules: A Review." *Renewable and Sustainable Energy Reviews* 12 (9): 2438–58. doi:10.1016/j.rser.2007.06.009.

[21] Hales, Thomas C. 1998. "An Overview of the Kepler Conjecture." *arXiv Preprint math/9811071*. http://arxiv.org/abs/math/9811071.

[22] Bezdek, Andréas, and Wlodzimierz Kuperberg. 1990. "Maximum Density Space Packing with Congruent Circular Cylinders of Infinite Length." *Mathematika* 37 (01): 74–80.

[23] Bourne, Stephen, and Atila Novoselac. 2016. “Improved Performance in Tube-Encapsulated Phase Change Thermal Energy Stores for HVAC Applications.” *Building and Environment* 98 (March): 133–44. doi:10.1016/j.buildenv.2015.12.023.

[24] Bourne, Stephen, and Atila Novoselac. 2015. “Compact PCM-Based Thermal Stores for Shifting Peak Cooling Loads.” *Building Simulation*, July. doi:10.1007/s12273-015-0243-6.

[25] Bourne, Stephen, and Atila Novoselac. 2015. “PCM-Based High-Density Thermal Storage Systems for Residential and Small Commercial Retrofit Applications.” *Procedia Engineering* 121: 536–43. doi:10.1016/j.proeng.2015.08.1025.

[26] Bourne, Steve, and Atila Novoselac. 2014. “Compact Phase Change Based Thermal Storage: Experimental Apparatus, Methodology, and Results.” *ASHRAE Transactions* 120 (1): 1–8.

[28] Cengel, Yunus A., Robert H. Turner, and John M. Cimbala. 2008. *Fundamentals of Thermal-Fluid Sciences*. 3rd ed. New York, NY: McGraw Hill.

[29] McAdams, William H. 1942. *Heat Transmission*. 2nd ed. New York: McGraw-Hill.

[30] He, B, V Martin, and F Setterwall. 2004. “Phase Transition Temperature Ranges and Storage Density of Paraffin Wax Phase Change Materials.” *Energy* 29 (11): 1785–1804. doi:10.1016/j.energy.2004.03.002.

[31] O’Neill, M. J. 1966. “Measurement of Specific Heat Functions by Differential Scanning Calorimetry.” *Analytical Chemistry* 38 (10): 1331–36.

[32] He, Bo, and Fredrik Setterwall. 2002. “Technical Grade Paraffin Waxes as Phase Change Materials for Cool Thermal Storage and Cool Storage Systems Capital Cost Estimation.” *Energy Conversion and Management* 43 (13): 1709–23.

[33] American Society of Heating, Refrigerating and Air-Conditioning Engineers. 2009. *2009 ASHRAE Handbook: Fundamentals*. American Society of Heating, Refrigeration and Air-Conditioning Engineers.

[34] Lide, David R. 2001. *Handbook of Chemistry and Physics*. 82nd ed. Boca Raton, FL: CRC Press LLC.

[35] Kousksou, T., A. Jamil, T. El Rhafiki, and Y. Zeraouli. 2010. “Paraffin Wax Mixtures as Phase Change Materials.” *Solar Energy Materials and Solar Cells* 94 (12): 2158–65.

Symbols

General

A	Area (general) [m^2]
A_a	Area associated with advection [m^2]
A_C	Area associated with convection [m^2]
A_i	Area of the inside surface of a node volume
A_k	Area associated with conduction [m^2]
A_o	Area of the outside surface of a node volume
A_P	Area associated with conduction into the PCM [m^2]
A_T	Area associated with conduction around the encapsulation tube
a	Constant (general)
C	Constant (general)
C_f	Specific heat of the heat transfer fluid
D_h	Hydraulic diameter [m]
ε_p	PCM fraction of cross sectional area of thermal store [%]
ε_r	Energy recovery fraction [%]
$\varepsilon_{r'}$	Energy recovery fraction corrected for height [%]
F_{lpm}	HTF flow rate [L/min]
H(t)	Latent enthalpy of a model volume element at time t
Hf	Heat of fusion [J]
h	Thermal convection coefficient [$W/(m^2 \cdot ºK$]
k	Conductivity (general) [$W/(m \cdot °K)$]
k_{eff}	Conductivity, effective (general) [$W/(m \cdot °K)$]
k_f	Conductivity of the heat transfer fluid [$W/(m \cdot ºK$]

k_p Conductivity of the PCM

k_t Conductivity of the encapsulation material

K_R Ratio of conductivities

L Length (general) [m]; arbitrary height length [m]

L_P Characteristic length of conduction into the PCM cylinder [m]

LR Loss rate through tank shell [W/ºK]

L_T Characteristic length of conduction along the encapsulation tube

Nu Nusselt number [ ]

Pr_r Prandtl number [ ]

r Radius [m]

r_i Inside radius of the encapsulation tube

r_o Outside radius of the encapsulation tube

R_c Resistance of convection to the encapsulation tube

R_p Resistance of conduction into the PCM

R_R Ratio of average tube size to thickness; $\frac{\left(r_o + r_i\right)/2}{\left(r_o - r_i\right)}$

R_t Resistance of conduction around the encapsulation tube

Re Reynolds number [ ]

Reo Outside radius of the encapsulation tube(s) [m]

Rei Inside radius of the encapsulation tube(s) [m]

t time [s, min, or hr]

T Temperature (general) [ºC or ºK]

T_{amb} Ambient temperature [ºC or ºK]

T_f Freezing temperature

T_m Lowest temperature at which PCM begins to melt [C]

T_{out} Output HTF temperature

T_s Highest temperature at which PCM begins to solidify

t Time (general) [s]

V_f Volume associated with a HTF node [m3]

w Vertical heat transfer fluid velocity [m/s]

z Vertical dimension (general) [m]

z_R Reference vertical dimension (for parametric data); 1, 2, or 3m

Special characters

α Thermal diffusivity (general) [m^2/s]

α_f Thermal diffusivity of the heat transfer fluid [m^2/s]

θ Angle (general) [rad]

ϱ Density (general) [kg/m^3]

ϱ_f Density of the HTF (heat transfer fluid) [kg/m^3]

Δr radial step dimension [m]

Δt Time step interval [s]

Δz Vertical step dimension or change in vertical height [m]

Subscripts

p PCM parameter

f Heat transfer fluid (HTF) parameter

s Surface of encapsulation tube

t Encapsulation tube parameter

m Row identifier

n Column identifier

Superscripts

t	time parameter [s]
$t + \Delta t$	time at next time step [s]

Bibliography

Abhat, A. 1983. "Low Temperature Latent Heat Thermal Storage: Heat Storage Materials." Solar Energy Vol 30 (4): 313–332.

Agyenim, Francis, Neil Hewitt, Philip Eames, and Mervyn Smyth. 2010. "A Review of Materials, Heat Transfer and Phase Change Problem Formulation for Latent Heat Thermal Energy Storage Systems (LHTESS)." Renewable and Sustainable Energy Reviews 14 (2) (February): 615–628. doi:10.1016/j.rser.2009.10.015.

Alexiades, Vasilios, and Alan D Solomon. 1993. Mathematical Modeling of Melting and Freezing Processes. Washington: Hemisphere Pub. Corp.

Andrepont, John S. 2012. "Applications of Low Temperature Fluid (LTF) in Thermally Stratified Thermally Stratified Thermal Energy Energy Storage (TES)." *ASHRAE Transactions* 118: 487.

ASHRAE. 2009. *2009 ASHRAE Handbook: Fundamentals*. Atlanta GA: American Society of Heating, Refrigerating and Air Conditioning Engineers.

ASHRAE. 2007. *2007 ASHRAE Handbook: HVAC Applications*. Atlanta GA: American Society of Heating, Refrigerating and Air Conditioning Engineers.

ASHRAE. 2004. *2004 ASHRAE Handbook: HVAC Systems and Equipment*. Atlanta GA: American Society of Heating, Refrigerating and Air Conditioning Engineers.

Assis, E., L. Katsman, G. Ziskind, and R. Letan. 2007. "Numerical and Experimental Study of Melting in a Spherical Shell." *International Journal of Heat and Mass Transfer* 50 (9): 1790–1804.

Baetens, Ruben, Bjørn Petter Jelle, and Arild Gustavsen. 2010. "Phase Change Materials for Building Applications: A State-of-the-Art Review." Energy and Buildings 42 (9): 1361–68. doi:10.1016/j.enbuild.2010.03.026.

Bentley, W. G., and John C. Evelyn. 1986. "Customer Thermal Energy Storage a Marketing Opportunity for Cooling Off Electric Peak Demand." Power Systems, IEEE Transactions On 1 (4): 57–61.

Bezdek, Andréas, and Wlodzimierz Kuperberg. 1990. "Maximum Density Space Packing with Congruent Circular Cylinders of Infinite Length." Mathematika 37 (01): 74–80.

Bilir, Levent, and Zafer İlken. 2005. "Total Solidification Time of a Liquid Phase Change Material Enclosed in Cylindrical/spherical Containers." Applied Thermal Engineering 25 (10) (July): 1488–1502. doi:10.1016/j.applthermaleng.2004.10.005.

Bourne, Stephen, and Atila Novoselac. 2015. "Compact PCM-Based Thermal Stores for Shifting Peak Cooling Loads." *Building Simulation*, July. doi:10.1007/s12273-015-0243-6.

Briggs, Tyler. 2013. “N-Tetradecane Pricing,” (email). December 18.

Budihardjo, Indra, Graham L. Morrison, and Masud Behnia. 2007. “Natural Circulation Flow through Water-in-Glass Evacuated Tube Solar Collectors.” *Solar Energy* 81 (12): 1460–72. doi:10.1016/j.solener.2007.03.002.

Cengel, Yunus A., Robert H. Turner, and John M. Cimbala. 2008. Fundamentals of Thermal-Fluid Sciences. 3rd ed. New York, NY: McGraw Hill.

Chen, Chun-Long, and Nihad Dukhan. 2012. “Metal-Foam Enhanced PCM Storage System: The Cylinder-in-Cylinder Geometry.” ASHRAE Transactions 118 (Part 1): 293–300.

Choi, Eunsoo, Young I. Cho, and Harold G. Lorsch. 1992. “Thermal Analysis of the Mixture of Laboratory and Commercial Grades Hexadecane and Tetradecane.” International Communications in Heat and Mass Transfer 19 (1): 1–15.

City of Austin. 2016. “Approved Rate Schedules for City of Austin.” *Austin Energy - More than Electricity*. austinenergy.com/wps/portal/ae/rates/approved-rates-schedules.

Croome-Gale, D. J., and B. M. Roberts. 1975. *Air Conditioning and Ventilation of Buildings*. 1st ed. Elmsford, NY: Pergamon Press.

Dimaano, Maria Natalia R., and Takayuki Watanabe. 2002. “The Capric–lauric Acid and Pentadecane Combination as Phase Change Material for Cooling Applications.” Applied Thermal Engineering 22 (4): 365–377.

Doggett, Trip. 2013. “ERCOT - A Strategic View of the Future.” presented at the Gulf Coast Power Association Fall Annual Conference, October 2. http://www.ercot.com/content/news/presentations/2013/GCPA - 02 Oct 2013 FINAL.pdf.

Fan, Liwu, and J. M. Khodadadi. 2011. “Thermal Conductivity Enhancement of Phase Change Materials for Thermal Energy Storage: A Review.” Renewable and Sustainable Energy Reviews 15 (1): 24–46.

Farid, Mohammed M, Amar M Khudhair, Siddique Ali K Razack, and Said Al-Hallaj. 2004. “A Review on Phase Change Energy Storage: Materials and Applications.” Energy Conversion and Management 45 (9-10): 1597–1615. doi:10.1016/j.enconman.2003.09.015.

Feldman, D., M. M. Shapiro, and D. Banu. 1986. “Organic Phase Change Materials for Thermal Energy Storage.” Solar Energy Materials 13 (1): 1–10.

Gur, Ilan, Karma Sawyer, and Ravi Prasher. 2012. “Searching for a Better Thermal Battery.” Science, March 23.

Hajiah, Ali, and Moncef Krarti. 2012. “Optimal Control of Building Storage Systems Using Both Ice Storage and Thermal Mass – Part I: Simulation Environment.”

Energy Conversion and Management (April). doi:10.1016/j.enconman.2012.02.016. http://linkinghub.elsevier.com/retrieve/pii/S0196890412000799.

Hajiah, Ali, and Moncef Krarti. 2012. "Optimal Controls of Building Storage Systems Using Both Ice Storage and Thermal Mass – Part II: Parametric Analysis." Energy Conversion and Management 64 (December): 509–515. doi:10.1016/j.enconman.2012.02.020.

Hale, D, M Hoover, and M O'Neill. 1971. "Phase Change Materials Handbook". United States. http://hdl.handle.net/2060/19720012306.

Hales, Thomas C. 1998. "An Overview of the Kepler Conjecture." arXiv Preprint math/9811071. http://arxiv.org/abs/math/9811071.

Hasan, A., and A. A. Sayigh. 1994. "Some Fatty Acids as Phase-change Thermal Energy Storage Materials." Renewable Energy 4 (1): 69–76.

Hasnain, S.M. 1998. "Review on Sustainable Thermal Energy Storage Technologies, Part I: Heat Storage Materials and Techniques." Energy Conversion and Management 39 (11) (August 1): 1127–1138.

He, B, V Martin, and F Setterwall. 2004. "Phase Transition Temperature Ranges and Storage Density of Paraffin Wax Phase Change Materials." Energy 29 (11) (September): 1785–1804. doi:10.1016/j.energy.2004.03.002.

He, Bo, Viktoria Martin, and Fredrik Setterwall. 2003. "Liquid–solid Phase Equilibrium Study of Tetradecane and Hexadecane Binary Mixtures as Phase Change Materials (PCMs) for Comfort Cooling Storage." Fluid Phase Equilibria 212 (1): 97–109.

He, Bo, and Fredrik Setterwall. 2002. "Technical Grade Paraffin Waxes as Phase Change Materials for Cool Thermal Storage and Cool Storage Systems Capital Cost Estimation." Energy Conversion and Management 43 (13): 1709–1723.

He, Bo, E. M. Gustafsson, and F. Setterwall. 1999. "Tetradecane and Hexadecane Binary Mixtures as Phase Change Materials (PCMs) for Cool Storage in District Cooling Systems." Energy 24 (12): 1015–1028.

Hermanns, Holger, and Holger Wiechmann. 2009. "Future Design Challenges for Electric Energy Supply." In Emerging Technologies & Factory Automation, 2009. ETFA 2009. IEEE Conference on, 1–8. http://ieeexplore.ieee.org/xpls/abs_all.jsp?arnumber=5347150.

Humphries, William, and Edwin Griggs. 1977. "A Design Handbook for Phase Change Thermal Storage Control and Energy Storage Devices". National Aeronautics and Space Administration Scientific and Technical Information Office. http://hdl.handle.net/2060/19780007491.

Incropera, Frank, David Dewitt, Theodore Bergman, and Adrienne Lavine. 2007. Fundamentals of Heat and Mass Transfer. 6th ed. Hoboken, NJ: John Wiley and Sons.

Ismail, K.A.R., and M.M. Goncalves. 1999. "Thermal Performance of a PCM Storage Unit." Energy Conversion and Management 40: 115–38.

Ismail, K.A.R., and R.I.R. Moraes. 2009. "A Numerical and Experimental Investigation of Different Containers and PCM Options for Cold Storage Modular Units for Domestic Applications." International Journal of Heat and Mass Transfer 52 (19-20) (September): 4195–4202. doi:10.1016/j.ijheatmasstransfer.2009.04.031.

Jesumathy, Stella P., M. Udayakumar, and S. Suresh. 2012. "Heat Transfer Characteristics in Latent Heat Storage System Using Paraffin Wax." Journal of Mechanical Science and Technology 26 (3): 959–965.

Jiji, Latif M., and Salif Gaye. 2006. "Analysis of Solidification and Melting of PCM with Energy Generation." Applied Thermal Engineering 26 (5): 568–575.

Kalaiselvam, S., M. Veerappan, A. Arul Aaron, and S. Iniyan. 2008. "Experimental and Analytical Investigation of Solidification and Melting Characteristics of PCMs inside Cylindrical Encapsulation." *International Journal of Thermal Sciences* 47 (7): 858–74. doi:10.1016/j.ijthermalsci.2007.07.003.

Kanwischer, Herbert, and Rainer Tamme. 1985. "Development of Media for Dynamic Latent Heat Storage for the Low-Temperature Range. Part I: Thermal Analysis of Selected Salt Hydrate Systems." National Aeronautics and Space Administration.

Kenisarin, Murat, and Khamid Mahkamov. 2007. "Solar Energy Storage Using Phase Change Materials." Renewable and Sustainable Energy Reviews 11 (9): 1913–1965.

Kousksou, T., A. Jamil, T. El Rhafiki, and Y. Zeraouli. 2010. "Paraffin Wax Mixtures as Phase Change Materials." Solar Energy Materials and Solar Cells 94 (12): 2158–2165.

Larsen, Floyd W., and James P. Hartnett. 1961. "Effect of Aspect Ratio and Tube Orientation on Free Convection Heat Transfer to Water and Mercury in Enclosed Circular Tubes." *Journal of Heat Transfer* 83 (1): 87–93.

Li, Gang, Yunho Hwang, and Reinhard Radermacher. 2012. "Review of Cold Storage Materials for Air Conditioning Application." International Journal of Refrigeration 35 (8): 2053–2077.

Lide, David R. 2001. Handbook of Chemistry and Physics. 82nd ed. Boca Raton, FL: CRC Press LLC.

Masters, Gilbert M. 2004. Renewable and Efficient Electric Power Systems. Hoboken, NJ: John Wiley & Sons, Inc.

McAdams, William H. 1942. Heat Transmission. 2nd ed. New York: McGraw-Hill.

Munson, Bruce R., Donald F. Young, Theodore H. Okiishi, and Wade W. Huebsch. 2009. Fundamentals of Fluid Mechanics. 6th ed. United States: John Wiley & Sons, Inc.

O'Neill, M. J. 1966. "Measurement of Specific Heat Functions by Differential Scanning Calorimetry." Analytical Chemistry 38 (10): 1331–36.

Rathod, M. K., and J. Banerjee. 2014. "Experimental Investigations on Latent Heat Storage Unit Using Paraffin Wax as Phase Change Material." *Experimental Heat Transfer* 27 (1): 40–55. doi:10.1080/08916152.2012.719065.

Regin, A. Felix, S.C. Solanki, and J.S. Saini. 2008. "Heat Transfer Characteristics of Thermal Energy Storage System Using PCM Capsules: A Review." Renewable and Sustainable Energy Reviews 12 (9) (December): 2438–2458. doi:10.1016/j.rser.2007.06.009.

Ruvalcaba, Daniel. 2012. "Certificate of Analysis, n-Tetradecane, Techical Grade."

Shamsundar, N, and Sparrow, E.M. 1975. "Analysis of Multidimensional Conduction Phase Change Via the Enthalopy Method". ASME. http://heattransfer.asmedigitalcollection.asme.org.ezproxy.lib.utexas.edu/article.aspx?articleid=1436183.

Sharma, Atul, V.V. Tyagi, C.R. Chen, and D. Buddi. 2009. "Review on Thermal Energy Storage with Phase Change Materials and Applications." Renewable and Sustainable Energy Reviews 13: 318–345.

Stevenson, A. R. 1929. "Refrigeration." Journal of the Franklin Institute 208 (2): 143–187.

Stoecker, W.F. 1989. Design of Thermal Systems. 3rd ed. McGraw-Hill.

Trp, Anica. 2005. "An Experimental and Numerical Investigation of Heat Transfer During Technical Grade Paraffin Melting and Solidification in a Shell-and-tube Latent Thermal Energy Storage Unit." Solar Energy 79 (6) (December): 648–660. doi:10.1016/j.solener.2005.03.006.

U.S. Census Bureau. 2013. American Housing Survey for the United States: 2011. https://www.census.gov/content/dam/Census/programs-surveys/ahs/data/2011/h150-11.pdf.

U.S. EIA Energy Information Administration. "Frequently asked Questions: How much electricity is used for cooling in the United States?". 21 Jan 2012. [Accessed 10 Mar 2013]. http://www.eia.gov/tools/faqs/faq.cfm?id=98&t=3

U.S. EIA Energy Information Administration. "Annual Energy Outlook 2013". Apr 2013. [Accessed 25 Sep 2013]. http://www.eia.gov/forecasts/aeo/pdf/0383(2013).pdf

Velraj, R., R. V. Seeniraj, B. Hafner, C. Faber, and K. Schwarzer. 1999. “Heat Transfer Enhancement in a Latent Heat Storage System.” Solar Energy 65 (3): 171–80.

Wattles P (2011). ERCOT Demand Response—Overview and Status Report. Available at http://www.ercot.com/content/meetings/dswg/ keydocs/2011/0830/3_ERCOT_presentation_workshop_083011. pdf.

U.S. Energy Information Administration. 2006. “Commercial Building Energy Consumption Survey”. U.S. Energy Information Administration. http://www.eia.gov/consumption/commercial/about.cfm.

Versteeg, H. K., and W. Malalasekera. 1995. *An Introduction to Computational Fluid Dynamics*. Essex, England: Pearson Education Limited.

Zalba, Belen, José Ma Marín, Luisa F. Cabeza, and Harald Mehling. 2003. “Review on Thermal Energy Storage with Phase Change: Materials, Heat Transfer Analysis and Applications.” Applied Thermal Engineering 23 (3): 251–83.

Vita

Stephen Bourne attended the University of California at Berkeley, where he earned a B.S. degree in Civil Engineering in 2007. Stephen continued at Berkeley, receiving his M.S. degree in Civil Engineering in 2009. In 2010, Stephen entered the Ph.D. program in Civil Engineering at the University of Texas at Austin. This dissertation is the culmination of his graduate work at the University of Texas.

Permanent address (or email): gaborkin@utexas.edu

This dissertation was typed by Stephen Bourne.